ELECTROTHERMAL BEHAVIOR OF FREESTANDING AND ATTACHED DIAMOND RESISTORS

By

Puteri Saidatul A. Megat Hamari

Dissertation

Submitted to the Faculty of the

Graduate School of Vanderbilt University

in partial fulfillment of the requirements

for the degree of

DOCTOR OF PHILOSOPHY

in

Electrical Engineering

December, 2010

Nashville, Tennessee

Approved:

Professor Jim L. Davidson

Professor Weng P. Kang

Professor Bharat L. Bhuva

Professor Alvin M. Strauss

Professor Norman H. Tolk

To my dearest husband, Fuad

To our wonderful children Nadia, Adam and Natasha

And

To my beloved parents, Megat Hamari and Nadzirah, and the rest of my family

ACKNOWLEDGEMENTS

The simple truth is that I have only gotten to this point because of a tremendous amount of guidance, support, assistance, understanding, and love from some incredible people. If a person is the sum of all their experiences up to a particular point in time, then the following people are largely responsible for where I am now.

I cannot begin by thanking anyone other my advisor, Dr. Jim L. Davidson for giving me the guidance, insight, encouragement, and independence to pursue a challenging project. His contributions to this work were so integral that they cannot be described in words here. His visions and dedication always inspire me. I would like to thank to Dr. Weng P. Kang and Dr. Bharat Bhuva who are also serve as the members of my committee for their unlimited patience in answering my questions when I needed them the most. I am also grateful to the other members of my committee, Dr. Norman Tolk and Dr. Alvin Strauss for many educational and stimulating discussions.

I would like to thank to our lab engineer, Mr. Mick Howell for helping and teaching me to operate the diamond machines as well as for keeping them running. I would like to extend my gratitude to my colleagues at the Vanderbilt Diamond Group, Patrick Taylor, Supil Raina and Nikkon Ghosh for the endless discussions and their cooperation have contributed substantially to this work.

A special thank you to Mr. Charles Ellis and the Alabama Microelectronics Science and Technology Center, your assistance and open door policy made it possible for the completion of this research.

Thank you to my parents, Megat Hamari and Nadzirah, my brothers and sisters. You have always believed in me. Mak and Abah, thank you for giving me every opportunity, for teaching me right from wrong, and for setting the examples I use to live my life every day. All of my achievements, past, present, and future, have begun with your love and generosity. Thank you.

Last but not least, and with all of my love and thanks, to my husband Fuad. It has been quite a ride. You have believed in me more than I may have deserved. I could struggle for another five years to try to find words necessary to express my feelings for you and for what our marriage means to me, but I suspect you would like me to graduate…now. So instead, I hereby dedicate this document to you. Last but not least, I wish to thank my three wonderful children, Nadia, Adam and Natasha, who provide unending inspiration.

TABLE OF CONTENTS

Page

ACKNOWLEDGEMENTS ... iii

LIST OF FIGURES ... vii

LIST OF TABLES ... xiii

NOMENCLATURE ... xiv

Chapter

I. INTRODUCTION ... 1

1.1 Motivation ... 1
1.2 Objectives of the work ... 2
1.3 Thesis Structure ... 3
1.4 Diamond Material Properties ... 4
1.4.1 Structural and Electrical Characteristics ... 4
1.4.2 Classification of Diamond ... 6
1.4.3 Thermal Characteristics ... 8
1.4.4 Thermal Transport ... 9
1.5 Microwave (MW) Plasma Enhanced (PE) CVD ... 10
1.6 Substrate ... 11
1.6.1 Bulk Micromachining Process Technology ... 12
1.6.2 Surface Micromachining Process Technology ... 13
1.7 Nucleation Process ... 14
1.8 Doping ... 14

II. BACKGROUND ... 16

2.1 Heat Transfer: Basic Concepts in Thermal Modeling ... 16
2.1.1 Conduction ... 16
Specific Heat Capacity ... 17
Thermal Diffusivity ... 17
2.1.2 Convection ... 18
2.1.3 Radiation ... 18
2.2 Electrical Equivalent of Thermal Parameters ... 21
2.3 Joule Heating ... 23
2.3.1 Electrical Resistance ... 23
2.3.2 Physics of Joule Heating ... 26
2.4 Boron Ionization in P-Doped Diamond ... 30
2.5 Hole Concentration Calculation ... 32
2.6 Heating and Cooling Principles ... 35
2.7 The Electromagnetic Spectrum ... 44

2.7.1 Basic Concept: The Blackbody 46

III. DEVICE FABRICATION AND EXPERIMENTATION 49
Part I: Fabrication of Attached and Freestanding Diamond Resistor 49
3.1 Resistor Layout and Design 49
3.2 Resistors Fabrication 52
3.2.1 Challenge on diamond deposition on SiO_2 60
Part II: Testing Characterization 66
3.3 Pulse Heating Measurement Setup 68
3.4 Experimentation to Determine Activation Energy 72

IV. EXPERIMENTAL RESULTS AND DISCUSSION 74
4.1 Thickness Measurement 74
4.2 Determination of Activation Energy 77
4.2.1 Temperature Dependence of Resistance 83
4.3 Preliminary Test Results 85
4.4 Attached Diamond Resistors 93
4.4.1 Lower Pulse Voltage Response Characterization 93
4.4.2 Higher Pulse Voltage Response Characterization 99
4.4.2.1 Discussion of the Rate of Change in Temperature over Pulsing Time 114
4.4.3 Examination of Power and Current at the Attached Diamond Resistor Limit 116
4.5 Freestanding Diamond Resistors 120
4.5.1 Lower Pulse Voltage Response Characterization 120
4.5.2 Higher Pulse Voltage Response Characterization 128
4.5.2.1 Temperature Effect on Carrier Concentration 148
4.5.3 Examination of Power and Current at the Freestanding Diamond Resistor Limit 154
4.6 Comparing Attached and Freestanding Diamond Resistors 160

V. SUMMARY AND FUTURE WORK 163
Summary 163
Future Work 164

Appendix

A. RESISTANCE AND CONDUCTANCE 165
B. P-SPICE SIMULATION 167
C. PRELIMINARY TEST 171
Resistor Free_B11 171
D. TEMPERATURE TABLE 174

REFERENCES 175

LIST OF FIGURES

Figure 1.1: Conventional unit cube for diamond (zinc blende crystal structure). 5

Figure 1.2: Schematic representation of a MWCVD reactor.. 11

Figure 1.3: Surface micromachining (left) of Texas Instruments Digital
Micromirror Device and bulk micromachining (right) of silicon gear. 12

Figure 2.1: Energy balance of the resistor. 27

Figure 2.2: Response to on-off control. 39

Figure 2.3: Schematic shows maximum and minimum temperature rise of resistor
in the state of dynamic equilibrium (steady state) with pulse voltage supply. 42

Figure 2.4: Transient process in R_T-R circuit for action on input of pulses of supply
voltage. Time t in seconds. 44

Figure 2.5: The electromagnetic spectrum.. 45

Figure 2.6: Distribution of energy from a blackbody as a function of wavelength. 47

Figure 3.1: Three resistors, R1, R2 and R3 with dimensions of 50µm × 10µm,
100µm × 50µm and 500µm × 100µm respectively. 50

Figure 3.2: Diamond resistor with necking design to concentrate the current
flow through the resistor body. 50

Figure 3.3: Mask layout consists of mask for resistor (red) and contact (blue)
on a 2cm × 2cm substrate for attached resistors... 51

Figure 3.4: Mask layout consists of mask for resistor (red), contact (blue)
and cavity (green) on a 2cm × 2cm substrate for freestanding resistors. 51

Figure 3.5: Steps of fabricating freestanding diamond resistors...................................... 55

Figure 3.6: Schematic of ASTeX Microwave Plasma Assisted Chemical Vapor
Deposition System 56

Figure 3.7: SEM image shows a well defined resistor delineation after RIE process. 57

Figure 3.8: (A) Micrograph picture of attached resistor, R3 with dimension
of 500µm × 100µm. (B) SEM picture of 50µm × 10µm attached diamond resistor. 57

Figure 3.9: Top view of SEM micrograph of complete freestanding diamond resistors. 58

Figure 3.10: (A) A close up SEM image of 500µm x 100µm diamond resistor. Inset shows the Boron doped diamond film. (B) Image of the freestanding diamond resistor with cavity and metal contact shown. 58

Figure 3.11: (A) SEM picture of 50µm × 10µm freestanding diamond resistor. (B) A close up SEM of the diamond resistor body; inset: shows the diamond resistor was a freestanding and the cavity height was about 1µm. 59

Figure 3.12: High mask area-to-sample size ratio contributed to edge effect. 60

Figure 3.13: Clusters of diamond on SiO_2 shows non-uniform layer of diamond growth. 62

Figure 3.14: SEM image of scratch found after contact pattern. 62

Figure 3.15: SEM picture of diamond nucleation in diamond machine 1.5kW. 64

Figure 3.16: SEM picture of diamond surface following the diamond growth in diamond machine 5kW (same sample after nucleation process in 1.5kW machine). .. 64

Figure 3.17: High magnified view of polycrystalline diamond film (from diamond machine 5kW). 65

Figure 3.18: Schematic of a rectangular pulse. 67

Figure 3.19: Schematic of the set- up for pulse heating test. 69

Figure 3.20: Detail of test set- up for the pulse heating experiment. 70

Figure 4.1: Outline sketch of DekTak IIA. 75

Figure 4.2: Graphic output for thickness sample **Free_A**. 75

Figure 4.3: Graphic output for thickness sample **Free_B**. 76

Figure 4.4: Graphic output for thickness sample **Att_C**. 76

Figure 4.5: Resistance vs. Temperature plot for both freestanding resistor samples, sample **Free_A** (A) and sample **Free_B** (B); inset: corresponding Arrhenius plots. 79

Figure 4.6: Resistance vs. Temperature plot for attached resistor sample, **Att_C**. 80

Figure 4.7: Typical current-voltage plots at room temperature for freestanding diamond resistors. A: sample **Free_A**, B: sample **Free_B**. 82

Figure 4.8: Typical current-voltage plot at room temperature for attached resistors sample **Att_C**. 82

Figure 4.9: Current waveform of resistor **Free_A5** at 160V. 87

Figure 4.10: Corresponding resistance waveform of resistor **Free_A5**. 87

Figure 4.11: I-V plot of resistor **Free_A5** post pulse. 88

Figure 4.12: Voltage, resistance and temperature waveforms of resistor **Free_A8**. 90

Figure 4.13: Resistance and current pulse for **Free_A8**. 91

Figure 4.14: Image of resistor glowed during the high power pulse. 91

Figure 4.15: Resistor failed after the high **Free_A8** power pulse. 92

Figure 4.16: The arrow on the Planckian locus shows the blackbody's color for the estimated temperature before the failure. 92

Figure 4.17: Input voltage and corresponding resistance and current waveform for resistor **Att_C5**. 96

Figure 4.18: Change in the current over time (**Att_C5**). 97

Figure 4.19: Corresponding change in resistance of $i(t)$ in Figure 4.18 over pulsing time. 97

Figure 4.20: Average current per pulse over cumulative pulsing time for resistor **Att_C5**. 98

Figure 4.21: Calculated average temperature per pulse over cumulative pulsing time for resistor **Att_C5**. 98

Figure 4.22: Current waveform for resistor **Att_C6** at 1s < t < 76s.The possible leakage current was observed after t > 73s. 100

Figure 4.23: Corresponding resistance waveforms of $i(t)$ in Figure 4.22. 101

Figure 4.24: High leakage current observed in resistor **Att_C6** after $t \geq$ 76s leading to electrical overstress. 102

Figure 4.25: Corresponding resistance waveform of resistor **Att_C6** after t>76s. Resistance became very low indicate it was failed to a short. 103

Figure 4.26: Typical resistance profile of resistor **Att_C8** shows near constant value of resistance in the pulse. In this display, the profile was at t = 70s. 105

Figure 4.27: Current profile of resistor **Att_C8** at t=150s. 105

Figure 4.28: Resistance profile of resistor **Att_C8** at t = 150s shows resistance decreases across the pulse (transient). 106

Figure 4.29: Sequential current behavior of resistor **Att_C8** with successive pulses for $\boldsymbol{t}$ > 60s. Possible leakage current was observed after 164s of pulsing. 107

Figure 4.30: Sequential current behavior of resistor **Att_C8** with successive pulses over pulsing time before the leakage current. 109

Figure 4.31: Plot of average resistance (in each pulse) ove time before the leakage current. 109

Figure 4.32: Plot of average current (in each pulse) over time. 110

Figure 4.33: Sequential calculated temperature with successive pulses. 112

Figure 4.34: Plot of temperature vs. power shows that the temperature increases as the power increases. 113

Figure 4.35: Plot of rate of change in temperature vs. cumulative pulsing time for resistor **Att_C8**. 115

Figure 4.36: Average power dissipation vs. calculated average temperature for both resistors **Att_C8** and **Att_C6**. 118

Figure 4.37: Average resistance vs. average current density over pulsing intervals for both resistors **Att_C8** and **Att_C6**. 119

Figure 4.38: Input voltage and corresponding resistance and current waveform for resistor **Free_A10**. 122

Figure 4.39: Change in the average current over time. 123

Figure 4.40: Average current per pulse over cumulative pulsing time for resistor **Free_A10**. 124

Figure 4.41: Calculated average temperature per pulse over cumulative pulsing time for resistor **Free_A10**. 125

Figure 4.42: Heating and cooling follow the same principle 127

Figure 4.43: The peak temperature in the resistor reached from a given power pulse can be less than the steady-state temperature at the same power applied DC. 127

Figure 4.44: Current waveform over time shows that the sawtooth effect is less pronounced when t < 20s but is more marked when t > 55s. 129

Figure 4.45: Sequential current behavior with successive pulses. 130

Figure 4.46: Plot of average resistance (in each pulse) over time. 132

Figure 4.47: Plot of average current (in each pulse) over time. 132

Figure 4.48: Sequential calculated temperature with successive pulses. 134

Figure 4.49: Plot of temperature vs. power shows that the temperature increases as the power increases and at high temperatures regime, the radiation mechanism is dominant and consistent with T^4. 136

Figure 4.50: The natural log of the measured power versus the natural log of the inferred temperature. The slope of the curve fit is 3.21. 140

Figure 4.51: Plot of $ln(P)$ vs. $ln(T)$. A: Redrawn plot with new predicted temperatures. B: Plot with initial calculated temperatures. 141

Figure 4.52: Sequential current behavior with successive pulses. 142

Figure 4.53 : Details of the current waveforms for time, t at 77s, 78s and 79s which focuses on the scenario at high currents. 143

Figure 4.54: Energy balance of the resistor. 145

Figure 4.55: Ratio of ionized boron to boron concentration 180 K< T < 2400K (-93 < T< 2000°C). 150

Figure 4.56: Plot of rate of change in temperature vs. cumulative pulsing time. 151

Figure 4.57: Plot of rate of change in temperature in the first 50s of pulsing time. 152

Figure 4.58: Plot of rate of change in temperature from 50s of the pulsing time until the resistor failed open. 153

Figure 4.59: Power and current density over pulsing intervals. 155

Figure 4.60: Power dissipation vs. theoretical temperature. 155

Figure 4.61: Resistance vs. current density over pulsing intervals. 156

Figure 4.62: Waveforms of input voltage, resistance and current when the resistor failed. 157

Figure 4.63: Before (left) and after (right) picture of resistor **Free_A10** at 120V power pulse. 158

Figure 4.64: Damaged contact pads after voltage cycles. 158

Figure 4.65: Sequential current behavior with successive pulses for freestanding resistors, (A): resistor **Free_A10** with 120V voltage pulse, (B): resistor **Free_B11** with 80V voltage pulse. 161

Figure 4.66: Sequential current behavior with successive pulses for attached resistors, (A): resistor **Att_C8** with 80V voltage pulse, (B): resistor **Att_C6** with 100V voltage pulse. 162

Figure C.1: Current waveforms over pulsing intervals. 172

Figure C.2: Resistance waveforms over pulsing intervals. 172

Figure C.3: SEM image of resistor **Free_B11** failed during pulse test. 173

LIST OF TABLES

Table 1.1: Structural and electrical characteristics 6

Table 1.2: Thermal, mechanical and optical properties 9

Table 2.1: Summary of the relationship between temperature and heat flux
for the three modes of heat transfer. 20

Table 2.2: Analogy between thermal and electrical parameters 22

Table 3.1: Diamond seeding process parameters. 63

Table 4.1: Summary of measurements and calculations on all samples. 85

Table 4.2: Parameters upper limit for attached resistors observed before
leakage current. 117

Table D.1: Tabulated table of calculated temperatures from Arrhenius relationship
and predicted temperatures that correlate to ideal Stefan-Boltzmann relationship. 174

NOMENCLATURE

Symbol	Description
PDF	Polycrystalline Diamond Film
CVD	Chemical Vapor Deposition
κ	Thermal conductivity (W/mK)
c_p	Specific heat (J/gK)
α	Thermal diffusivity (m^2/s)
ε	Emissivity
k , σ_s	Stefan Boltzmann constant 5.67×10^{-8} W/m^2K^4 8.62×10^{-5} eV
σ	Electric conductivity (Ω^{-1})
ρ	Resistivity (Ω·cm)
μ_p	Hole mobility (m^2/Vs)
μ_n	Electron mobility (m^2/Vs)
ξ	Electric field (V/m)
J	Current (A)
β	Spin degeneracy
m_h^*	Density of states effective hole mass (kg)
n	Electron concentration (cm^{-3})
p	Hole concentration (cm^{-3})
N_A	Acceptor concentration (cm^{-3})
N_D	Donor concentration (cm^{-3})
N_v	Valence band effective density of states
h	Planck constant 4.13×10^{-15} eV 6.63×10^{-34} Js
R	Resistance (Ω)
T_∞	Ambient Temperature (K or ^oC)
sccm	Standard cubic centimeters per minute, a unit of gas flow
Δ	Spin-orbit splitting energy (eV)
E_A	Activation energy (eV)

CHAPTER I

INTRODUCTION

1.1 Motivation

Diamond is touted as a superior semiconductor due to its many unique properties. The French chemist Antoine L. Lavoisier determined the carbon composition of diamond by studying the product of diamond combustion. Its cubic structure was determined by the father and son team of Sir William Henry Bragg and Sir William Lawrence Bragg through x-ray diffraction.

In recent years the knowledge of growing diamond, the defects inherent in the process and the methods of controlling it have grown immensely. This resulted in the availability of chemical vapor deposition (CVD) diamond of increasingly improved quality. Research efforts were now directed at improving specific properties of diamond to increase its viability for different uses. These efforts often attempt to fabricate CVD diamond with qualities that approach those of type IIa diamond, which is the highest quality natural diamond.

The physical properties of diamond such as high thermal conductivity, small thermal coefficient of expansion and hardness, present intriguing possibilities for the fabrication of microstructures which benefit from extended dynamic range, faster response, or reduced wear. The best known property of diamond, its extreme hardness, was the first to be successfully applied. Diamond is now commonly used as a coating to

protect equipment that may otherwise be quickly worn down. Another property that has been utilized is diamond's thermal conductivity (24W/cmK), which is the highest of any solid at room temperature. This allows it to dissipate heat efficiently. Hence it is suitable as a heat spreader (heat sink). Diamond is also excellent for temperature cycling due to its extremely small thermal coefficient of expansion ($1.1 \times 10^{-6}K^{-1}$). Diamond's optical properties have also been successfully exploited. Diamond is optically transparent from the infrared to the ultraviolet region and has been used successfully as optical windows. A property of diamond that has the greatest potential is its ability to act as a semiconductor when doped. Diamond-based electronics could potentially offer everything that silicon currently offers as well as excellent heat conduction. Diamond also has an effectively negative electron affinity value, which means that electrons are readily emitted from diamond if it is biased negatively in a vacuum. This means that diamond may be an effective field emitter and may have potential uses in display devices (1).

1.2 Objectives of the work

Increasing needs for higher power density power electronics places greater demands on improving the understanding of interactions between thermal and electrical properties of semiconductor devices. Power systems now have greater density and reduced sizes. As a result, electrothermal models are more important than ever before. The objective of this study was to produce a series of electrically viable attached and freestanding doped diamond resistors and to characterize the resistors at the level necessary for blackbody radiation to occur and for the device to fail. The diamond

resistors were fabricated in a process similar to conventional thin film resistors. The freestanding diamond resistors were doped with boron to be sufficiently conductive to have controlled Joule heating under applied power. The electrothermal dynamics of the diamond resistors were also characterized by applying pulsed voltages to understand and characterize their response. The characterization compares the response of the attached diamond resistors to freestanding diamond resistors. Transient electrothermal behavior of diamond is an interesting area to examine, since dynamic thermal and electrical variables may have strong and nonlinear dynamic interactions in the operating condition of interest.

1.3 Thesis Structure

At the beginning, Chapter I provides an overview of diamond’s unique properties and the motivation for the development of diamond resistors. Finally, the objective of the research is mentioned. Chapter II outlines the heat transfer mechanisms and the analogy between thermal and electrical systems. The information is useful in understanding the complexity of thermal characteristics. We will also discuss in great detail the effects of Joule heating and the boron ionization in p-doped diamond with respect to temperature. A brief review of the heating and cooling principles is given, before introducing the approach adopted herein. The chapter concludes with a brief review of electromagnetic spectrum and blackbody radiation.

Chapter III describes the details of fabrication process and experimentation involved in this work. Next, in Chapter IV presents the electrical and thermal

characterization of the resistors. Finally, in Chapter V, the conclusion and future perspectives are presented.

1.4 Diamond Material Properties

Before describing the layout and processing steps that will be used to produce the structures for this work, the properties of diamond will be briefly reviewed. Diamond is a more expensive material compared to silicon. Its use is justified, however for applications where its properties confer upon it an advantage that is greater than the cost penalty incurred. Special attention is then given to such features and characteristics.

1.4.1 Structural and Electrical Characteristics

Diamond and other Group IV compounds possess the zincblende (or sphalerite) crystallographic structure which is made up of two face-centered cubic (fcc) sublattices displaced by a vector (¼, ¼, ¼), with a primitive basis of two carbon atoms, as illustrated in **Figure 1.1**. This is similar to shifting a second fcc lattice by one-fourth along the diagonal of the first, creating the diamond structure. The lattice constant a = 0.356 nm, where a is the edge of the conventional cubic cell (2).

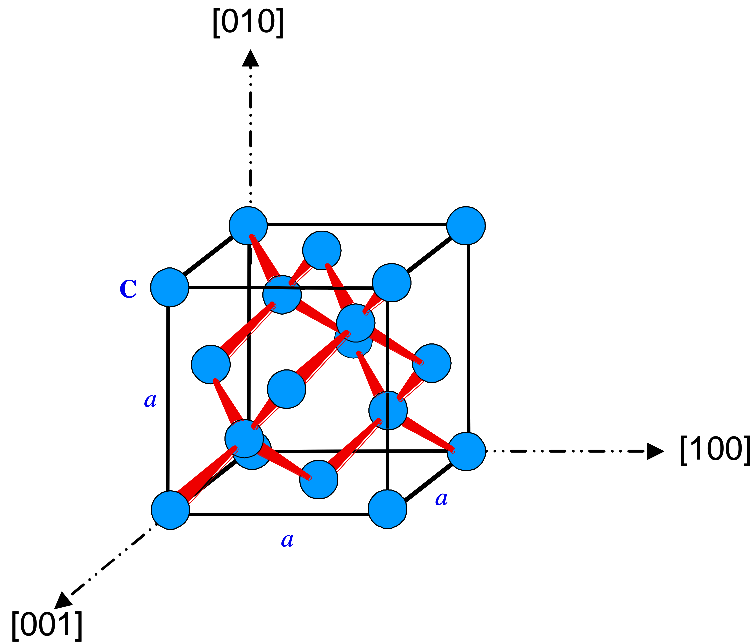

Figure 1.1: Conventional unit cube for diamond (zinc blende crystal structure).

In 1797 it was discovered that diamond was an allotrope form of carbon. Since that day work has been done on ways to synthesize diamond. **Table 1.1** shows some properties of single crystal diamond, compared with the conventional semiconductor Si, which is commonly used for microelectronic applications. Looking at this table, it becomes apparent that diamond is superior not only to silicon but all other semiconductor materials in all the fields. However, several factors are responsible for diamond's under utilization in industry. Natural diamond is scarce, expensive and impossible to obtain in any standard shape or quality. The qualities listed in the table are for a perfect crystal of diamond, however all natural diamonds have defects to a certain degree. These may be intrinsic (dislocations, vacancies etc) or extrinsic (boron, hydrogen etc impurities) and

affects the electronic, mechanical, thermal and optical properties. N-type natural diamond has yet to be achieved and this handicaps the use of diamonds in electronics.

Table 1.1: Structural and electrical characteristics (3).

Properties	Diamond	Silicon
Crystal structure (space group)	diamond	diamond
Lattice constant a (Å)	3.5668	5.4311
Crystal density ρ (g/cm^3)	3.5	2.3290
Bandgap energy *Eg* (eV)	5.45	1.12
Carrier mobility (cm2/V.s)		
Electron	2200	1500
Hole	1600	600
Thermal expansion (x 10^{-6} K^{-1})	1.1	2.6
Breakdown voltage (x 10^5 V cm^{-1})	100	3
Dielectric constant	5.5	11.8
Resistivity (Ω cm)	10^{13}	10^3
Thermal conductivity (W cm^{-1} K^{-1})	20	1.5
Refractive index	2.42	3.5
Hardness (GPa)	98	9.8

1.4.2 Classification of Diamond

The currently used classification system of diamond is based on differences in optical absorption caused by a few occurring elements and/or defects in diamond. The most important element in this respect is nitrogen. Of all natural diamonds, about 98% contains enough nitrogen to be detectable by optical absorption. Also boron and hydrogen-related defects play a role in the categorization of natural, high pressure-high temperature (HPHT) as well as chemical vapor deposited (CVD) diamonds.

The presence of impurities gives rise to very typical features in the absorption spectra, making it possible to distinguish between the different sorts. More specifically,

the absorption in the infrared region of the spectrum is very sensitive to intrinsic and extrinsic impurities. By disturbing the perfect crystal structure, the lattice symmetry is broken. This causes certain phonon modes of diamond, which normally does not exist because of symmetry reasons, to be active in the IR region.

The first important subdivision is based on the amount of nitrogen present in the diamond. Roughly one can say that type I diamond contains a lot of nitrogen and type II diamonds don't. Within these two types, further subdivisions are possible, which will now be summarized briefly (4); (5); (6); (7).

Type I crystals are further divided into sub-types depending on the way the N-atoms are incorporated in the diamond lattice.

- *Type Ia*: to be graded as a pure Ia diamond, the amount of single substitutional nitrogen atoms should be lower than 10^{16} cm^{-3} (7). These crystals are most common in nature.
- *Type Ib*: covers all diamond with atomically dispersed nitrogen, showing the paramagnetic signal for substitutional nitrogen. Synthetic HPHT diamonds usually are of this type, and are commonly used as substrates for doping experiments. The substitutional nitrogen forms a deep donor (E_i= 2.2 eV) (6), making it suitable for electronic applications.
- *Type Ic*: this category is almost never used. Unlike the previous two, this labeling is not based on the presence of nitrogen, but covers all diamonds with high concentrations of dislocations.

Type II diamonds don't show any nitrogen-related optical absorption features nor paramagnetic signals.

- *Type IIa*: the purest form of diamond. It shows no forbidden one-phonon absorption due to boron or hydrogen impurities, only allowed intrinsic two- and three-phonon process are present. Therefore IIa is optically the most transparent of all diamonds. Being colorless and very rare, this type is very much appreciated as a gemstone used in jewellery.
- *Type IIb*: natural p-type semiconducting diamond are grouped in this class. Boron is the shallow acceptor (E_i=0.37eV) (8) responsible for the p-type conductivity. In nature, these diamonds, which are very rarely found, have a maximum boron concentration of 10^{17} cm^{-3}. On the other hand, the manmade equivalents by HPHT as well as CVD techniques can contain as much as $10^{20}cm^{-3}$ boron atoms.
- *Type IIc*: equal to Ic, this name is not commonly used. It includes type II diamonds with a specific hydrogen-related absorption.

When classifying diamonds using these categories, care has to be taken. As many crystals are inhomogeneous, a mix of different types may be present in the same diamond sample.

1.4.3 Thermal Characteristics

In the standard theory, the carriers of heat are phonons which are quantized lattice vibrations. The Debye temperature, θ_D is a useful parameter in solid-state problems because of its inherent relationship to lattice vibration. The parameter θ_D can be used in characterizing the excitation of phonons and to describe various thermal phenomena, such as specific heat and lattice thermal conductivity. The heat capacity or specific heat

of the solid is one of the most essential thermal parameters. The heat capacity c_p for diamond is 0.52J/(g.K), while for silicon it is 0.71J/(g.K). **Table 1.2** summarizes the thermal and mechanical properties of diamond compared to GaAs and Si.

Table 1.2: Thermal, mechanical and optical properties (9), (10).

Properties	Diamond	GaAs	Silicon
Melting point T_m (^oC)	4000	1238	1413
Specific heat C_p (J/g.K)	0.52	0.35	0.71
Thermal resistivity (K.cm/W)	0.05	0.64	2.27
Thermal expansion coefficient α_{11} (10^{-6}/K)	1.1	6.4	2.6
Thermal conductivity, κ (W/cmK)	24	0.55	1.5
Young's modulus for <100> (GPa)	910	85	190
Hardness Hv (100) (GPa)	100	7	10
Debye temperature $\theta_{D\,(K)}$	1860	370	463

1.4.4 Thermal Transport

The diamond property that has been most widely utilized in advanced electronics and optoelectronics systems is its extremely high thermal conductivity. This applicability of diamond as a thermal management material has been growing due to the increasing availability of diamond in the form of high quality thin films.

Polycrystalline diamond films are fabricated through several processes like CVD, microwave or laser-assisted deposition that yields polycrystalline films with different microstructure and thickness. Thermal properties are often determined by the size of the crystallites which in turn, are dependent on the deposition rate, the film thickness and the process gas mixture.

Transport properties of diamond are determined by intrinsic defects, and extrinsic contaminants or dopants, most prominently nitrogen and boron, as well as different structural morphologies (e.g. polycrystalline). Boron is an effective acceptor with a ground state level 0.37eV above the valence band edge and therefore causes p-type conductivity (8). In natural diamond, boron doped crystals (named IIb) are very rare and contain less than 1 ppm boron. Synthetic HPHT can contain up to 1000 ppm of boron. CVD diamond has been doped in the regime of 10^{16} cm^{-3} to 10^{21} cm^{-3} by adding gaseous compounds of boron to the plasma.

1.5 Microwave (MW) Plasma Enhanced (PE) CVD

Figure 1.2 shows a schematic representation of a microwave deposition system as used by Vanderbilt Diamond Technology to deposit the diamond films. The generated microwave of 5000W is coupled into the deposition chamber from above via a rectangular and circular waveguide through a dielectric window. The pressure used in this system is about 120Torr. Substrate temperature is between $800^{o}C$ – $850^{o}C$. The choice of a good gas mixture is important, but the substrate temperature and pressure in the growth chamber play an equally important role in the deposition process. Through collisions with the gas atoms and molecules, energy is transferred. This process dissociates molecules into reactive species, suitable as precursors for diamond growth. This type of glow discharge is very stable, provides up to 25% hydrogen atoms, and is perfectly suited for long runs.

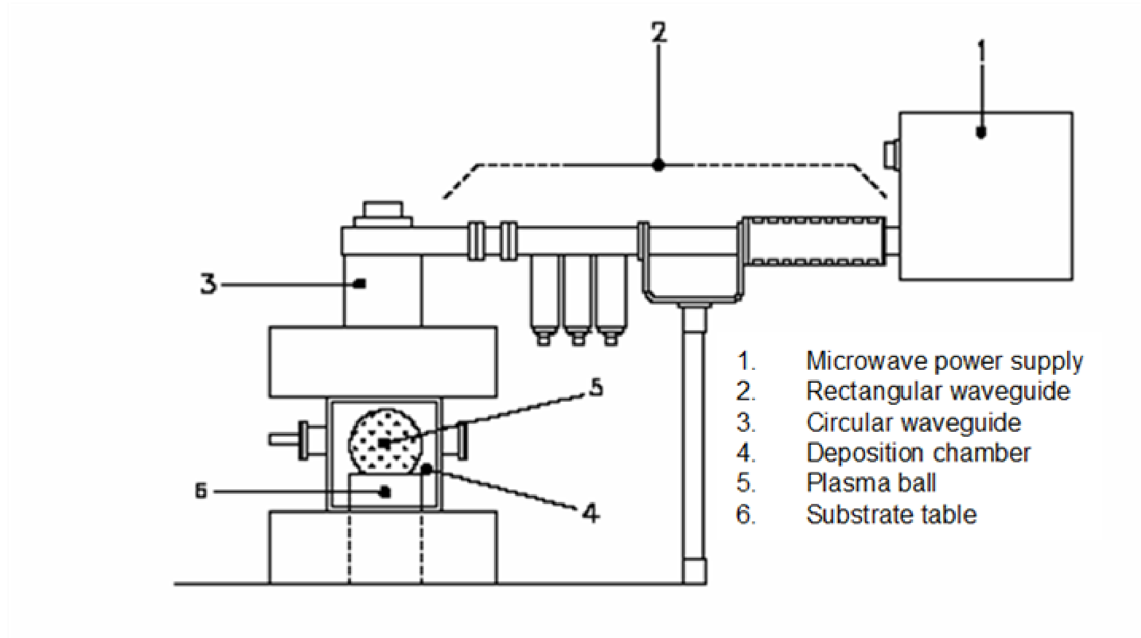

Figure 1.2: Schematic representation of a MWCVD reactor.

1.6 Substrate

The substrate plays an essential role in the final quality and properties of diamond film. The chosen material must have a melting point at the process pressure higher than the temperature required for diamond growth. Other parameters are the thermal expansion coefficient and the chemical/metallurgical stability. A small thermal coefficient assures a good adhesion between substrate and diamond coating that is relatively unaffected by temperature changes. Chemical stability is required to avoid any reaction between the substrate and the carbon or other gas-phase components during diamond growth.

Silicon is a material that is readily available at a low price and it possesses some necessary properties: a thermal expansion coefficient comparable to that of diamond and

the ability to form an oxide layer, which will be the sacrificial layer in the fabrication process (silicon micromachining).

Silicon micromachining can be broadly categorized into bulk micromachining and surface micromachining (**Figure 1.3**). The former involves etching structures into the substrate (removal of material), and the latter involves the deposition and subsequent etching of thin films of sacrificial and structural materials (additive processes). Although the details of the processing are beyond the scope of this work, the author will highlight and briefly discuss some of the popular methods that are relevant to this work

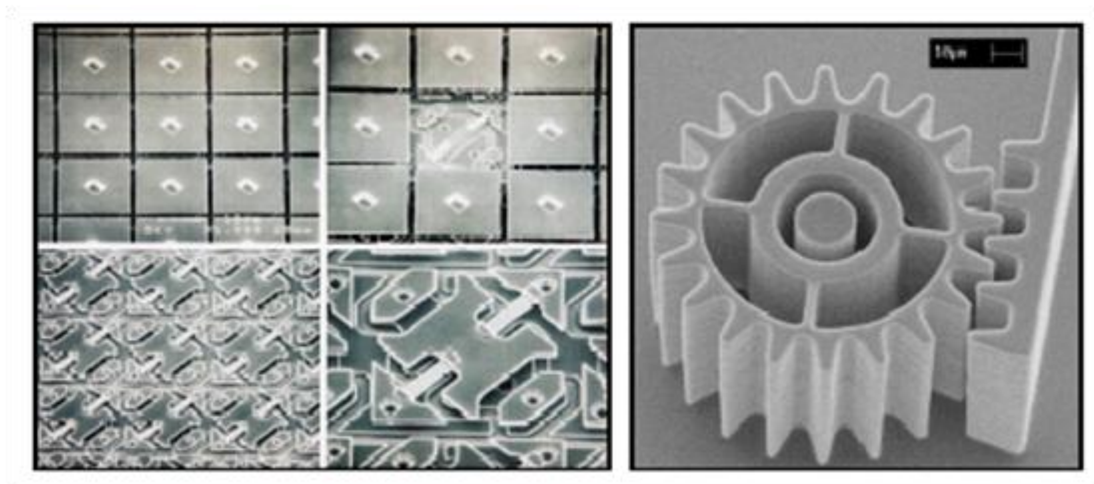

Figure 1.3: Surface micromachining (left) of Texas Instruments Digital Micromirror Device and bulk micromachining (right) of silicon gear.

1.6.1 Bulk Micromachining Process Technology

Several methods have been used for the removal of the material from the bulk of the wafer. Wet or dry etchants are selected based on selectivity to etch masks, availability of etch stop methods, etch rate, cost, etch geometry, and many other criteria. The most

common anisotropic wet etchant is KOH, which etches preferentially along the <100> surface of the wafer, leaving the <111> surfaces exposed. When high aspect ratios are desired, dry etching methods are used, such as DRIE (deep reactive ion etching). High aspect ratios can also be obtained with thick photoresists such as SU8 and molding/electroplating processes.

1.6.2 Surface Micromachining Process Technology

Surface micromachining consists of the deposition, patterning, etching and release of thin films of material (11). Techniques that fall under this category are sometimes called additive processes since material is added to the surface of the substrate. Unlike bulk micromachining, there is no removal of material from the substrate. In order to obtain functional electromechanical microsystems, both insulating and conductive films are required. Hence, in order to create freestanding microstructures, sacrificial layers are used. These layers are deposited between mechanical layers, and removed near the end of processing. Silicon dioxide (SiO_2) is certainly the most commonly available dielectric in silicon fabrication laboratories and is commonly used as a sacrificial layer. SiO_2 is usually deposited using LPCVD (low pressure chemical vapor deposition) or PECVD as opposed to fabrication through thermal oxidation. However, at the Vanderbilt Diamond Laboratory, SiO_2 is achieved through thermal oxidation.

1.7 Nucleation Process

In order for continuous film growth to occur, a sufficient density of crystallites must be formed in the early stages of growth. In general, the substrate must undergo a nucleation enhancing pre-treatment to allow this. Substrates may be pre-treated by a variety of methods such as abrasion with small (~µm sized) hard grits (i.e. diamond) or ultrasonication of samples in slurry of hard grit.

The pre-treatment produces scratches, which are favorable sites for nucleation. There is a possibility that small (~nm sized) flakes of diamond, which are a result of the abrasion with diamond grit, become embedded in the substrate. The deposited CVD diamond will then grow on these flakes. Evidence for homogeneous nucleation of diamond in the gas phase has also been presented, however this is not believed to be the dominant process when, for example, manual abrasion is used (12).

It would be desirable to produce nucleation sites without damage to the underlying substrate. This is particularly important for some applications such as diamond electronics and optical components. One method for encouraging nucleation without damaging the substrate material has been developed: bias enhanced nucleation (BEN) (13), (14). This process is however still relatively new.

1.8 Doping

As mentioned before (*Section 1.5*), MWPECVD is a very flexible method allowing the use of different carbon precursors. This fact is also valid for addition of other gasses, unlike HF CVD (hot filament chemical vapor deposition), where adding halogens or oxygen would destroy the filament. This also means that in-situ doping

experiments can easily be performed by just adding a gas compound that contains the atom targeted to be included in the diamond lattice. It is evident that the growth chemistry is influenced by the addition of other gases. A boron source is usually introduced into the gas-phase for doping of the diamond lattice during its growth, in order to make conductive diamond. Boron acts as an effective acceptor and fits well into the diamond lattice (15).

CHAPTER II

BACKGROUND

2.1 Heat Transfer: Basic Concepts in Thermal Modeling

Heat transfer occurs when energy is transferred between an object and its environment due to a temperature difference between them. The three basic mechanisms for heat transfer are through conduction, convection, and radiation. They are usually described individually for simplicity but a system will usually have heat transfer through all three processes simultaneously. In almost all problems, the energy transfer rate, q, will vary with time. This initial period is known as the *transient* period. Eventually, the energy transfers at a constant rate known as *steady state* rate or equilibrium rate.

2.1.1 Conduction

Conduction is the heat transfer mechanism through a medium in direct contact with surfaces of different temperatures. The first requirement for conduction is that the medium is static. Thus the medium must be a rigid solid or a fluid with no circulating currents. The law that governs this heat flow is Fourier's law of heat conduction, Eqn. (2.1), which states that the heat flux is proportional to the negative of the local temperature gradient. Where q is the heat flux, or heat flow per unit area perpendicular to the flow direction (W/m^2), T is the local temperature (K or ^{o}C), x is the coordinate in the

flow direction (m) and κ is the thermal conductivity (W/m·K) of the material. The *negative sign* indicates that heat is transferred in the direction of decreasing temperature.

$$q = -\kappa \frac{dT}{dx} \tag{2.1}$$

<u>*Specific Heat Capacity*</u>

Specific heat capacity (c_p), also sometimes known simply as specific heat, is defined as the amount of thermal energy required to raise the temperature of a unit mass of a material by a unit measure of temperature at a constant pressure. For example, the specific heat of a substance could be measured in J/gK, or the number of joules of thermal energy required to raise the temperature of one gram of the material one Kelvin. As noted in **Chapter I**, the specific heat for diamond is 0.52 J/gK.

<u>*Thermal Diffusivity*</u>

The thermal diffusivity of a material (α) is defined as the ratio of thermal conductivity to volumetric heat capacity. It has the units of m^2/s. High thermal diffusivity materials heat and cool very quickly, and therefore take less time to reach thermal equilibrium with their surroundings. The opposite would be true if thermal diffusivity is lower. A high value of thermal diffusivity can arise either due to a high thermal conductivity or due to a small heat capacity value of the material. Thermal diffusivity can be expressed as (16):

$$\alpha = \frac{\kappa}{\rho c_p} \quad (2.2)$$

where ρ is the density of the material. Transient heat transfer problems occur when the temperature distribution changes with time. The fundamental quantity that enters into heat transfer situations not at steady state is the thermal diffusivity. It is related to the steady state thermal conductivity through the Eqn. (2.2).

2.1.2 Convection

A fluid (e.g., water, air), by virtue of its temperature, can transport energy. Convection is the transport of energy by bulk motion of a medium from a surface to a moving fluid. There are essentially two types of convection: forced and natural convection.

$$q_c = h_c(T_s - T_c) \quad (2.3)$$

Where q_c is the heat flux by convection in Eqn. (2.3), T_s is the surface temperature, T_c is the fluid temperature and h_c is the convective heat transfer coefficient, this value varies for forced and natural convection.

2.1.3 Radiation

Radiation is the mechanism of heat transfer where energy is emitted due to an object's temperature. Therefore any object at a temperature above absolute zero will

radiate energy. This energy is called radiant energy and is measured in joules. This term is used to describe the entire amount of energy radiated from a source in a given time interval. The energy is transported by electromagnetic waves (or photons). Radiation requires no medium for propagation. Radiant heat transfer is the name given to heat transfer by way of thermal radiation. Radiant exchange between surfaces is maximized when no material occupies the intervening space. A perfectly emitting or absorbing body is called a *blackbody*. The rate at which it emits radiant energy is given by the Stephen-Boltzmann law of thermal radiation (17)

$$E = \frac{q}{A} = \varepsilon \sigma_s T_b^4 \tag{2.4}$$

where emissivity, ε is a property of the surface characterizing how effectively the surface radiates compared to a blackbody ($0 \leq \varepsilon \leq 1$). $E = q/A$ (W/m^2) is the surface emissive power. σ_s is the Stefan-Boltzmann constant ($\sigma_s = 5.67 \times 10^{-8}$ $W/(m^2K^4)$). T_b is the absolute temperature of the surface (in Kelvin). The relations discussed in this section are summarized in **Table 2.1** (18).

Table 2.1: Summary of the relationship between temperature and heat flux for the three modes of heat transfer.

Heat Transfer Mode	Model, or "Law"	Coefficient Defined by Model	Range of Temperature Exponent
Conduction	Fourier's law $q = -\kappa \nabla T$	Thermal conductivity κ	1.0 – 1.1
Convection	Newton's law of cooling $q = h_c \Delta T$	Heat transfer coefficient h_c	1.0 – 2.0
Radiation	The Stefan-Boltzman law $q = \varepsilon \sigma_s T^4$	Emissivity ε	4.0 – 5.0

Since heat transfer is in essence a transfer of kinetic energy between particles, it cannot be instantaneously conveyed from one part of an object to another. Rather, it diffuses over time throughout objects, and to the surrounding environment.

Heat is actually a form of motion, although not on the macroscopic scale. It is a result of kinetic energy due to the motion of molecules and within those molecules, through vibrational and rotational motions. This kinetic energy is in a constant state of transfer, dispersing itself throughout the object from areas of high energy to low energy, and to the surroundings. The rate of this transfer of energy is proportional to the magnitude of the difference in temperature that exists, as can be seen in the basic definition of a temperature gradient (19)

$$\frac{\partial T}{\partial z} = \frac{(T_2 - T_1)}{(z_2 - z_1)} \tag{2.5}$$

where T_1 and T_2 are temperatures at two points in space, z_1 and z_2 are locations of the respective points, and $\frac{\partial T}{\partial z}$ is the gradient driving heat transfer between those points. Naturally, if the temperature throughout an object or between an object and its surroundings is uniform, there will be no heat transfer as there will be no gradient to facilitate the transfer of thermal energy.

In this research, we are interested in heat conduction and radiation. These are the dominant effects at the range of operation of the powered diamond resistors.

2.2 Electrical Equivalent of Thermal Parameters

For electrical engineers it is commonly easier to evaluate systems in terms of electrical parameters. Fortunately, the behavior of thermal and electrical systems is mathematically described by the same equations. Thus, temperature and heat flux are fundamental variables, equivalent to voltage and current in an electrical circuit, while heat capacity and thermal resistance describes the basic properties of a system and correspond respectively, to capacitance and electrical resistance (20) (21).

Therefore, the analogy between thermal and electrical systems, summarized in **Table 2.2**, enables us to describe thermal systems as equivalent electrical circuits, which is convenient because of the many excellent tools available for electrical circuit analysis and the familiarity of solving electrical network problems.

Table 2.2: Analogy between thermal and electrical parameters (22).

Thermal Parameters	Electrical Parameters
Temperature T (K)	Voltage V (V)
Heat flow → Power P (W)	Current I (A)
Heat Q (J=W.s)	Charge Q (C =A.s)
Resistance R (K/W)	Resistance R (Ω=V/A)
Conductance G (W/K)	Conductance G ($S = \Omega^{-1}$)
Capacity C (J/K)	Capacitance C (F = A.s/V)
Thermal resistivity ρ_{th} (K.m/W)	Electrical resistivity ρ_{el} (Ω.m)
Thermal conductivity κ (W/K.m)	Electrical conductivity σ (S/m)
Specific heat c_p (J/kg.K)	Permitivity ε (F/m)

Note that, even though in the true physical sense thermal power and electrical power are equivalent, thermal power is equivalent to an electrical current, but there is no thermal equivalent for electrical power. Moreover, while geometrical dependence is similar for both electrical and thermal resistances and conductances, they differ from capacitances. The thermal capacitance is directly proportional to the volume of the body and thus, for bodies of equal composition and shape (congruent bodies), to the third power of the linear scaling factor. The electrical capacitance of congruent bodies, however, increases in direct proportion to the linear scaling factor. Finally, there is no known thermal equivalent to an electrical inductor (22). The real behavior of a thermal system is obviously non-linear because of the heat capacity and thermal resistance are generally temperature dependent.

2.3 Joule Heating

Joule heating is also known as resistive or ohmic heating. The discovery of Joule heating by James Prescott Joule in 1841 has provided for an efficient way of producing heat through conversion of electrical energy to thermal energy (23). It is a process by which electric current passes through a conductor thereby generating heat. From molecular perspective, Joule heating occurs when electrons collide with atomic ions that make up the bulk of the conductor. These collisions result in the increase of kinetic energy manifesting into heat as byproduct. From the thermodynamical perspective, efficiency of Joule heating can be explained from the first law of thermodynamics which describe the conservation of energy. Essentially, electrical energy is transferred to thermal energy at nearly 99% since no work is done by the system. The benefits of this technology make it suitable for number of applications such as toasters, electric stoves, thermistors and recently in scene projectors.

2.3.1 Electrical Resistance

The following discussion is taken from a section in Stephen Senturia's *Microsystem Design* book to demonstrate the Joule heating effects from electrical resistance. Ohm's law, in continuum form, is written

$$J = \sigma \xi \tag{2.6}$$

where J is the current density, with units Amperes/m^2, ξ is the electric field, and σ is the electric conductivity. In a semiconductor material, the conductivity at low electric field is

$$\sigma = q\mu_n n + q\mu_p p \tag{2.7}$$

where q is the electronic charge (1.6×10^{-19} Coulombs), n and p are the concentrations of free electrons and free holes, respectively, and μ_n and μ_p are electron and hole mobilities, with units of m^2/V-s . In doped semiconductors, only the majority carrier will contribute significantly to the conductivity. Given that $p\mu_p >> n\mu_n$ for p-type semiconductor, the above equation simplifies to:

$$\sigma = q\mu p \tag{2.8}$$

The electric field is the gradient of the electrostatic potential ϕ

$$\xi = -\nabla\phi \tag{2.9}$$

and the electric field inside the resistor has the magnitude of

$$\xi = \frac{V}{L} \tag{2.10}$$

where V is the potential difference applied between the ends of the resistor and L is the resistor length. The current density inside the resistor is then uniform and has magnitude

$$J = \frac{\sigma V}{L} \tag{2.11}$$

The total current I is the integral of J over the cross section of the resistor, yielding

$$I = \frac{\sigma A}{L} V \tag{2.12}$$

where A is the cross section area. This can be expressed in the more usual Ohm's law form as

$$V = \left(\frac{\rho L}{A}\right) I \tag{2.13}$$

where ρ is the resistivity, the reciprocal of the conductivity, σ. We recognize the quantity in parenthesis as the resistance of the resistor, given by

$$R = \frac{\rho L}{A} = \frac{L}{\sigma A} \tag{2.14}$$

This proves the effect of current flow on the resistance. When the current flows through the resistor, it encounters resistance and some electrical energy is transformed into thermal energy (Joule heating). The larger the current, the greater the Joule heating. A large current occurs when the resistance of the resistor is decreased. Eqn. (2.15) shows the Joule heating occurs when the resistor is heated as the current flows through it.

$$P_{joule} = I^2R \tag{2.15}$$

Since the current I is squared, even a small amount of current can produce substantial heating.

2.3.2 Physics of Joule Heating

As mentioned in the previous section, James Prescott Joule discovered that when current travels across a resistive material, heat is generated. Specifically, he found that the rate of heat generation (Q) is proportional to the current (I) squared and directly proportional to resistance (R) as shown in Eqn. (2.16).

$$Q = I^2R \tag{2.16}$$

With the understanding of how heat is generated, we can now look at how energy regulates in the resistor. **Figure 2.1** shows the scheme (energy balance) of a resistor.

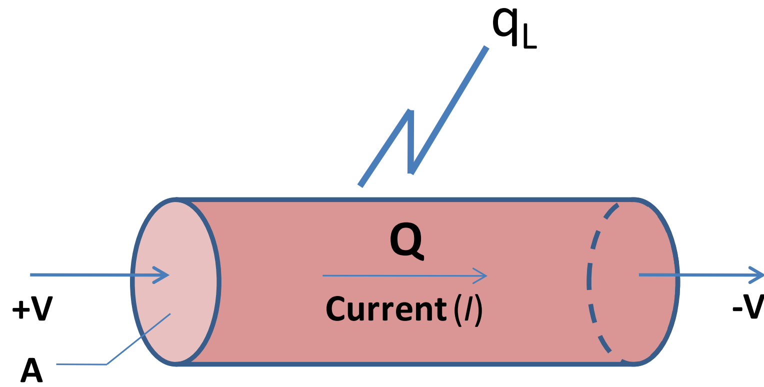

Figure 2.1: Energy balance of the resistor.

As a result, we can control the thermal energy generated (Q) by adjusting the inherent resistance of the material or current going through the resistor due to its relationship to Ohms law (see **Appendix A**). We can predict the rate of heat generated by knowing the *mass* (m), *specific heat* (c_p) of the sample and *power supplied* (I^2R) to resistor, hence Eqn. (2.17):

$$mc_p\frac{\Delta T}{\Delta t} = RI^2 \tag{2.17}$$

Considering the cylinder as the resistor, voltage supplied to the system will result in current flowing through the resistor which generates heat (Q), while heat lost to environment (q_L) can be due to conduction, convection and radiation. In these experiments, the convective term is negligible as the experiments were performed in a vacuum chamber (5.9×10^{-7}Torr). Details of the experiment setup will be discussed in

Chapter III. The conduction term occurs due to contact between the resistor and the oxide layer in the attached resistor scenario and can be described using Fourier's Law (Eqn. (2.1)). The heat loss due to radiation can be modeled using Stefan-Boltzmann Law (Eqn. (2.4)). Incorporating all mechanisms responsible for heat lost to the environment results in Eqn. (2.18) for **attached resistors** and Eqn. (2.19) for the **freestanding resistors**.

$$mc_p \frac{\Delta T}{\Delta t} = Q - [q_{L1(conduction)} + q_{L2(radiation)}] \tag{2.18}$$

$$mc_p \frac{\Delta T}{\Delta t} = Q - q_{L2(radiation)} \tag{2.19}$$

For the attached resistors, combining both heat loss (Eqn. (2.1) and Eqn. (2.4)) with Eqn. (2.18), yields Eqn. (2.20)

$$mc_p \frac{\Delta T}{\Delta t} = Power - \left[\kappa \frac{dT}{dt} + \varepsilon \sigma_s (T_f^4 - T_i^4)\right] \tag{2.20}$$

For the freestanding resistors, Eqn. (2.19) yields to

$$mc_p \frac{\Delta T}{\Delta t} = Power - [\varepsilon \sigma_s (T_f^4 - T_i^4)] \tag{2.21}$$

Once a plateau temperature or steady state is achieved, Eqn. (2.20) and Eqn. (2.21) simplify to Eqn. (2.22) and Eqn. (2.23) respectively.

$$Power = \left[\kappa \frac{dT}{dt} + \varepsilon \sigma_s A (T_f^4 - T_i^4)\right] \tag{2.22}$$

$$Power = \varepsilon \sigma_s A (T_f^4 - T_i^4) \tag{2.23}$$

To accurately identify the Joule heating effect, a sample could be placed under an infrared camera system to measure the temperature without making contact with the resistor. A qualitative image will be produced to show the resistor's temperature distribution. However, no infrared camera is available to use in this work. The resistor's temperature will be estimated from the temperature dependence of resistance of the Arrhenius relationship. This will be discussed in further detail in *Section 4.2*.

In this work, the effect of Joule heating is also responsible for the time dependence of the measured currents when different level of voltage pulses are applied to the resistor. A train of voltage pulses will be applied at the start of the test, ($\sim t$ = 1s) to the resistor circuit. Measurements will be taken at 1s interval (see testing setup in **Chapter III** for further discussion). This will result in an increasing current in the resistor due to Joule heating and thus increases the resistor temperature and reduces its resistance.

2.4 Boron Ionization in P-Doped Diamond

The concentration of free majority carriers is one of the most important quantities that determine the electrical properties of semiconductor devices. Li (24) and Li and Thurber (25) have calculated the percentage of ionized dopant atoms in boron-doped Si and phosphorus-doped Si for doping concentrations up to 3×10^{18}cm^{-3}. Their model is based on a simple single impurity level theory, with the additional assumption that the activation energy of a donor or acceptor level decreases with doping and eventually vanishes as the doping concentration approaches the level of about 3×10^{18}cm^{-3}. This assumption is inferred from the experiments (26) indicating that the concentration of majority carriers does not depend on temperature for doping concentrations about 3×10^{18}cm^{-3}. This result was considered as evidence that at doping concentrations about 3×10^{18}cm^{-3} all the dopant atoms in Si are ionized at room temperature. Thus, the dopant concentration can be substituted for the carrier concentration.

Conversely, this is different with diamond. In diamond, the dopants (boron) are not fully ionized (partially thermally activated) at room temperature and more ionize as the temperature rise (27). In this case, the carrier concentration is proportional to the ionized dopant concentration. An ionized dopant provides a carrier, either an electron in the conduction band or a hole in the valence band. The carrier concentration rises with increasing temperature as dopants are ionized, thereby decreasing the resistivity.

Resistivity as it relates to resistance is described by Eqn. (2.24):

$$R = \rho \frac{L}{A}$$

$$\rho = R \frac{A}{L} \tag{2.24}$$

$$\sigma = \frac{1}{\rho} = q\mu p = q\mu N_a$$

where R is resistance, L is length, A is cross-section area, ρ is resistivity in Ω-cm. Eqn. (2.24) gives the relationship of conductivity, σ, or resistivity, ρ, to the product of charge, q, mobility, μ, and carrier (hole) concentration, p, for a p-type material. Thus, conductivity of a material is determined by two factors: the concentration of free carriers available to conduct current and their mobility. In semiconductor, both mobility and carrier concentration are temperature dependent.

We start the discussion on the temperature dependence of mobility. For conventional semiconductors, there are two basic types of scattering mechanisms that influence the mobility of electrons and holes: lattice scattering and impurity scattering. In the context of metals, lattice vibrations (*lattice scattering*) cause the mobility to decrease with increasing temperature. However, the mobility of the carriers in semiconductor is also influenced by the presence of *charged impurities* (ionized dopants). At lower temperatures, carriers move more slowly, so there is more time for them to interact with ionized dopants. As a result, as the temperature decreases, impurity scattering increases, and the mobility decreases. Impurity scattering is typically only seen at *very* low temperatures when not all dopants are ionized (i.e. Si). In the temperature range of interest, only the influence of lattice scattering will be expected.

However, unlike conventional semiconductors, mobility increases with increasing temperature in diamond, at least to a point. Kiyota and Deguchi determined that point for diamond to be nominally 500K (28) (29). Another report found that mobility increases up to 400K (30). In excess of these temperatures, the mobility of diamond plateaus and eventually decreases with increasing temperature, similar to conventional semiconductors.

As we have mentioned earlier, carrier concentrations are also temperature dependent. In diamond, dopants are not fully ionized at room temperature and more ionize as the temperature rise. Increasing temperatures increases the ionization of the dopants and more thermally generated carriers (holes) are created.

Consequently, the increase in the hole concentration leads to lower resistivity even though there is a reduction in carrier mobility at elevated temperatures. The increase in conductivity from the increased hole concentration overcomes the impact of the reduced mobility that arises from rising temperatures.

2.5 Hole Concentration Calculation

As discussed in the *Section 2.3.1,* the power entering a resistor when it has voltage V and is carrying current I is VI, which using Ohm's law for linear resistor, is equal to I^2R. All positive resistors absorb power, regardless of the direction of current. This is an example of an intrinsically dissipative element. Whenever a resistor carries a current, it is absorbing net power, which must be converted to heat.

For a p-type semiconductor, the current density J due to an externally applied electric field ξ, (from Eqn. (2.6)) is given by

$$J = \sigma\xi = \frac{1}{\rho}\xi = qp\mu\xi \tag{2.25}$$

where σ, ρ, q, p and μ have been defined previously. For a non-degenerate p-type semiconductor (or equivalent for n-type material) containing a density N_D of compensating donor, the density of holes p at a given temperature T can be calculated using:

$$\frac{p(p + N_D)}{(N_A - N_D - p)} = \frac{2}{\beta}\left\{\frac{2\pi m^* kT}{h^2}\right\}^{3/2} exp\left[-\frac{E_A}{kT}\right] \tag{2.26}$$

where N_A and N_D are the acceptor and donor densities, β is the spin degeneracy of acceptors, h is the Planck constant and m^* is the density of states effective hole mass given by:

$$m^* = \left[m_h^{3/2} + m_l^{3/2}\right]^{3/2} \tag{2.27}$$

where m_h and m_l are the heavy and light hole masses, assuming that the split-off-band is not degenerate.

When an impurity level is created by splitting of states from the conduction or valence band with multiple or degenerate extrema, the impurity level spin degeneracy β will be larger than two. For acceptor levels introduces by group III impurities in Si and Ge, β = 4, because the heavy hole and light hole band are generated at k = 0 and the spin-

orbit splitting energy Δ = 44 meV in Si and 295 meV in Ge is much larger than kT, so that in general the split-off band is well separated and thermally occupied only to a negligible degree (31). In diamond however, spin-orbit coupling is weak; Δ = 6meV (31) so that a threefold band degeneracy with β = 6 at temperatures above about 70K can be expected. Below 70K, a twofold band degeneracy with β = 4 is a better approximation (31).

As mentioned before, the dopants in diamond are only partially thermally activated at room temperature. In a p-type semiconductor, normal band-conduction occurs in the valence band through the transport of holes, which result from the ionization of acceptors at an energy E_A above the valence band edge. In the high temperature regime, holes are thermally excited from acceptor states into the valence band. The hole concentration, p in the valence band of a non-degenerate p-type semiconductor is the solution to the equation (26)

$$\frac{p(p+N_D)}{N_A-N_D-p} = N'_V \tag{2.28}$$

with

$$N'_V = \frac{N_v}{\beta} e^{-E_A/kT} \tag{2.29}$$

assuming that both acceptors and compensating donors are present with concentration N_A and N_D, respectively, and with $N_A > N_D$.

$$N_v = 2\left(\frac{2\pi m^* kT}{h^2}\right)^{3/2} \tag{2.30}$$

is the valence band effective density of states. In this work, the donor concentration N_D is presumed to be negligible and the equation can be simplified as

$$\frac{p^2}{N_A - p} = N'_V \tag{2.31}$$

and obtains for the *hole concentration* (a solution to Eqn. (2.31))

$$p = \sqrt{\left(\frac{N'_V}{2}\right)^2 + N'_V(N_A)} - \frac{N'_V}{2} \tag{2.32}$$

2.6 Heating and Cooling Principles

This section will discuss the principle of heating and cooling that occurs during a thermal process. Most thermal systems are generally complex, which made up of sub-systems, each one of which can be analyzed and computed. But when put together presents massive computational problem. For this reason, approximations has to be made

to the mathematical model. The heating and cooling mechanism possess similar effect as a pulse, with heating as the "on" and cooling as the "off" of the pulse. Hence, we can apply the effect of the heating and cooling concept to the heating pulse during the transient period. The following derivation of the heating and cooling principle is reproduced from (32).

Consider a body that is cooled from its surface by convection to environment with a constant ambient temperature T_∞. It also has an internal heat source $Q(t)$ to compensate for this heat loss, and the control objective is to maintain the temperature of the body as a given level by manipulating the heat source. Under lumped approximation, the body can be considered to have a uniform temperature $T(t)$, and the energy balance is given by

$$mc_p \frac{dT}{dt} + h_c A_s (T - T_\infty) = Q(t) \tag{2.33}$$

where m is the mass of the body, c_p is its specific heat, h_c is convective heat transfer coefficient and A_s is the surface area for convection. In the case of *on-off* control which is a common form of thermal control in which the heating or cooling is turned *off* at a predetermined temperature and turned *on* at another, Eqn. (2.33) becomes

$$mc_p \frac{dT}{dt} + h_c A_s (T - T_\infty) = \begin{cases} Q_0 & \text{on} \\ 0 & \text{off} \end{cases} \tag{2.34}$$

where for the moment we take the ambient temperature, T_∞ to be constant. The heat rate is $Q = Q_0$ when the system is *on* and $Q = 0$ when the system is *off*. With the system in its

off mode, as $t \to \infty$, $T \to T_{min} = T_\infty$ and in its *on* mode $T \to T_{max} = T_\infty + Q_0/h_c A$. Note that with the nomenclature T_{min} and T_{max}, we have implicitly assumed that we are dealing with a heater, though the analysis is also applicable to cooling; in this case Q_0 would be negative and T_{min} would be higher than T_{max}.

Taking the non-dimensional temperature to be

$$\theta = \frac{T - T_{min}}{T_{max} - T_{min}} \tag{2.35}$$

and non-dimensional time variable to be

$$\tau = \frac{t}{mc_p/h_c A_s} \tag{2.36}$$

the governing equation is

$$\frac{d\theta}{d\tau} + \theta = \begin{cases} 1 & \text{on} \\ 0 & \text{off} \end{cases} \tag{2.37}$$

The solution is

$$\theta = \begin{cases} 1 + C_1 e^{-\tau} & \text{on} \\ C_2 e^{-\tau} & \text{off} \end{cases} \tag{2.38}$$

We will assume that the heat source comes *on* when temperature falls below a value T_L, and goes *off* when it is above T_U. These lower and upper bounds are non-dimensionally

$$\theta_L = \frac{T_L - T_{min}}{T_{max} - T_{min}} \tag{2.39}$$

$$\theta_U = \frac{T_U - T_{min}}{T_{max} - T_{min}} \tag{2.40}$$

The result of applying this form of control is an oscillatory temperature that looks like in **Figure 2.2**. The heat source in *on* for a time interval τ_{on} during which time the system temperature goes from θ_L to θ_U. The heater source is then switched *off* and the system goes from θ_U back to θ_L in time τ_{off}. These temperature conditions can be applied to the solution Eqn. (2.38).

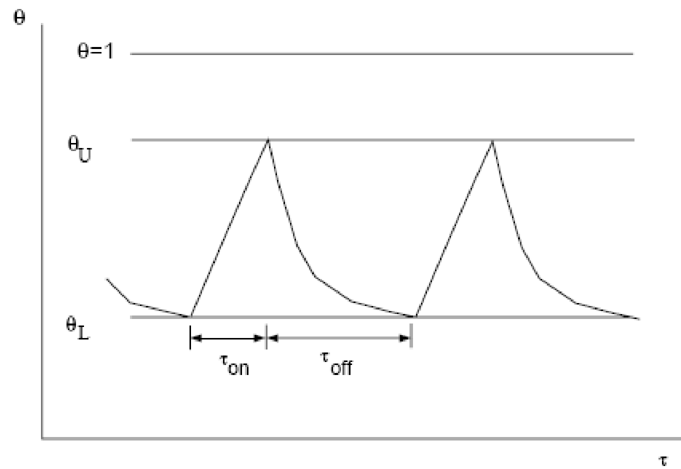

Figure 2.2: Response to on-off control.

As mentioned before, the same concept can be applied to the pulsing mechanism. Voltage pulse will be applied to the diamond resistors to characterize their dynamic thermal behavior. Detail on the test setup will be discussed in **Chapter III**.

A more extensive *mathematical model* temperature distribution of steady state and transient response based on the heating and cooling principles were studied by Minkin *et al*. Minkin *et al.* described a measurement method called “subtraction and extrapolation” in a system that contains a semiconducting thermistor and linear resistor in a circuit (33) to model the transient response in an R_T-R circuit accompanying voltage pulses at its input. The method was utilized to determine basic parameters characterizing a pulsed thermistor-linear resistor temperature measuring circuit and ensuring increased sensitivity to temperature changes while conserving a given accuracy of measurement. The semiconducting material of the thermistor involved in the study was not reported. The

structural circuit diagram modeled in this method is conceptually similar to the test set up for the pulse heating experiment of the diamond resistor studied in this work. A transfer function of the system was introduced to utilize the structural circuit diagram on the basis of linearized differential equations describing the electrothermal processes in the circuit. The theoretical analysis that was carried out in this method describes the test results observed from the diamond pulse test. The change in temperature of the thermistor due to the application of a train of pulses at the input of the circuit was analyzed. The overall character of the variation of the output quantity of the pulses system can be expressed with the aid of a so-called "envelop", the curve joining the maximum or minimum values of the output quantity in the transient process. This transient process will be discussed in detail for freestanding resistor in *Section 4.5.2.*

As the number of pulses increase, i.e. $n \to \infty$, a state of dynamic equilibrium (*steady state*) sets in the pulse system, and the envelopes converge to constant values corresponding to the maximum and minimum values of the steady state (quasistationary) temperature. The equations that describe this phenomenon are as follows;

$$\Delta T_{max,s.s} \approx \Delta T[\infty, \gamma] = \frac{2\Delta V_{cir} V_0}{k(1 - D_0\delta)(R_{T0} + R)} \frac{1 - e^{-\alpha\gamma}}{1 - e^{-\alpha}} \tag{2.41}$$

$$\Delta T_{min,s.s} \approx \Delta T[\infty, 0] = \frac{2\Delta V_{cir} V_0}{k(1 - D_0\delta)(R_{T0} + R)} \frac{e^{\alpha\gamma} - 1}{1 - e^{-\alpha}} \tag{2.42}$$

where:

$t_p = \text{pulse duration}$

$\tau = \text{pulse repetition period}$

$t_{int} = \text{interval between pulses}$

$n = \text{arbitrary pulse repetition period}$

$\varepsilon = \text{relative time} = \dfrac{\Delta t}{\tau}$

$\Delta V_{cir} = \text{circuit voltage supply}$

$\Delta V_0 = \text{initial voltage across thermistor at working point}$

$\gamma = \dfrac{t_p}{\tau} = \text{duty ratio}$

$k = \text{dissipation constant}$

$D = \text{dynamic constant}$

$R_{T0} = \text{initial resistance thermistor at working point}$

$\delta = \dfrac{R_{T0} - R}{R_{T0} + R}; \text{dimensionless parameter}$

$\alpha = \dfrac{\tau}{\tau_\theta}$

$\tau_\theta = \dfrac{\tau_0}{(1 - D_0\delta)}, \tau_\theta = \text{time constant of } R_T \text{ - R circuit, } \tau_0 = \text{thermistor time constant}$

These expressions show an unbalanced signal during pulses and pauses of the input pulses and is illustrated in **Figure 2.3**.

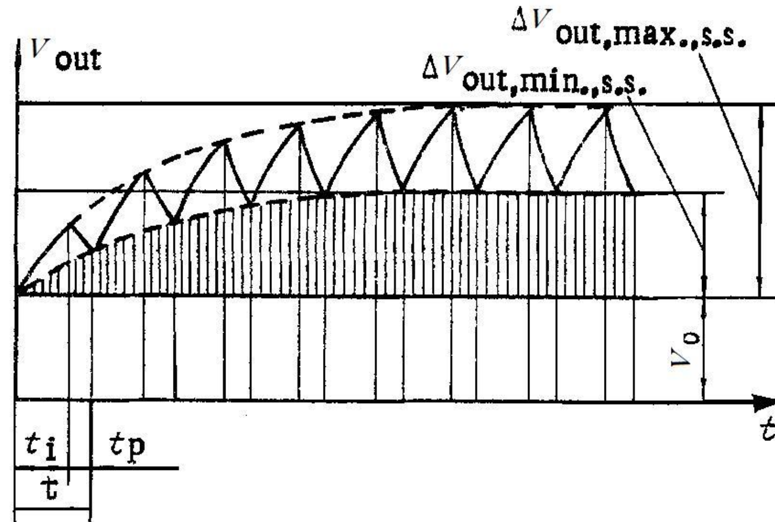

Figure 2.3: Schematic shows maximum and minimum temperature rise of resistor in the state of dynamic equilibrium (steady state) with pulse voltage supply.

According to Minkin, the steady state value of the output quantity is achieved when the number of repetition periods n for which the envelopes differ from the respective steady state values by less than 5%. This condition can be used to determine the end of the transient process, i.e. steady state condition has reached.

Continuing the discussion from the steady state, the theoretical analysis of the *transient* process in an $R_T - R$ circuit accompanying voltage pulses at its input was modeled by Minkin *et al*. The study showed that the temperature rise of the thermistor due to the application of a train of pulses at the input of the circuit can be described by the following equations (33):

during the pulse ($0 \leq \varepsilon \leq \gamma$)

$$T[n,\varepsilon]=\frac{2\Delta V_{cir}V_0}{k(1-D_0\delta)(R_{T0}+R)}\left\{1-\frac{e^{-\alpha\varepsilon}}{1-e^{-\alpha}}[(1-e^{-\alpha(1-\gamma)})-(1-e^{\alpha\gamma})e^{-\alpha(n+1)}]\right\} \quad (2.43)$$

In the intervals between pulses ($\gamma \le \varepsilon \le 1$)

$$\Delta T[n,\varepsilon]=\frac{2\Delta V_{cir}V_0}{k(1-D_0\delta)(R_{T0}+R)}\frac{1-e^{\alpha\gamma}}{1-e^{-\alpha}}[e^{-\alpha(n+1)}-1]e^{-\alpha\varepsilon} \quad (2.44)$$

(The variables in the above equations were defined after Eqn. (2.42) was introduced). The principle of this method was that two consecutive readings of the output signal were taken separated by some time interval within the duration of one supply voltage pulse and the first reading was subtracted from the second one, whereupon the difference was subtracted from the first reading.

The expressions in Eqn. (2.43) and Eqn. (2.44) show that the temperature of the thermistor during a pulse and in the interval between pulses varies in accordance with an *exponential* law. The overall character of the variation of the output quantity of the pulse system can be expressed with the aid of the envelop, the curve encompassing the maximum or minimum values of the output quantity in the transient process. The maximum values of $\Delta T[n,\varepsilon]$ over the given repetition periods are attained at $\varepsilon=\gamma$ and the minimum values, at $\varepsilon=0$. Inserting these values into Eqn. (2.43) and Eqn. (2.44) gives the equations of the *envelop*:

$$\Delta T_{\max} = \Delta T[n,\gamma] = \frac{2\Delta V_{cir} V_0}{k(1 - D_0\delta)(R_{T0} + R)} \left\{ \frac{(1 - e^{-\alpha\gamma})(1 - e^{-\alpha(n+1)})}{1 - e^{-\alpha}} \right\} \quad (2.45)$$

$$\Delta T_{\min} = \Delta T[n,0] = \frac{2\Delta V_{cir} V_0}{k(1 - D_0\delta)(R_{T0} + R)} \left\{ \frac{(e^{\alpha\gamma} - 1)(1 - e^{-\alpha n})e^{-\alpha}}{1 - e^{-\alpha}} \right\} e^{-\alpha} \quad (2.46)$$

These expressions are visualized in **Figure 2.4**. We will observe this phenomenon in the freestanding resistor during the higher voltage characterization in *Section 4.6.2*.

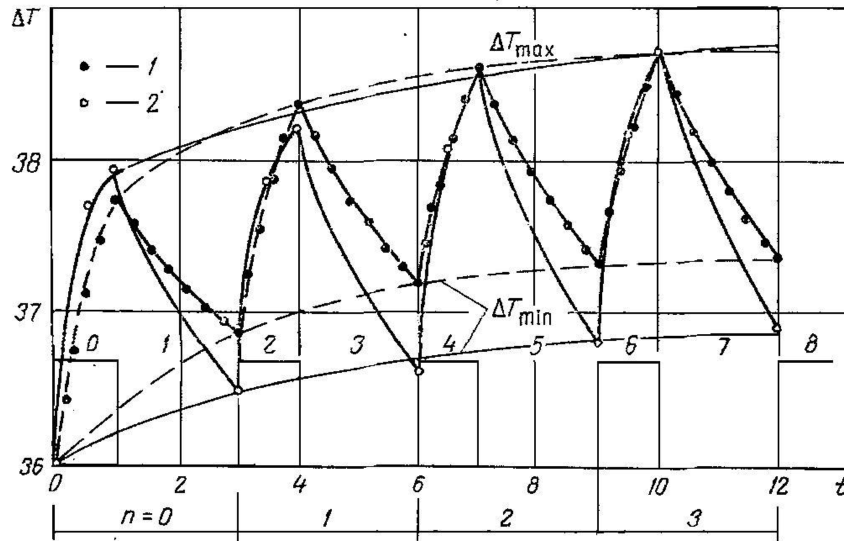

Figure 2.4: Transient process in R_T-R circuit for action on input of pulses of supply voltage. Time t in seconds (33).

2.7 The Electromagnetic Spectrum

It has already been stated that thermal radiation is an electromagnetic phenomenon (*Section 2.1.3*). Electromagnetic waves are capable of carrying energy from

one location to another, even in vacuum (34). Some essential features of the electromagnetic spectrum are illustrated on **Figure 2.5**. Visible light, ultraviolet light, radio waves, and X-rays are all examples of electromagnetic radiation, differing only in wavelength.

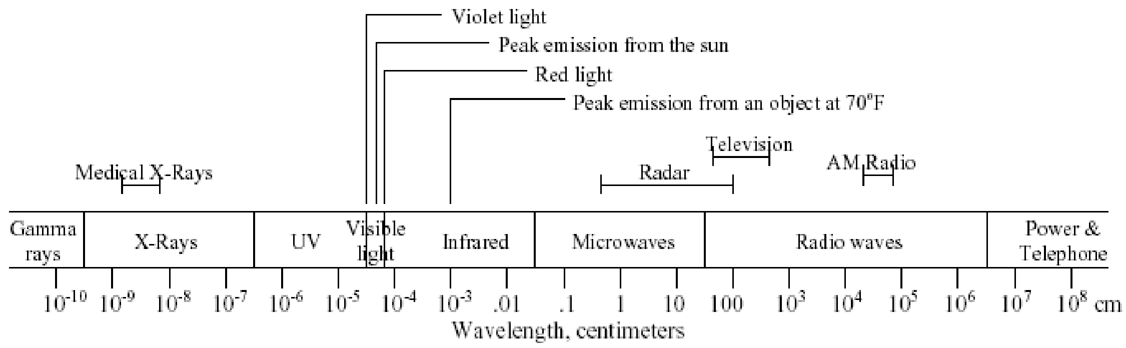

Figure 2.5: The electromagnetic spectrum

The frequency, v (Hz) of an electromagnetic wave is related to its wavelength λ (m) according to (34):

$$v = \frac{c}{\lambda} = \frac{c_0}{n\lambda} \tag{2.47}$$

where c (m/s) is the speed of light in the medium through which the radiation is passing, c_0 (≈ 2.9979×10^8 m/s) is the speed of light in a vacuum, and $n = c_0/c$ (-) is the *index of refraction.* Frequencies in the infrared are in the order of 10^{13} to 10^{14} Hz. There are no methods available for the direct measurement of such high frequencies; instead,

wavelength is measured and converted to frequency by Eqn. (2.47). Wavelength can be measured interferometrically to an accuracy of about one part in 10^7 (35). To preserve this increased accuracy we can use the *wavenumber* (υ), the number of waves per unit distance. If the distance is measured in centimeters, the units are reciprocal centimeters (cm^{-1}).

Infrared (IR) radiation is emitted by every object as a function of their temperature. An object at a higher temperature emits more intense infrared radiation at shorter wavelengths. The infrared radiation of an object at a moderate temperature (above 93°C (366K)) is already intense enough for a human body to detect its presence as heat. If the temperature increases above 650°C or 923K, the infrared radiation is intense enough and the wavelength short enough for it to cross into the visible light spectrum. This occurs at the threshold of red light which is the visible light with the longest wavelength. At this point, the heated object glows “red hot”. As the temperature increases even more, the emitted radiation traverses the visible light spectrum. An object at 2760°C, such as the tungsten filament of a light bulb, radiates infrared radiation whose wavelength is short enough to be visible as white light. Any object that is at a temperature above zero Kelvin will emit infrared light. Objects or regions at different temperatures will emit radiation at different wavelengths.

2.7.1 Basic Concept: The Blackbody

Solids and liquids radiate visible light at temperatures above 500°C and above (36). A surface which absorbed all incident radiant energy would appear black. Such surface would also be a complete radiator. Such idealized surfaces are called *blackbodies*.

A practical incandescent radiator will exhibit behavior similar to that of a blackbody (e.g. tungsten incandescent bulb).

The maximum wavelength emitted by a blackbody radiator is infinite. It also emits a definite amount of energy at each wavelength for a particular temperature, so standard blackbody radiation curves can be drawn for each temperature, showing the energy radiated at each wavelength. **Figure 2.6** illustrates the distribution of energy from a blackbody as a function of wavelength (37)

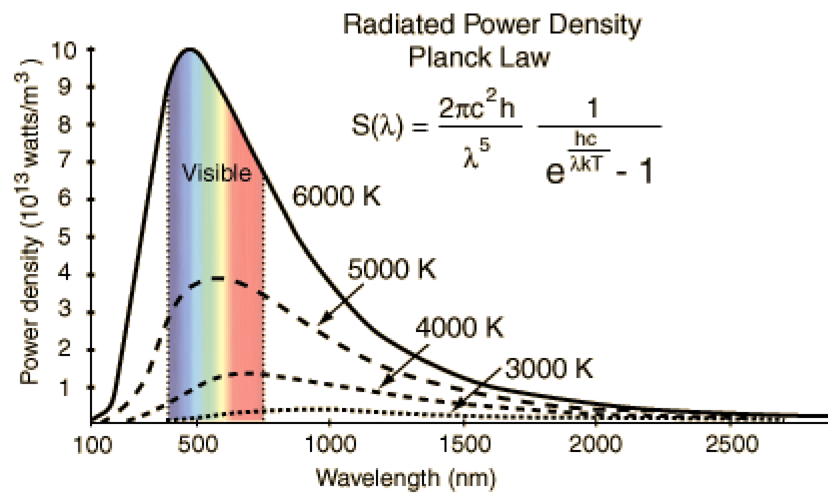

Figure 2.6: Distribution of energy from a blackbody as a function of wavelength.

The blackbody radiation curve shows that the blackbody does radiate energy at every wavelength. The curve gets infinitely close to the x-axis but never touches it. The curve touches at infinite wavelength. It also shows that the blackbody emits at a peak wavelength at which most of the radiant energy emitted. At 5000K the peak wavelength

is about 5×10^{-7} m (500 nm) which is in the visible light region in the yellow-green section. At each temperature the blackbody emits a standard amount of energy. This is represented by the area under the curve (38).

Classical theory can predict the spectrum contains standing electromagnetic waves in equilibrium. The result is

$$\frac{dE}{d\lambda} = \frac{8\pi kT}{\lambda^4} \tag{2.48}$$

(the Rayleigh – Jeans law). The measured spectrum agrees well with the Rayleigh-Jeans law at long wavelength but deviates badly at short wavelengths. This problem was therefore known as the *ultra-violet catastrophe*.

In 1899 Lummer and Pringsheim measured the behavior of $dE/d\lambda$ as a function of T and showed that it has the form shown in **Figure 2.6**. Note particularly that the maximum moves to shorter λ as T increases (the Wien displacement law). These curves explain why, as a body gets hotter and hotter, it first begins to glow dark red and eventually, at a sufficiently high temperature, appears more blue than red (“white hot”). The area under the curve is proportional to T^4 in accordance with Stefan’s law.

CHAPTER III

DEVICE FABRICATION AND EXPERIMENTATION

This chapter is divided into two major parts. The first part describes the processing techniques developed for the attached and freestanding diamond resistors. The second part will discuss the experimentation setup to analyze the electro thermal behavior of the diamond resistors.

Part I: Fabrication of Attached and Freestanding Diamond Resistor

3.1 Resistor Layout and Design

The basic design of both attached and freestanding resistors is a similar design used in the Master's thesis work (39). **Figure 3.1** shows the three dimensions of resistors, labeled as ***R1, R2*** and ***R3***. The dimensions are 50µm × 10µm, 100µm × 50µm and 500µm × 100µm respectively. However, in this work, we have focused **only** on resistor ***R3*** with the dimension of ***500µm*** × ***100µm***. Based on the previous work (39), the chances of arcing occurring for small resistors (*R1* and *R2*) is high for voltages at medium to high level due to the small separation between the electrical contacts. The power tolerance of diamond resistors leaves the smaller specimens vulnerable to the effects of localized electrical arcing at increased voltages.

The resistors were designed to have a 'necking' pattern as shown in **Figure 3.2**. This is to enhance and concentrate the current flow through the resistor body. The design

layout consists of clusters of the three resistors (*R1*, *R2* and *R3*). **Figure 3.3** shows the mask layout of the attached resistors on a 2cm × 2cm substrate area. Consequently, the process of fabricating freestanding resistors is exactly the same as the attached resistors but with an additional step to create a cavity underneath the resistor body. **Figure 3.4** shows the additional mask layer of cavity underneath the resistors body.

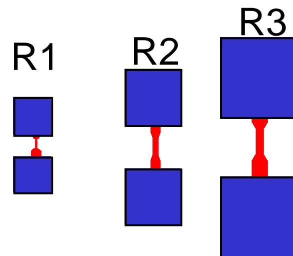

Figure 3.1: Three resistors, R1, R2 and R3 with dimensions of 50µm × 10µm, 100µm × 50µm and 500µm × 100µm respectively.

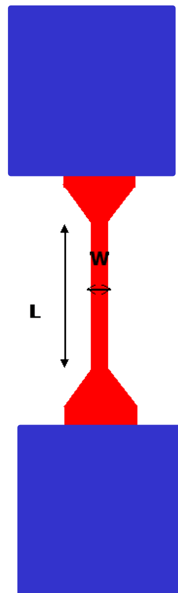

Figure 3.2: Diamond resistor with necking design to concentrate the current flow through the resistor body.

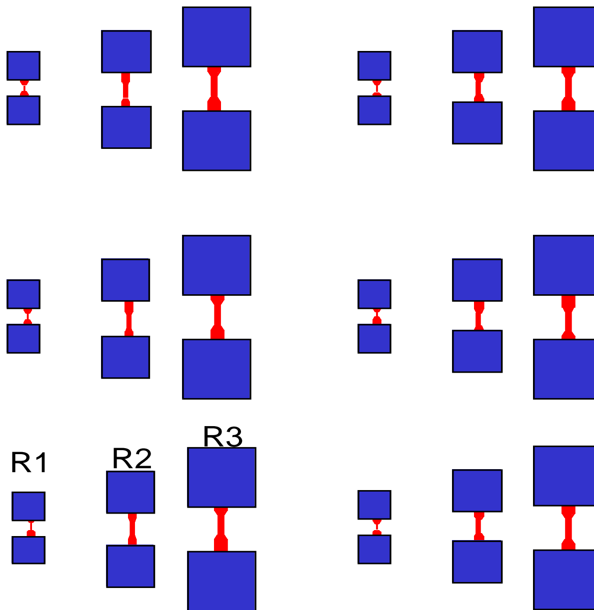

Figure 3.3: Mask layout consists of mask for resistor (red) and contact (blue) on a 2cm × 2cm substrate for attached resistors.

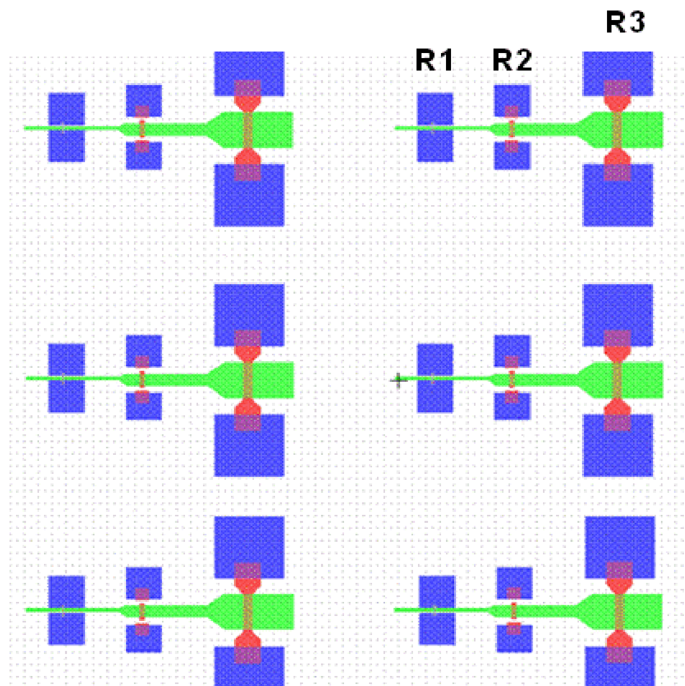

Figure 3.4: Mask layout consists of mask for resistor (red), contact (blue) and cavity (green) on a 2cm × 2cm substrate for freestanding resistors.

3.2 Resistors Fabrication

The fabrication process of the attached and freestanding diamond resistor is illustrated in **Figure 3.5**. The process stops at step #8 for attached resistors. The starting substrates were a SiO_2/Si wafers. The SiO_2/Si substrates used in this study were produced by a standard thermal oxidation method. Si (111) wafer was wet oxidized at 1100°C and the oxidation time was ~10 hours. Polycrystalline diamond films were deposited in an *ASTeX*® MPECVD system with a 5kW generator, operating at 2.45 GHz. The schematic of a typical MPECVD system is shown in **Figure 3.6.** The substrate temperature was set using an induction heater independent of the plasma. The growth system was coupled with a controlled gas handling system, allowing for precise control of the flow of all process gases. A gas mixture of methane (CH_4), hydrogen (H_2), and trimethylboron was employed for boron doped diamond growth. Trimethylboron ($B(CH_3)_3$) (hereafter referred to as TMB) gas was used as a dopant source to obtain p-doped CVD diamond films. The gases at flow rates of 18/478/12 sccm (CH_4/H_2/TMB) were introduced into the CVD system at a pressure of 120Torr. The substrates were heated to 800°C. The microwave plasma was maintained at a power of 5000W for ~3.5 hours to achieve a diamond thickness about 3 microns.

After the diamond growth, the substrates were deposited with ~0.5 micron thick of Titanium. Titanium was used as the masking material during the etching of the diamond layer. Previous work (39) had shown that the application of titanium as a masking layer was a repeatable process. The titanium was then patterned using a conventional lithography process (Mask #1 – *mask resistor*). The delineation of the diamond resistor was achieved using reactive ion etching (RIE) process. The etching uses

oxygen plasma to remove diamond. This method produces a well defined pattern as shown in **Figure 3.7**. RIE of diamond has been attempted by different researchers with moderate success. A low etch rate, non-uniform etching, and inadequate mask-defined selectivity for device-level micro patterning have been some of the issues encountered during the diamond etch. Experimental trials involving different plasma technology sources, etchant gas chemistries, power and pressure conditions, and masking materials of varied thicknesses established within the diamond group researchers have led to a successful recipe to etch the diamond. The utilization of an ICP-RIE system, based on the inductively-coupled plasma (ICP) technology, which combines a high conductance, high vacuum compatible process chamber with an ICP source to produce very high ion density at low pressures resulted in a diamond etch process with an etch rate of ~0.1µm/min. R.F.-assisted pure oxygen plasma chemistry was identified to be a very efficient and effective diamond etchant. A titanium masking layer of ~0.5µm thickness was found to offer good selectivity, allowing the patterned diamond structures to retain the beneficial properties of diamond. The ICP-RIE process parameters included a coil R.F. power of 700W, platen R.F. power of 100W, oxygen flow rate of 40sccm, at a pressure of 10mTorr. The etch conditions of high R.F. power and low pressure helped achieve good anisotropy, the high energy reactive ions with minimum ion scattering giving a high diamond etch rate and selectivity.

An ohmic contact to the resistor was achieved by depositing dual layer of metals, titanium and gold. A thin layer of titanium (~0.05µm) followed by a thickness of ~0.2µm of gold. The Ti/Au layer was deposited through evaporation after delineation of resistor's body and was chosen for its good performance in high temperature operation and

exhibited low resistance (40). A conventional lithography process was performed to remove the unwanted Ti/Au from the substrate (Mask #2 – *mask contact*). These steps complete the fabrication of the attached resistors. **Figure 3.8(A)** is a micrograph picture of attached resistor, *R3* with dimension of 500μm × 100μm. **Figure 3.8(B)** is the SEM image of 50μm × 10μm attached diamond resistor (*R1*).

The fabrication process was continued for a final step for freestanding resistors. After the contact patterning, the final lithography process was performed to define a selective area to form cavity underneath the resistor body (Mask #3 - *mask cavity*). The SiO_2 layer that acted as the sacrificial layer was wet etched using BOE (Buffered oxide etch). **Figure 3.9** shows an optical micrograph image of a top view of a substrate after the final fabrication process. **Figure 3.10(A)** shows the SEM image of the 500μm × 100μm diamond resistor before the cavity etch. **Figure 3.10(B)** is the SEM image after the cavity etch. A clear visible image of the small freestanding resistor is shown in **Figure 3.11**. **Figure 3.11(A)** is the SEM image of 50μm × 10μm freestanding diamond resistor (*R1*). **Figure 3.11(B)** is the close up image of the resistor showing the freestanding structure. **Figure 3.11(B)** inset: shows the diamond resistor was a freestanding and the cavity height was about 1μm. The same image could not be captured for resistor *R3* due to its position in the middle of the 2cm × 2cm sample. As was mentioned earlier, resistor *R1* was not tested in the experiments as its dimensions limited the currents to which it could be exposed.

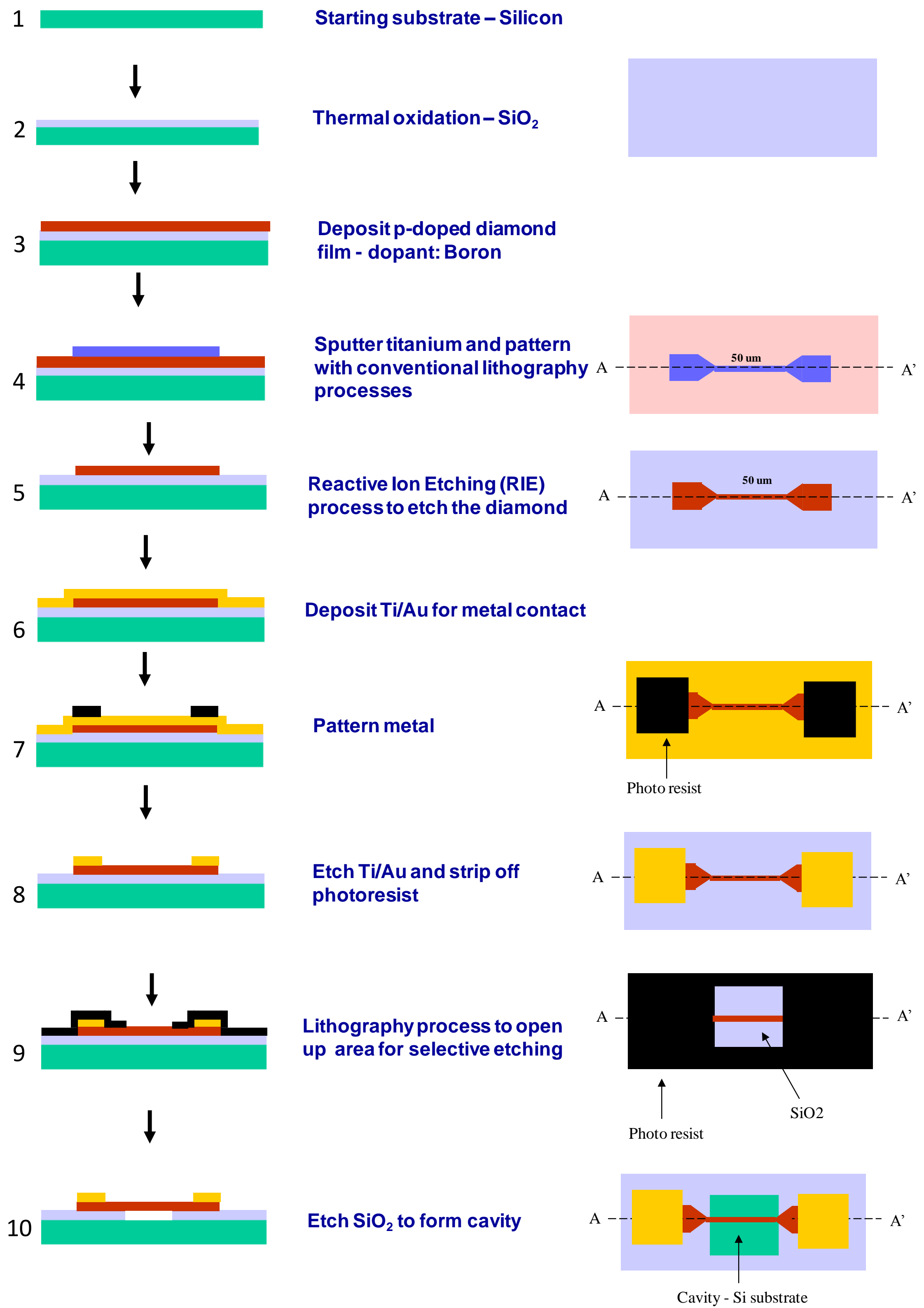

Figure 3.5: Steps of fabricating freestanding diamond resistors.

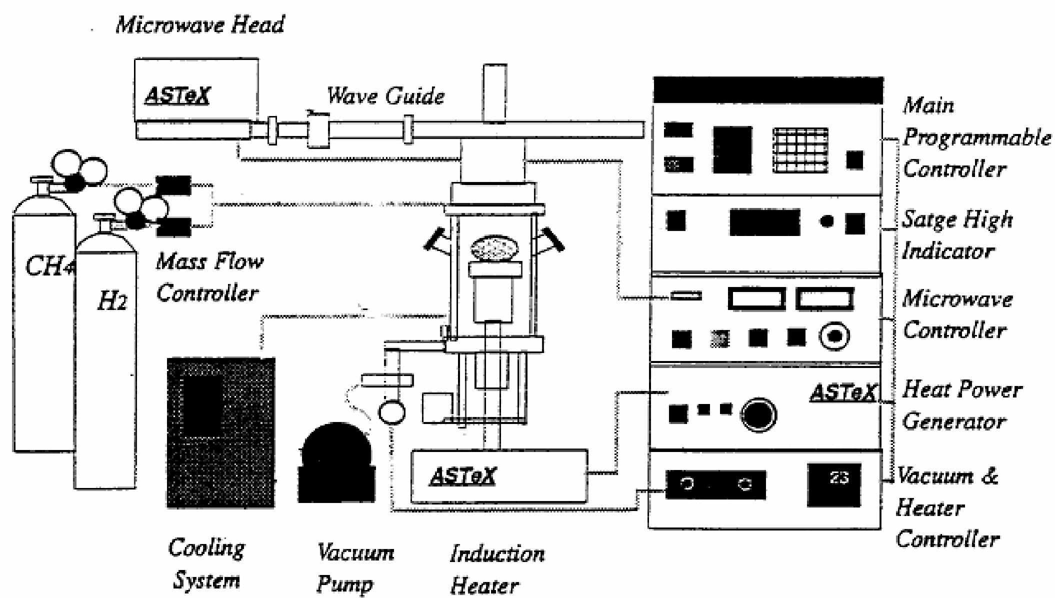

Figure 3.6: Schematic of ASTeX Microwave Plasma Assisted Chemical Vapor Deposition System (41).

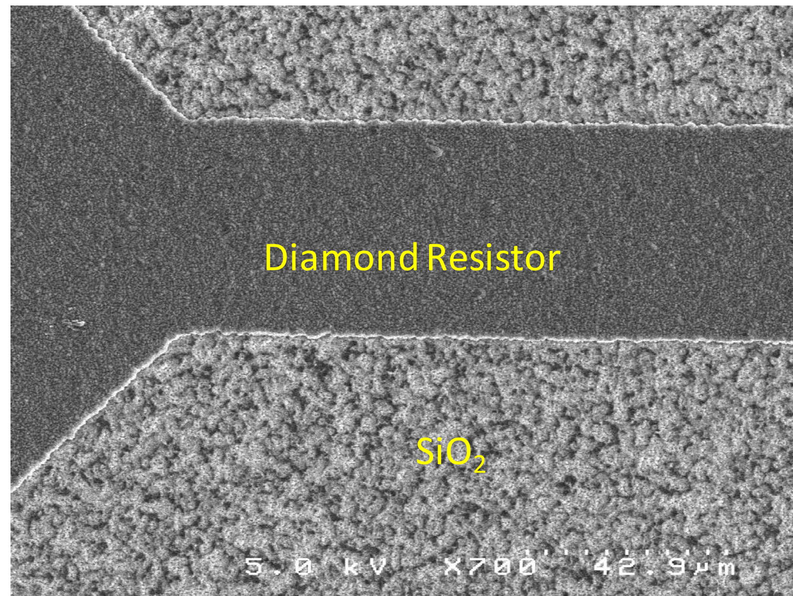

Figure 3.7: SEM image shows a well defined resistor delineation after RIE process.

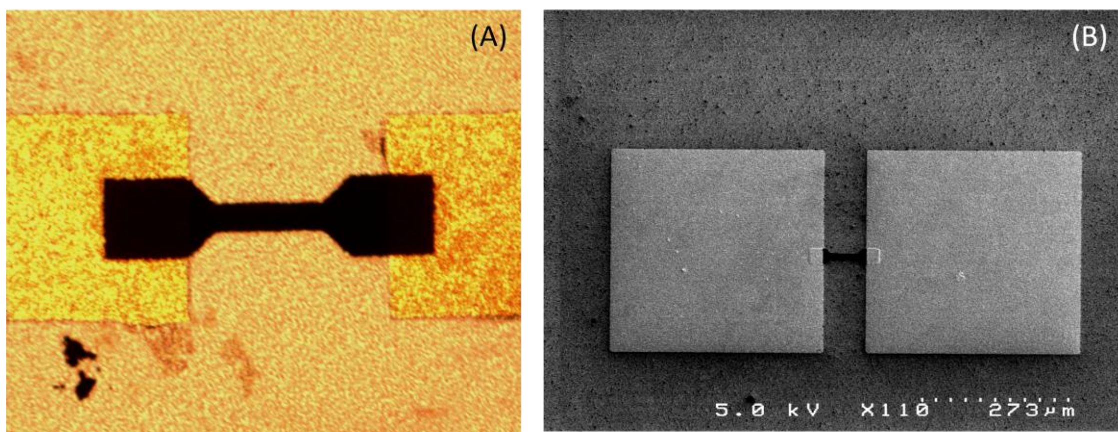

Figure 3.8: (A) Micrograph picture of attached resistor, R3 with dimension of 500μm × 100μm. (B) SEM picture of 50μm × 10μm attached diamond resistor.

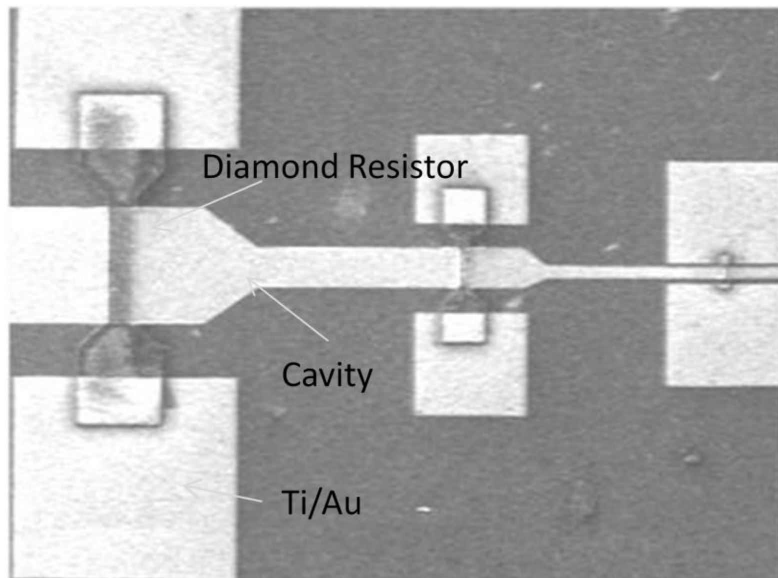

Figure 3.9: Top view of SEM micrograph of complete freestanding diamond resistors.

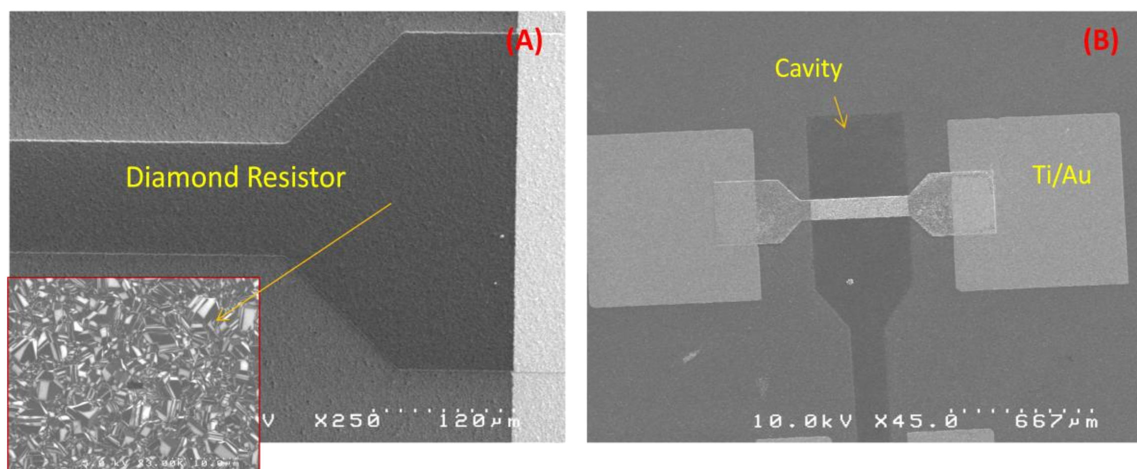

Figure 3.10: (A) A close up SEM image of 500μm × 100μm diamond resistor. Inset shows the boron doped diamond film. (B) Image of the freestanding diamond resistor with cavity and metal contact shown.

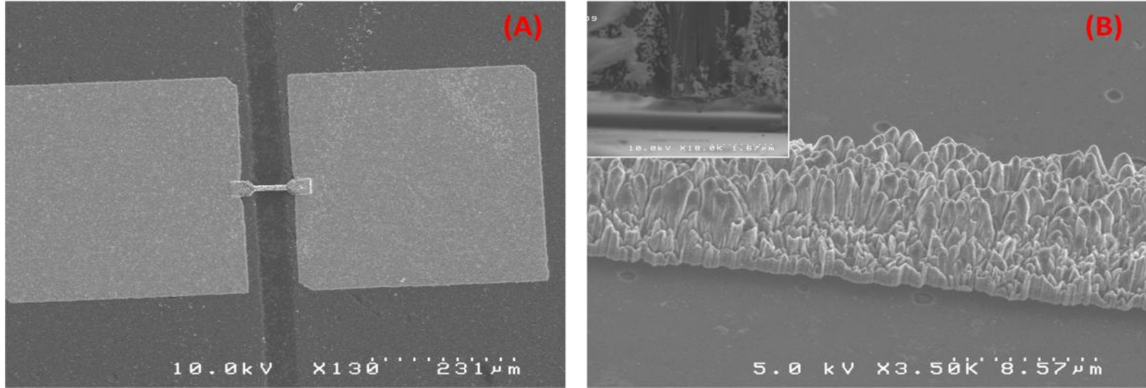

Figure 3.11: (A) SEM picture of 50μm × 10μm freestanding diamond resistor. (B) A close up SEM of the diamond resistor body; inset: shows the diamond resistor was a freestanding and the cavity height was about 1μm.

The dimension of the substrates ranged from less than ~ 2cm × 2cm to ~ 2.5cm × 2.5cm. Each substrate has eight to fifteen of these patterned resistors (***R3***). Edge effects typically led to six to eight resistors as viable test candidates out of the fifteen resistors patterned on one substrate (see **Figure 3.12**).

The samples achieved for testing were three sets of SiO_2 substrates. Two of the SiO_2 substrates are freestanding resistor samples identified as sample **Free_A** and sample **Free_B**. The other SiO_2 substrate is the attached resistor sample identified as sample **Att_C**. Each substrate consists of 6 to 8 of ***R3*** diamond resistors (dimension: 500μm × 100μm). From now on, this particular resistor will be referred to as *resistor* in this thesis content.

Figure 3.12: High mask area-to-sample size ratio contributed to edge effect.

3.2.1 Challenge on diamond deposition on SiO_2

Though there was previous report of successful attempts to grow diamond on SiO_2 (42), it had been a challenging experience to grow diamond on an oxide substrate i.e., clusters of diamond particle islands were found on the substrates (**Figure 3.13**). Multiple trials of diamond growth were attempted to have a successful uniform growth of diamond film.

There were two stages in the procedures that could contribute to the non-uniform diamond growth. The first stage was preparing the substrate for the growth which involved mechanically polishing the surface using a 2.5μm diamond powder suspended in an oil base to augment diamond nucleation on the smooth surface of SiO_2. Moderate pressure was applied manually in a circular motion for approximately 20 minutes. The diamond grit was removed by washing with deionized water followed by rinsing with acetone. Care was also taken not to damage the oxide surface as it is an important layer to provide electrical insulation for the high current testing and a sacrificial layer for the freestanding diamond resistors. Furthermore, extended abrasion process could result in visible scratches on the substrate that affects the ecstatic aspect of the resistor sample as well as the ability of the resistor to perform resistively. A few trial runs of diamond deposition that involved prolong abrasion process, in anticipation that diamond would nucleate better, had resulted in inoperative resistors as shown in **Figure 3.14**.

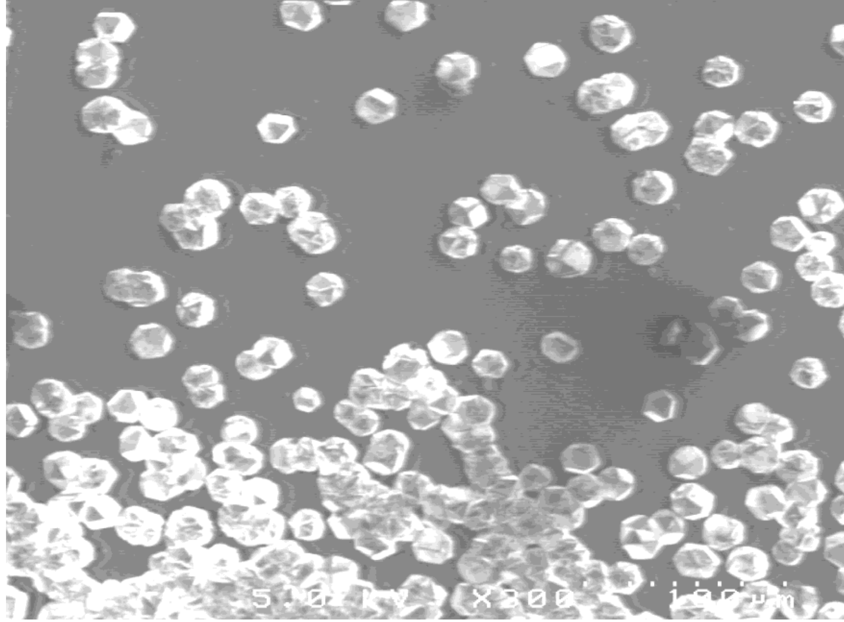

Figure 3.13: Clusters of diamond on SiO_2 shows non-uniform layer of diamond growth.

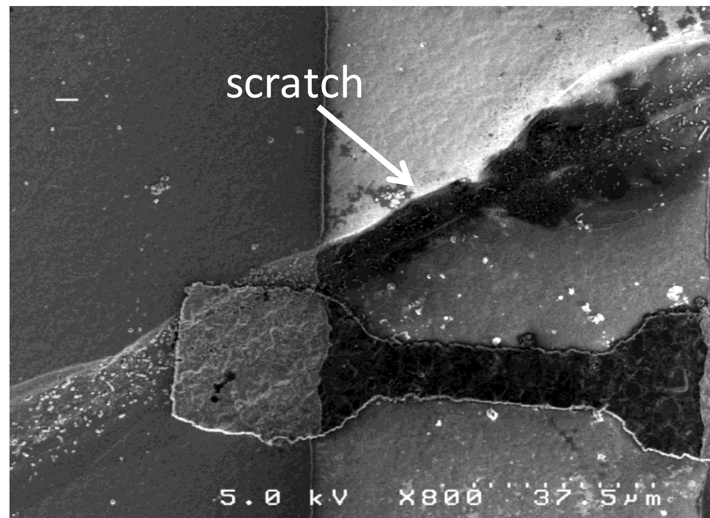

Figure 3.14: SEM image of scratch found after contact pattern.

The second stage that could contribute to the non-uniform diamond growth was during the growth of the diamond. The 5kW microwave diamond machine is designated for boron dopant use only to prevent cross-contamination between machines in the lab and resulted in a good conductive layer of polycrystalline p-doped diamond. However, the high power of the microwave could have resulted in an irregular growth of diamond on the glassy surface of SiO_2. After this possible issue was addressed, a successful attempt of uniform diamond growth was obtained by putting the substrate in a low power (1500W) microwave operated at 550W at 800°C for 6 hours with **no dopant** gas to get the diamond 'seed' *grown* on the SiO_2 surface. **Figure 3.15** shows the SEM picture of diamond nucleation from the 1.5kW diamond machine. The substrate was then transferred to the 5kW power microwave where the diamond growth was continued and doped with boron. **Figure 3.16** shows the SEM picture of the diamond surface following the diamond growth in the 5kW diamond machine. **Figure 3.17** is the high magnified view of polycrystalline diamond film. **Table 3.1** shows the process parameters for the diamond seeding process.

Table 3.1: Diamond seeding process parameters.

Hydrogen, H2	135 sccm
Methane, CH4	15 sccm
Pressure	13 Torr
Temperature	800C
Power	550W
Time	6 hours

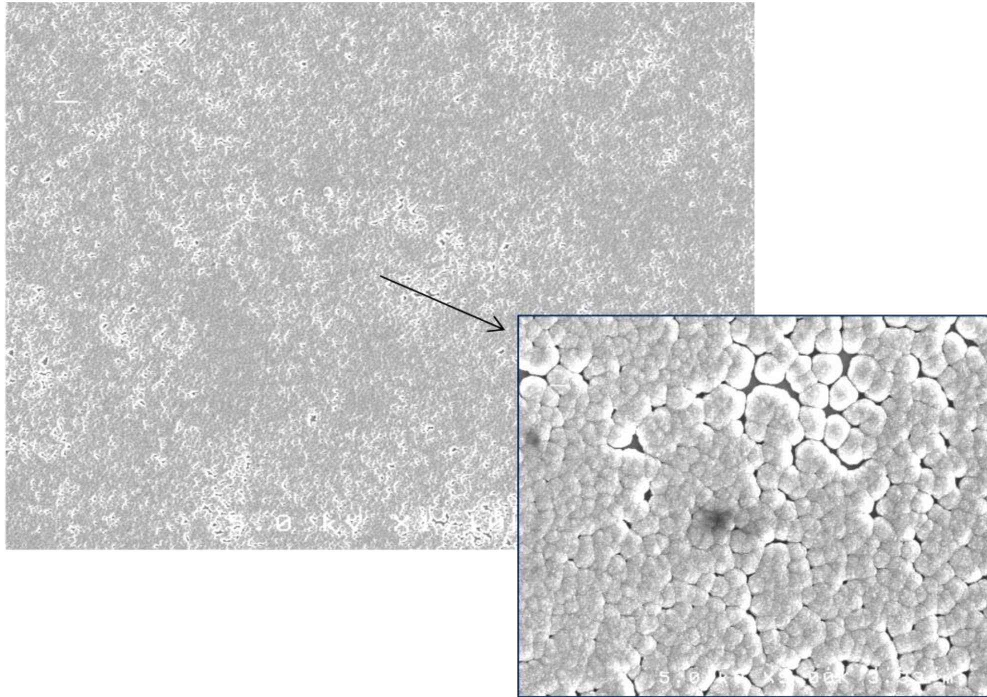

Figure 3.15: SEM picture of diamond nucleation in diamond machine 1.5kW.

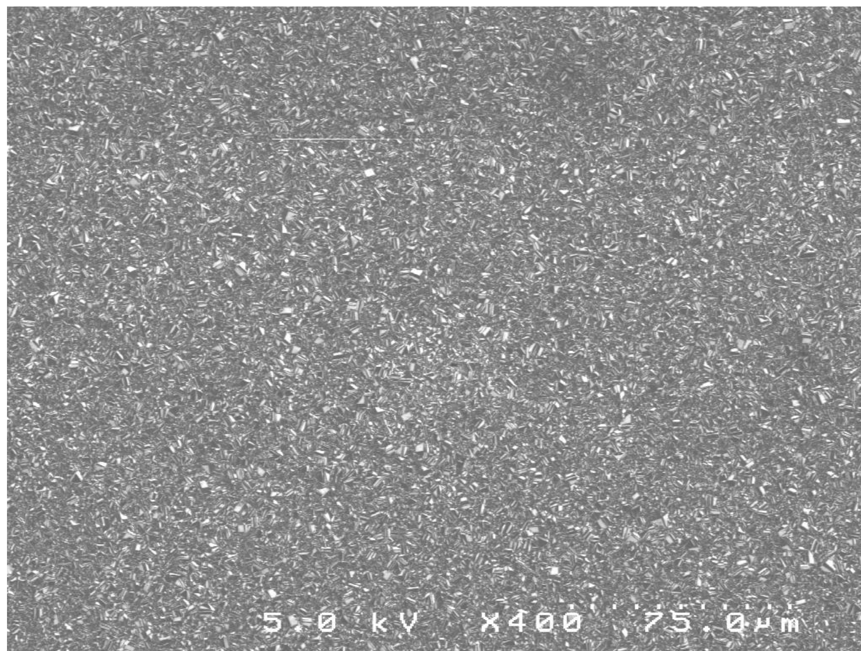

Figure 3.16: SEM picture of diamond surface following the diamond growth in diamond machine 5kW (same sample after nucleation process in 1.5kW machine).

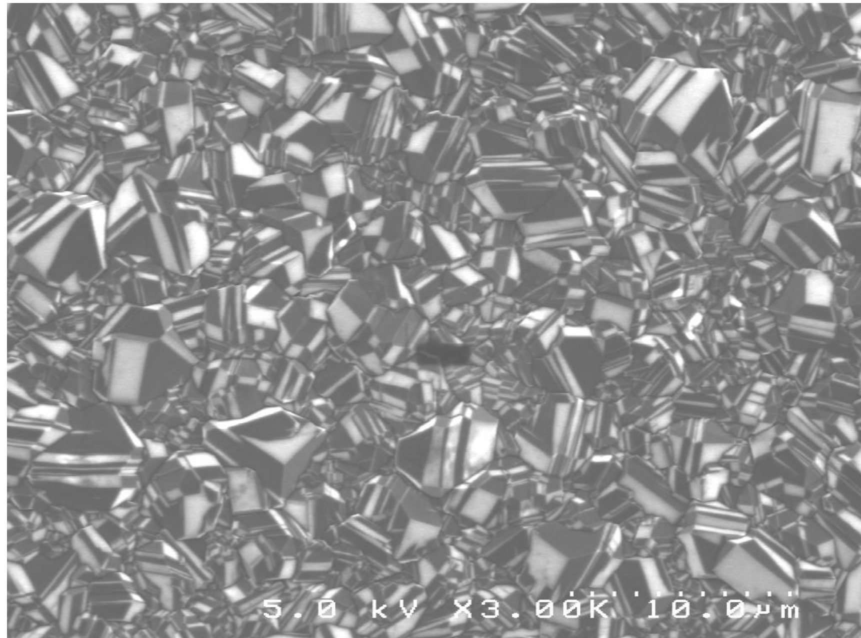

Figure 3.17: High magnified view of polycrystalline diamond film (from diamond machine 5kW).

Part II: Testing Characterization

Methods for testing dynamic systems are sometimes classified either as transient response or frequency response procedures. Although the classification is often considered to establish two independent techniques, it is recognized that the information yielded by one method is related to the other. The pulse method employs the transient response to a known input.

Electrical power pulse will be passed through the resistors to characterize the electrothermal responses. This technique is based on the rapid resistive self heating of the resistor up to a preset temperature and then maintaining the sample at that temperature under brief steady state conditions. The pulsed heating technique is considered a very accurate method for the measurement of several thermophysical properties (heat capacity, enthalpy, heat of fusion, electrical resistivity, hemispherical total emissivity, thermal expansion (43), at high temperatures. The oscillating temperature causes a periodic change in the resistor due to the nonzero temperature coefficient of resistance. This in turn influences the electrical power dissipated into the resistor. The pulse method has been shown to produce detailed curves of the experimental heat exchange frequency response (44). **Figure 3.18** shows the duration and amplitude of a rectangular pulse. The pulse strength is defined as the area under the pulse. For a specified duration, the pulse strength is determined by the amplitude. The experiment needs to be performed in a vacuum chamber to avoid chemical interaction of the device (resistor) with the environment.

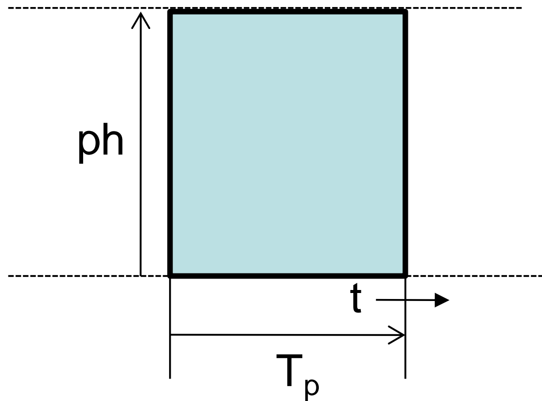

ph = pulse height (amplitude)
T_p = pulse duration
ph x T_p = pulse strength

Figure 3.18: Schematic of a rectangular pulse.

Several tests performed during the course of this research will be classified as "preliminary". These tests were typically simple current-voltage analysis (in air and vacuum), constant current (DC mode), thermal current-voltage analysis, threshold voltage analysis, trial testing for different setups with the data acquisition (DAQ) system to record data. Some of the procedures were performed to make observations before a subsequent test but the sample was destroyed prematurely before the next level of test was conducted. Although some of the preliminary tests did not have the results recorded, resistors were lost and reduced the number of samples available for further testing. The ensuing section put forward the test setup developed for testing the attached and freestanding diamond resistors.

3.3 Pulse Heating Measurement Setup

The measurement procedure utilizes resistive current-sensing. Resistive current sensing is a commonly used technique for measuring electrical current in circuits. According to Ohm's law, when detecting current through a resistor, the voltage drop across the resistor is a direct measure of the current. In this technique, a sense resistor, R_1 is inserted in series with the device under test (diamond resistor) to measure the current. An Agilent HP 54600B 100MHz, 20MSa/s dual channel digital oscilloscope is used to record the voltage drop across R_1. This oscilloscope has an advanced interface with remote control capability and GPIB for data storage. The oscilloscope uses Agilent BenchLink XL 54600 software to capture screen images, gathers waveform data, and stores instrument setups to MS Excel™. Using a stable low impedance, R_1 ,is important to accurately sense the current and minimizes power losses, yet achieve a sufficiently high voltage to differentiate the signal from noise. This method is also important for overload current protection by providing sufficient attenuation to limit the voltage on the oscilloscope when high voltages are applied to the diamond resistor.

The input voltage pulse is supplied from a controlled high voltage DC power supply generator (Magnavolt™ High Voltage DC Power Supply/Pulse Generator) that is capable of supplying up to 5A and a maximum voltage of 5kV. A voltage divider which consists of resistors RA and RB, was in the circuit (**Figure 3.19**) to allow accurate measurement of the voltage supplied by the Magnavolt™, which will be used in the circuit calculation. The combined resistive value of RA and RB is much greater than the combined resistive value of the diamond resistor (R_d) and R_1, routing most of the current through the resistive device under test.

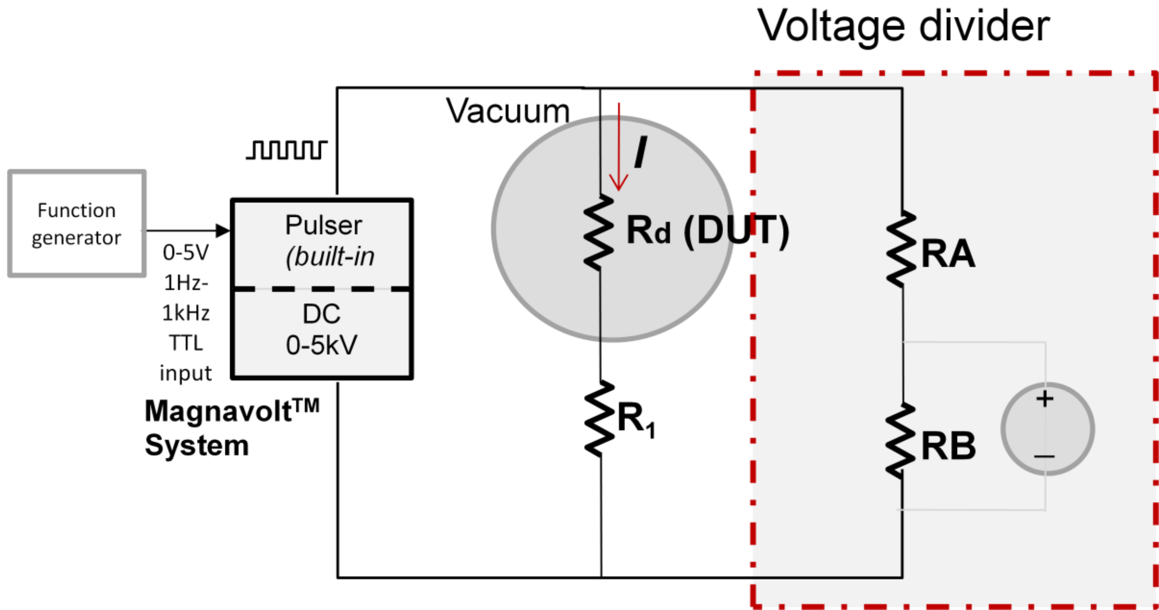

Figure 3.19: Schematic of the set- up for pulse heating test.

A detail schematic of the test set up is shown in **Figure 3.20**. Resistor R_1 as 100Ω, 50W aluminum housed power resistor which has a 1% tolerance of its rated value over 1000 hours operation. The current was calculated from the voltage drop across R_1 as measured with an oscilloscope. Using the calculated current, the resistance R_d was determined. Details of the calculation will be discussed later. The resistor R_1 has a power rating of 50W and throughout the experiment; the power across the resistor was much less than this. This ensures that test variables affect only the diamond resistor while R_1's characteristics remain constant. The values of RA and RB were 100kΩ and 1kΩ respectively. The voltage drop across the 1kΩ resistor is measured using the oscilloscope; this allows the input voltage to be recorded (using the voltage divider). Diamond resistors under test were placed in a vacuum environment (~10^{-7} Torr) during testing.

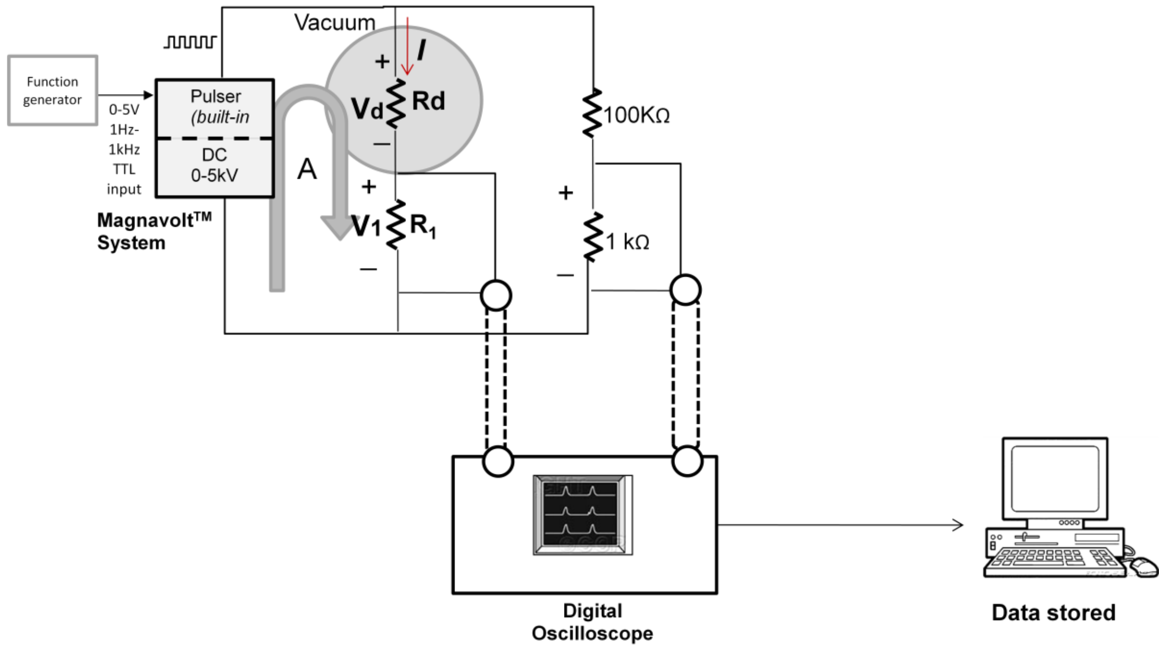

Figure 3.20: Detail of test set- up for the pulse heating experiment.

Following are the circuit calculations involved in the test configuration. Referring to **Figure 3.20**, we can define the current, I through R_d and R_1 as;

$$I = \frac{V_1}{R_1} = \frac{V_d}{R_d} \tag{3.1}$$

Apply Kirchhoff law in Loop A;

$$V_s = V_d + V_1 \tag{3.2}$$

$$V_d = V_s - V_1 \tag{3.3}$$

$$IR_d = V_s - V_1 \tag{3.4}$$

Hence, we get the resistance across the diamond resistor, R_d;

$$R_d = \frac{R_1(V_s) - R_1(V_1)}{V_1} \tag{3.5}$$

The input power to the diamond resistor circuit during the heating pulse can be computed from simultaneous measurement of the current flowing through the diamond resistor and the applied voltage for the duration of the defined as;

$$P_{inp}(t) = IV_s t \tag{3.6}$$

The power dissipation in the diamond resistor causes heating and is referred to as Joule heating (45). The amount of heat generated can be calculated:

$$P_d(t) = I\,V_d t = I^2 R_d t \tag{3.7}$$

where P_d is the power dissipated in the diamond resistor as a function of time (second), t. To verify these formulas, a PSpice simulation was performed. The complete spice file and data is in **Appendix B**. For an example, at a voltage input of 60V, R_1=100Ω and R_d is set at 5kΩ, following are the extracted circuit parameters:

I_{Rd}= 11.76 mA I_{RA} = 0.594 mA V_{Rd} = 58.82 V

I_{R1} = 11.76 mA V_{RB} = 0.594 V Vs = 60V

I_{RB} = 0.594 mA V_1 = 1.176 V

Substituting the above values of Vs, V_1 and R_1 into the Eqn. (3.5),

$$R_d = \frac{R_1(V_s) - R_1(V_1)}{V_1}$$

$$R_d = \frac{100(60) - 100(1.176)}{1.176}$$

$$R_d = 5002\ \Omega$$

This illustrates the formula to calculate R_d is accurate, as the calculated value well approximates the set value of R_d.

3.4 Experimentation to Determine Activation Energy

This is a thermal evaluation to determine the activation energy of boron dopant in the thin film diamond resistor. In doped semiconductor, both the charge carrier mobility and the charge carrier density depend upon temperature. The thermal vibration of the atoms can impart energy ($\sim kT$) to the holes such that some of them break free from their covalent bonds and migrate through the film as part of conduction current. The resistance temperature dependence dominates in the semiconductor and is given by the Arrhenius relationship:

$$R_T = R_0 \, e^{\frac{E_A}{kT}} \tag{3.8}$$

where E_A is the effective activation energy, k is the Boltzman constant, R_0 is a constant and T is temperature under consideration. The temperature of the thin film may be assumed to be uniform throughout the volume between the two metal contacts. This assumption is made due to the very high thermal conductivity of the diamond thin film and the very low thermal diffusivity of the air surrounding the resistor body, a very thin film thickness, and the short duration of the applied current pulse.

The basic test approach to determine the activation energy involves heating the diamond resistor and measuring the current to obtain the resistance. The sample was placed on a hot plate and probes were used to access the interconnect circuitry of the resistor. Voltage was supplied to the resistor from a Keithley 6517A electrometer and the current was measured and stored by LabView data acquisition. The experiment started at room temperature (25°C), and the current measured. The temperature was then increased in 25°C increments and the hot plate was allowed to stabilize at the new temperature for 10 minutes before the current was measured again. The steps were repeated to a maximum temperature of 350°C. The resistance at each of the temperature was determined from the slope of the I-V plot. The activation energy was determined from the Arrhenius plot (discussed in detail in *Section 4.2*).

CHAPTER IV

EXPERIMENTAL RESULTS AND DISCUSSION

4.1 Thickness Measurement

The thickness of the diamond films was determined after the delineation of the resistors. The thickness was measured using a DekTak IIA Surface Profile Measuring system. It has a micro-sensitive stylus that moves on a plane sensing any aberrations on the planarity of the surface. The deviations were measured digitally and recorded as graphical output. An outline sketch of the instrument is shown in **Figure 4.1**. The stylus was allowed to scan the film twice, with the sample turned 180° during the second run. The mean reading of the steps was taken to be the thickness of the film. The graphic outputs of the scan program in the instrument that reads the thickness are shown in **Figures 4.2** and **4.3** for freestanding samples and **Figure 4.4** for attached resistors. Resistors on sample **Free_A** have an average thickness of 2.5μm. The resistors on sample **Free_B** and **Att_C** have an average thickness of 2.8μm.

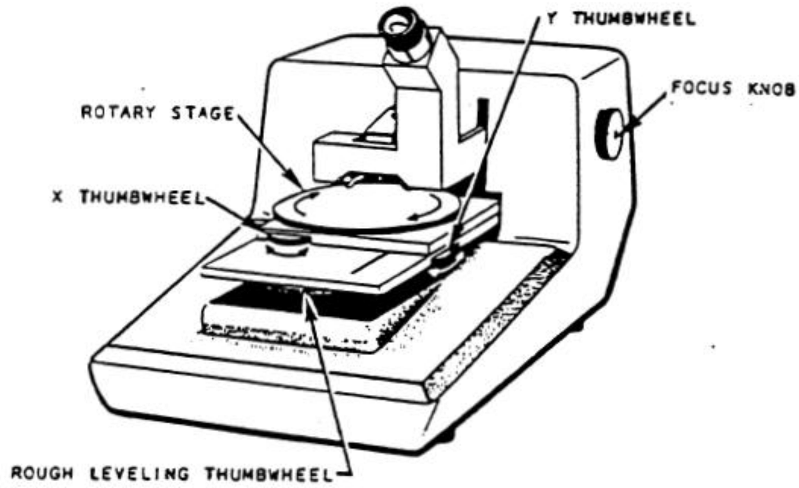

Figure 4.1: Outline sketch of DekTak IIA.

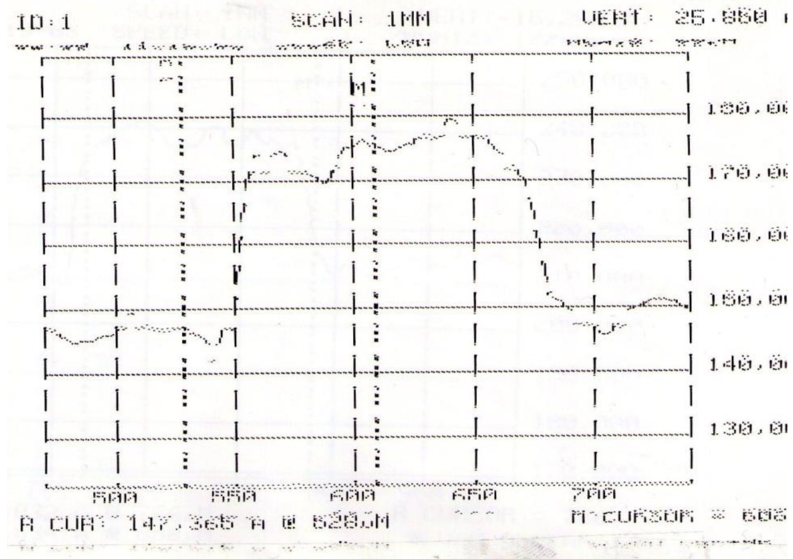

Figure 4.2: Graphic output for thickness sample **Free_A**.

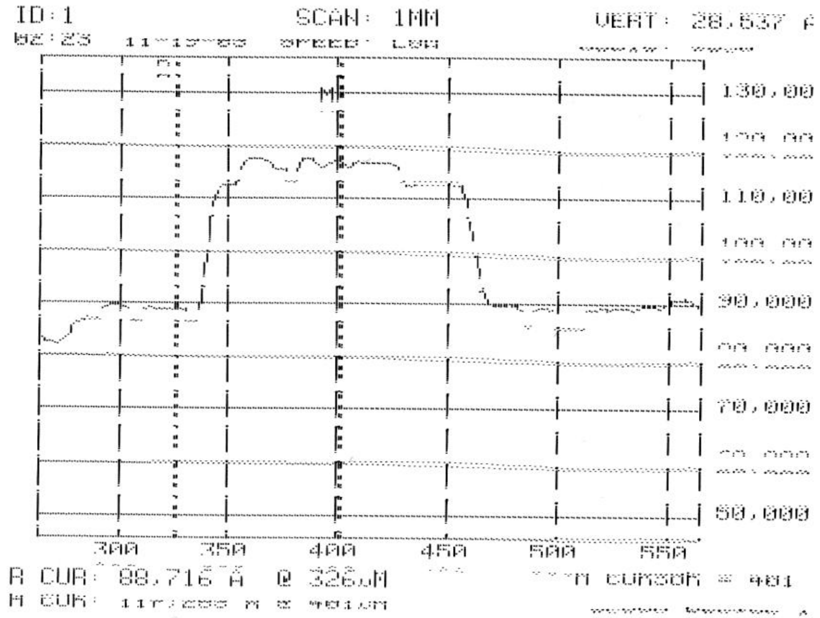

Figure 4.3: Graphic output for thickness sample **Free_B**.

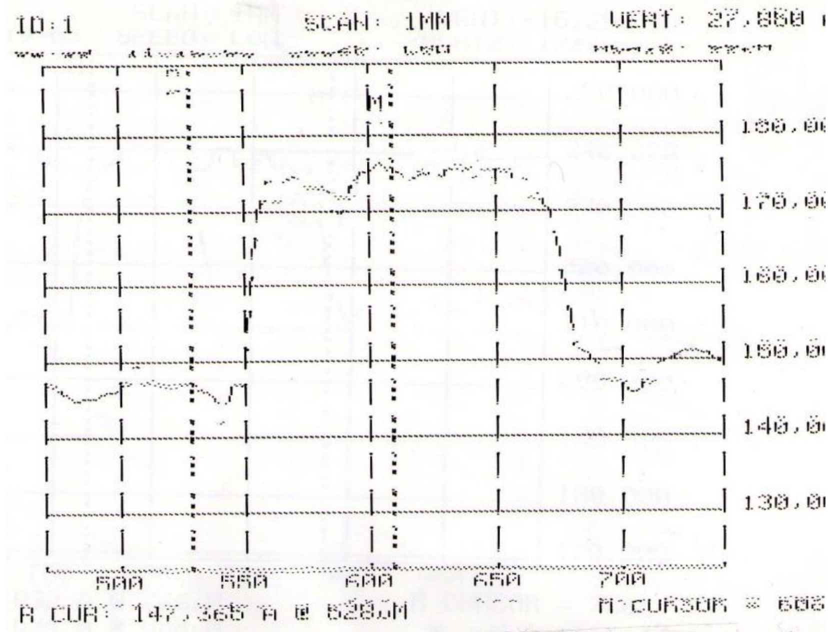

Figure 4.4: Graphic output for thickness sample **Att_C**.

4.2 Determination of Activation Energy

The activation energy of boron dopant in the diamond resistors can be obtained from the Arrhenius relation:

$$\rho_T = constant \times e^{\frac{E_A}{kT}} \tag{4.1}$$

where ρ_T is the resistivity at any given temperature and T is the temperature in Kelvin. The equation can be modified to give the relationship when resistance, R_T of the material at a given temperature is known,

$$R_T = R_0 \, e^{\frac{E_A}{kT}} \tag{4.2}$$

where R_T is the resistance of the material at a given temperature,

R_0 is a constant,

E_A is the activation energy of the sample and

k is the Boltzmann constant.

Taking the natural logarithm to both sides of the equation, we obtain

$$ln\, \mathrm{R_T} = ln\, \mathrm{R_0} + \mathrm{E_A/kT} \tag{4.3}$$

The *Current–Voltage* (*I-V*) measurements were taken for temperatures over the range of 25°C to 350°C on all samples. Details of the experimentation have been discussed in *Section 3.4*. **Figure 4.5** and **Figure 4.6** show Resistance vs. Temperatures for freestanding and attached resistor samples respectively. As we have discussed in **Chapter II**, the resistance decreases with an increase in temperature because of the increased numbers of charge carriers (holes) available for conduction. At room temperature, the boron dopants are not fully ionized. As the temperature increases, the ionization of the boron dopants increases. The ionized dopants create carriers that are holes in the valence band. The increasing number of carriers reduces the resistance of the diamond resistor, which corresponds to a negative temperature coefficient of resistance (TCR).

The Arrhenius plots for freestanding diamond resistors of samples **Free_A** and **Free_B** are shown in the inset of **Figure 4.5** and the Arrhenius plots for the attached diamond resistors of sample **Att_C** is shown in the inset of **Figure 4.6**. The natural log of resistance ($ln\ R_T$) was plotted against the inverse of the temperature in Kelvin ($1/T$). A straight line was obtained where the slope of the line is E_A/k. The activation energy, E_A can be calculated by substituting the Boltzmann constant, k into the slope equation. The activation energy was 0.1eV for sample **Free_A** (*freestanding*) and sample **Att_C** (*attached*) and 0.09eV for **Free_B** (*freestanding*).

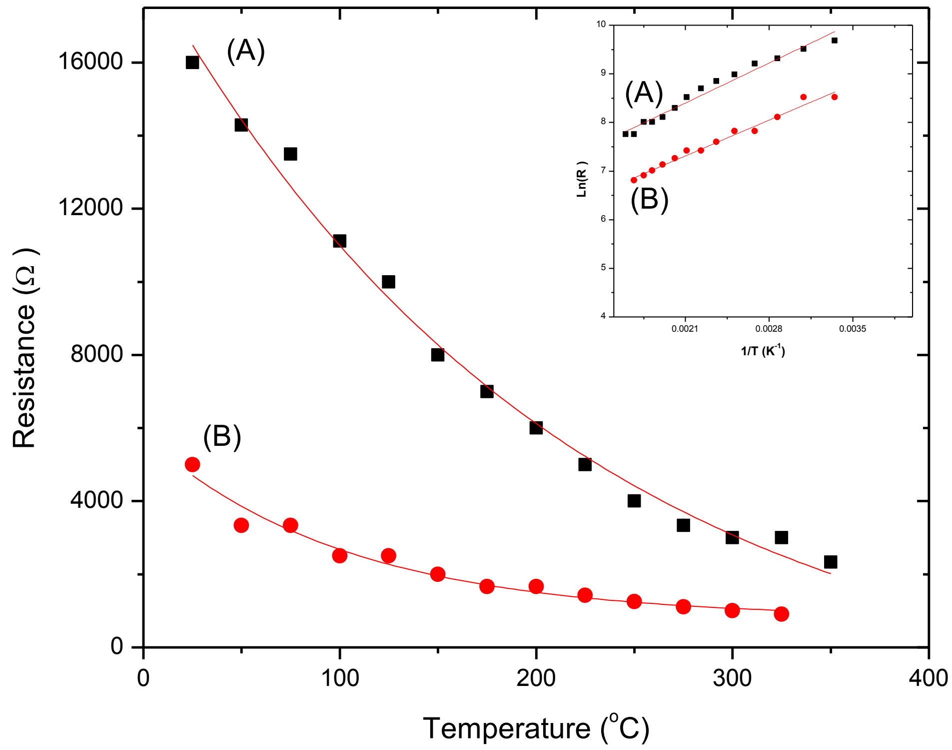

Figure 4.5: Resistance vs. Temperature plot for both freestanding resistor samples, sample **Free_A** (A) and sample **Free_B** (B); inset: corresponding Arrhenius plots.

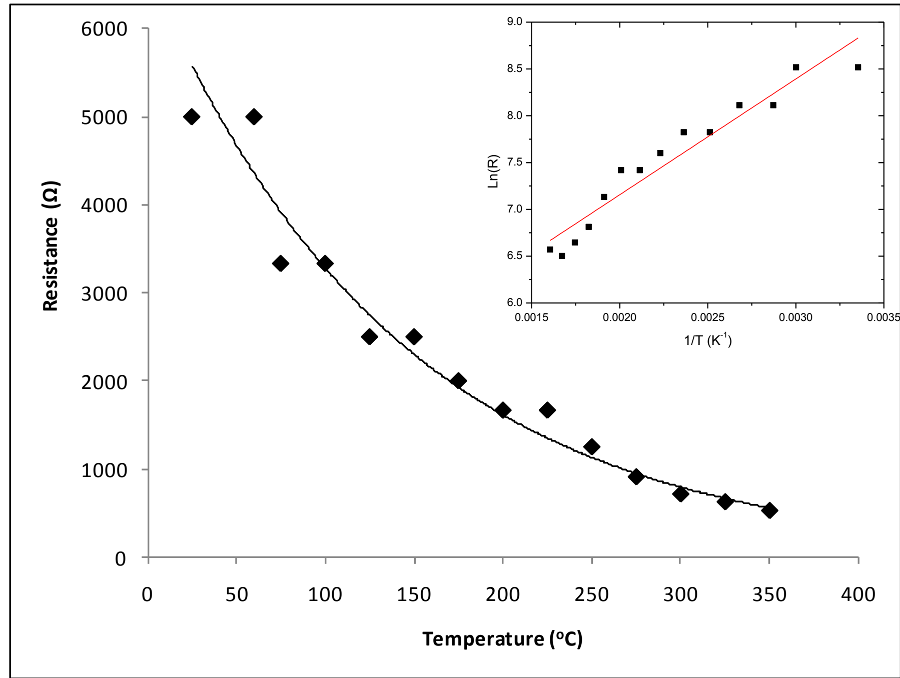

Figure 4.6: Resistance vs. Temperature plot for attached resistor sample, **Att_C**.

I-V measurements were performed to determine the resistive behavior of the diamond resistors. The typical resistance at room temperature for freestanding samples **Free_A** and **Free_B** were 16kΩ and 5kΩ respectively. The I-V plots are shown in **Figure 4.7**. The sample for attached resistors, **Att_C** has the same room temperature resistance as **Free_B** which was 5kΩ and the typical I-V plot at room temperature is shown in **Figure 4.8.** The variation in the measurement of the room temperature resistance for freestanding samples is believed to be due to the thickness difference which possibly occurred during the resistor delineation in the RIE process.

Knowing the resistance value at room temperature and the resistor's dimension, the diamond resistor resistivity at room temperature is calculated from Eqn. (A-1). Please refer to **Appendix A** for details. Below are the resistivity calculations for all the samples.

For sample **Free_A**:

$$R = \frac{\rho L}{A}$$

$$\rho = \frac{RA}{L} = \frac{16000 \cdot 100 \times 10^{-4} \cdot 2.5 \times 10^{-4}}{0.05}$$

$$\rho = 0.8\ \Omega \cdot cm \tag{4.4}$$

Same calculation is carried out for sample **Free_B**:

$$\frac{RA}{L} = \frac{5000 \cdot 100 \times 10^{-4} \cdot 2.8 \times 10^{-4}}{0.05}$$

$$\rho = 0.3\ \Omega \cdot cm \tag{4.5}$$

and sample **Att_C**:

$$R = \frac{\rho L}{A}$$

$$\rho = \frac{RA}{L} = \frac{5000 \cdot 100 \times 10^{-4} \cdot 2.7 \times 10^{-4}}{0.05} \tag{4.6}$$

$$\rho = 0.3\ \Omega \cdot cm$$

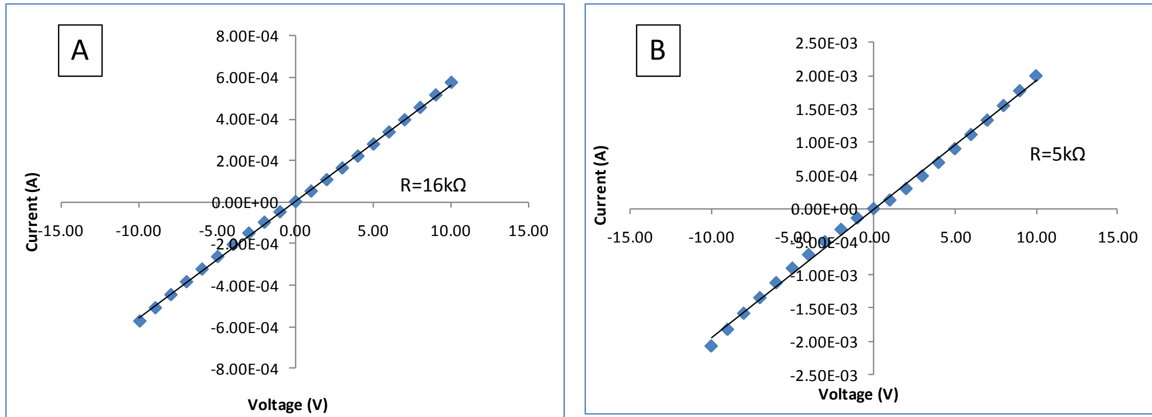

Figure 4.7: Typical current-voltage plots at room temperature for freestanding diamond resistors. A: sample **Free_A**, B: sample **Free_B**.

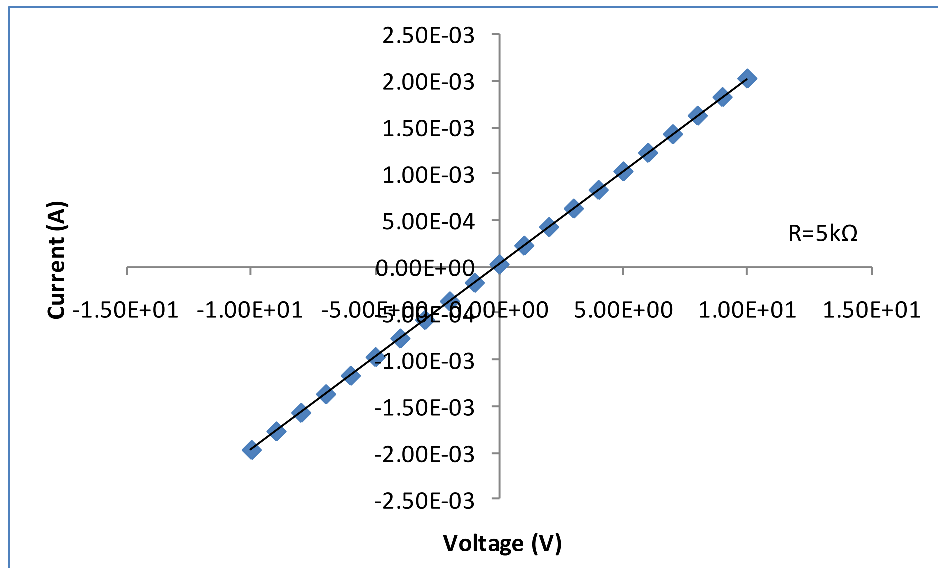

Figure 4.8: Typical current-voltage plot at room temperature for attached resistors sample **Att_C**.

4.2.1 Temperature Dependence of Resistance

We can infer the *heated* diamond resistor as a *thermistor*. After all, the name thermistor is derived from the words *thermal* and *resistor*. This is based on the fact that the electrical resistance of the diamond resistor changes as its temperature changes. A thermistor with negative temperature coefficient (NTC) will show a decrease in resistance with a temperature increase. Thermistors made of single crystal diamond have been reported before (46). Vereshchagin *et al*. concluded that p-type diamond was the most suitable material for thermistors as opposed to undoped diamond, n-type silicon carbide or undoped SiC. Nakahata *et. al.* then fabricated thermistor made from p-type polycrystalline thin film diamond (47).

Temperatures of the diamond resistors in this work are not measured directly due to equipment limitations. Instead they are calculated from the temperature dependence of resistance equation. The diamond resistors are utilized as thermistors and the temperature dependence of resistance of the pulse voltage test allows us to obtain the resistor temperature.

The dependence of resistance on temperature is given by the Arrhenius relationship, Eqn. (4.2). Given the values of activation energy, E_A, resistance at room temperature and Boltzmann constant, we can calculate the temperature dependence of the resistance constant, R_0. Eqn. (4.2) can be rewritten as:

$$T = \frac{E_A}{k}\left[\frac{1}{\ln\left(\frac{R_T}{R_0}\right)}\right] \tag{4.7}$$

To calculate R_0, here, we show an example for sample **Free_A** calculation. The resistance measured at room temperature (300K) for sample **Free_A** was 16kΩ and the E_A was 0.1eV. Substituting these values in the above equation, we have:

$$16000 = \mathrm{R}_0 \times \exp(\frac{0.1}{0.0258}) \tag{4.8}$$

$$\text{constant}, \mathrm{R}_0 = \frac{16000}{47.97} = 333.5\ \Omega \tag{4.9}$$

The R_0 was 333.5Ω for sample **Free_A**. Similar calculation was also performed for samples **Free_B**, and **Att_C**. The R_0 obtained was 153.5Ω and 103.7Ω respectively. Substituting these constant values and the resistance values (R_d) that were measured throughout the pulse heating experiment; the temperatures of diamond resistor as the pulses were applied can be calculated using Eqn. (4.7). **Table 4.1** shows the summary of the calculations performed on all the samples involved.

Table 4.1: Summary of measurements and calculations on all samples.

	Sample Free_A	Sample Free_B	Sample Att_C
Room temperature resistance, R (Ω)	16 k	5 k	5k
Thickness, t (μm)	2.5	2.8	2.7
Resistivity, ρ (Ω-cm)	0.80	0.30	0.30
Activation energy, E_A (eV)	0.1	0.09	0.1
Temperature dependence of resistance constant, R_0, (Ω)	333.5	153.5	103.7

4.3 Preliminary Test Results

In this section, we will present two of the preliminary results obtained during the series of trial tests. Trial tests were done more on the freestanding than attached resistors as more freestanding resistors were successfully fabricated compared to attached resistors. The results of the preliminary round of testing provided guidance for more scientific time bounded testing. To improve data clarity, an oscilloscope was setup to remotely store the waveform data using a GPIB interface (**Chapter III**). These results will be more comprehensible as we go on through this chapter. The discussion here will be brief intending to provide guidance for subsequent tests.

In this preliminary test, a current limit was set on the Magnavolt™ (power supply) and the voltage from the power supply was increased until the current limit was reached. This approach ensured that there was no overshoot voltage or current that could

cause catastrophic damage to the external circuit and the equipments involved when dealing with high voltages and currents.

The current limit was set to 15mA. The test was conducted on resistor **Free_A5**. The voltage on the Magnavolt™ was applied until the LED (on Magnavolt™) indicated that the current limit has been reached. The voltage reading was at 160V. The frequency was 10Hz with 30% duty cycle. **Figure 4.9** shows the current waveform of resistor **Free_A5**. The corresponding resistance waveform is depicted in **Figure 4.10**. The transient response was observed within the 0.03s of the driving pulse which indicates that the voltage pulse warms the resistor quickly, proceeding to a lower value until the pulse ends. The result from this preliminary test gave us imminent idea on how much voltage pulse (i.e. power) that the resistor could handle before any failure to occur and characterize transient response within the pulsing pulse. After the pulse test, the resistor was visually inspected under a microscope. Probe marks were found on the contact pads. The I-V plot shows non-linear characteristic after the pulse test, **Figure 4.11**. A current limit imposed by the instrument was also observed in **Figure 4.11** at ±7V.

The non-linear characteristic could be due to two possible scenarios. The first scenario was the possibility of junctions developing at both ends of the resistor, creating a mirror effect of the non-linear characteristic. The second scenario was the possibility of the development of a secondary current path through the Si substrate, creating a mirrored MOS diode effect on the vertical structure of the resistor (currents flowing through the contact pads (metal), passing the SiO_2 (oxide) and through the Si (semiconductor)).

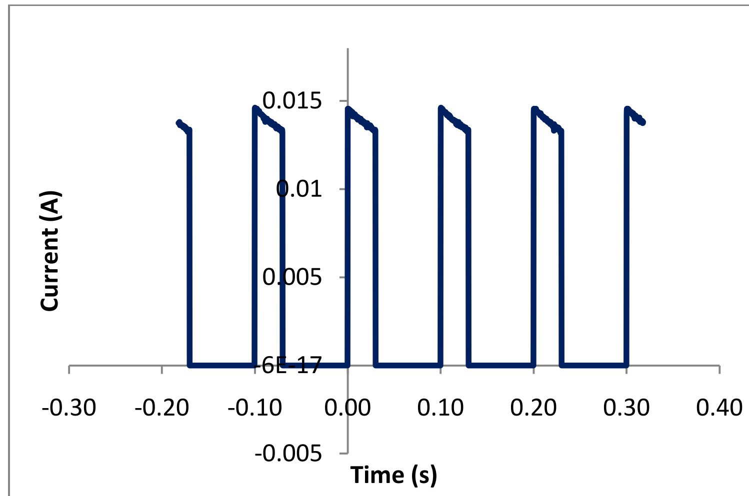

Figure 4.9: Current waveform of resistor **Free_A5** at 160V.

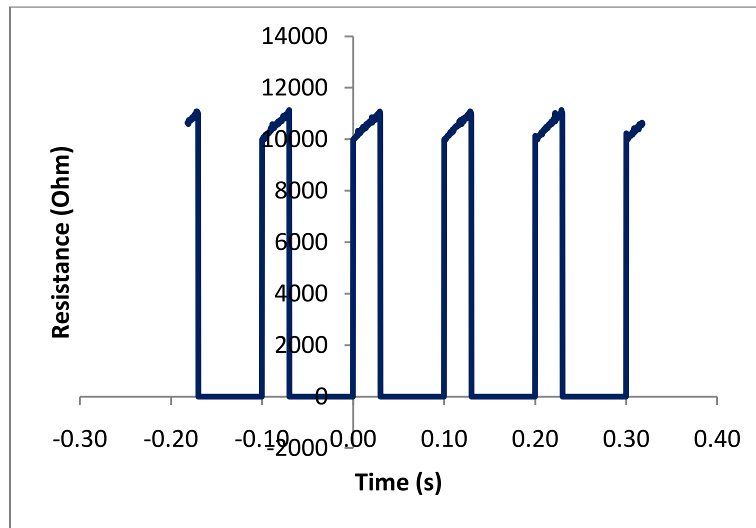

Figure 4.10: Corresponding resistance waveform of resistor **Free_A5**.

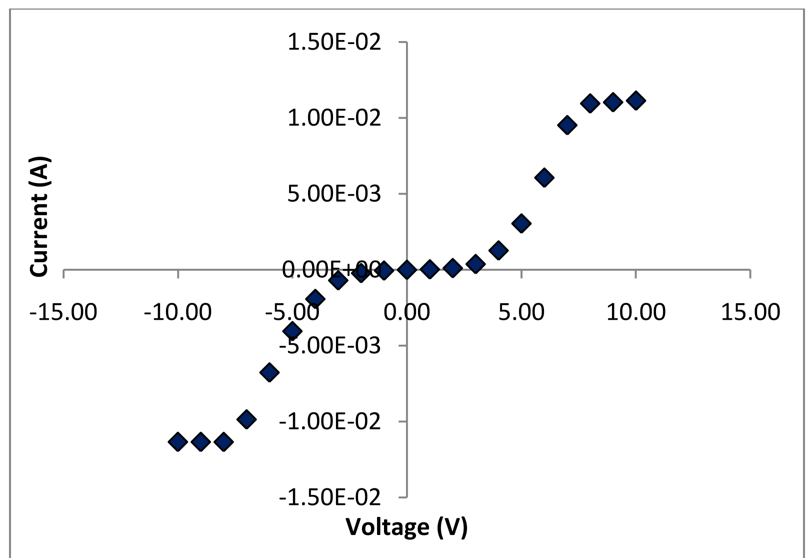

Figure 4.11: I-V plot of resistor **Free_A5** post pulse.

Another preliminary test result that will be discussed here is from a *single pulse characterization*. This was amongst the earlier tests in which overall testing was time independent. The purpose of this test was to investigate and characterize the resistance and current waveforms when the resistor was subjected to power pulses sufficient to cause the diamond resistor to glow. This test was conducted on resistor **Free_A8**. The Magnavolt^{TM} was set to limit the current at 0.5A. The voltage was increased until this current limit was achieved. For the 0.5A current limit, the input voltage pulse was ~470V. The frequency of the voltage pulse was set at 10Hz with a 5% duty cycle. In this test, the 5% duty cycle was chosen to keep the resistor from experiencing extended high stress in each pulsing pulse.

Resistor **Free_A8** was observed to be illuminated (visible radiation emission, red glow) at 0.5A and the single current pulse was measured at the time when the resistor was glowing. **Figure 4.12** shows the waveforms of the voltage drop across **Free_A8**, V_d, its resistance, R_d and temperature during the pulse. The I^2R heating of the diamond resistor causes a rapid current increase as shown in **Figure 4.13**. The current through the resistor causes significant power dissipation causing localized temperature rise, hence the change in the resistance. The change in resistance indicated that the resistor was heating up during the pulsing period. This phenomenon will be discussed in detail in the following sections when we discussed the experimentation results. The image of the resistor glowing during the pulsing was captured, **Figure 4.14**. **Figure 4.15** shows the SEM image of the diamond resistor post pulse test. The stress of the pulsing had caused the sample **Free_A** to crack along the resistor **Free_A8**. The lateral crack caused the remaining resistors along the line to be damaged and unusable for further testing. In

Figure 4.16 the Planckian locus, which is the path that the color of a blackbody takes as the temperature changes, estimates the temperature, visually matching with the resistor's radiant emission.

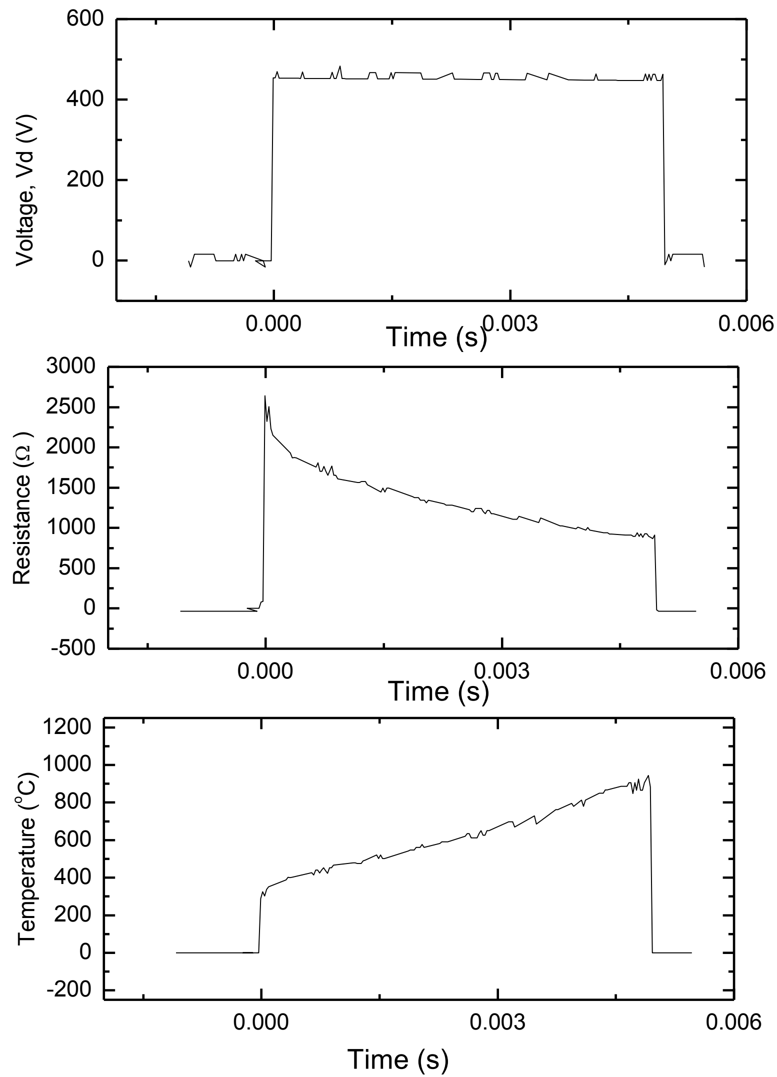

Figure 4.12: Voltage, resistance and temperature waveforms of resistor **Free_A8**.

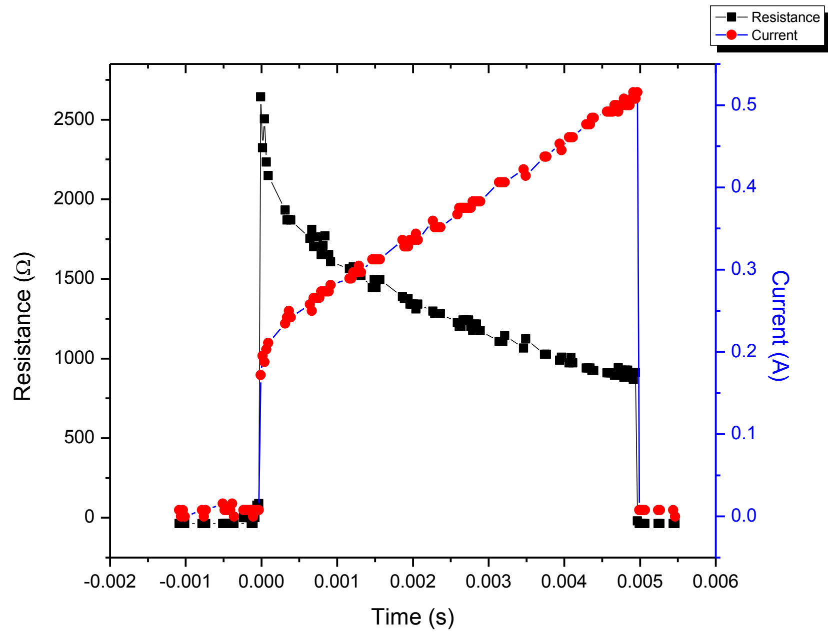

Figure 4.13: Resistance and current pulse for **Free_A8**.

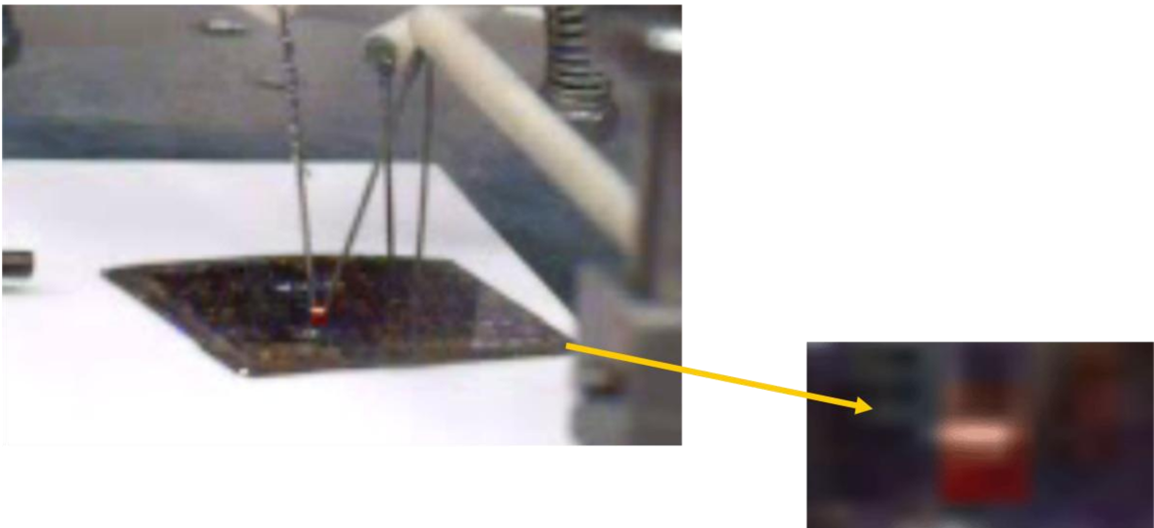

Figure 4.14: Image of resistor glowed during the high power pulse.

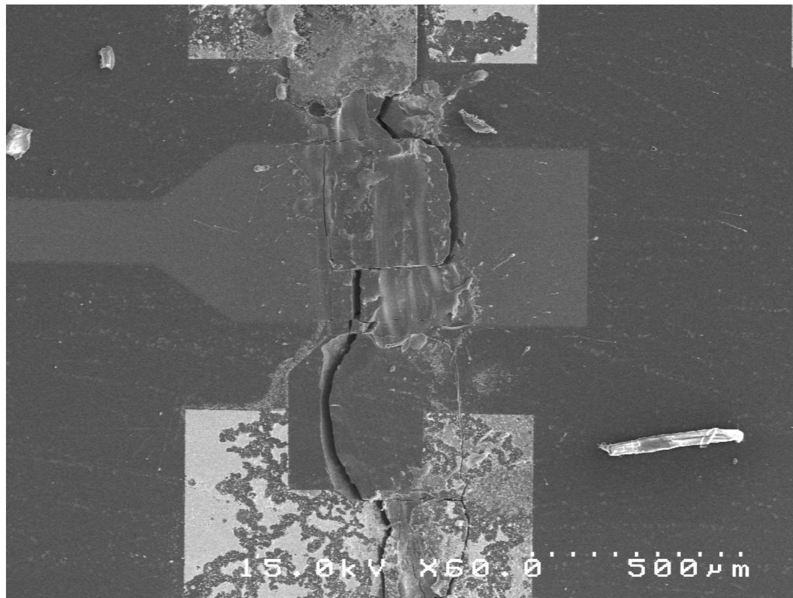

Figure 4.15: Resistor failed after the high **Free_A8** power pulse.

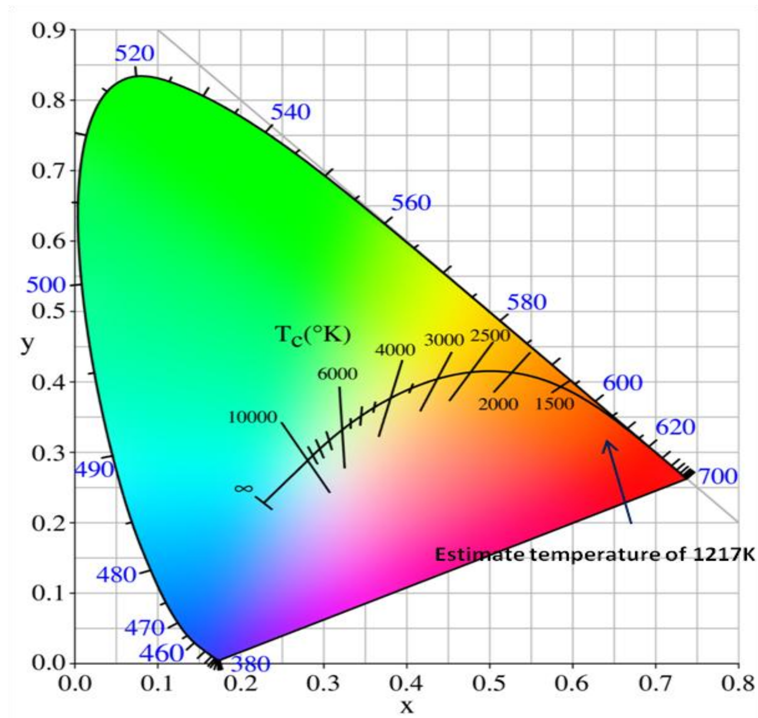

Figure 4.16: The arrow on the Planckian locus shows the blackbody's color for the estimated temperature before the failure.

4.4 Attached Diamond Resistors

In the following sections we will discuss the thermal behavior of the attached diamond resistors under lower and higher voltage pulses. We will also discuss the limit of the attached diamond resistors. Recall that the attached resistors were fabricated on a 1μm thick oxide layer (**Chapter III**). The oxide layer serves as a thermal isolation (48) to the substrate.

4.4.1 Lower Pulse Voltage Response Characterization

The attached diamond resistor described in *Section 3.2* and **Figure 3.8A** was examined under pulse conditions where the pulse duration and voltage were maintained low enough that the resistor would heat up to an equilibrium temperature as a result of the pulse power, and sustain said pulsing and not fail or suffer irreversible damage. This pulsing condition was determined by trial pulsing many resistors to failure and found to be a 60V pulse with a pulse frequency of 10Hz and 10% duty cycle. These conditions allowed us to observe how the diamond resistor behaves as it heats up under the effect of power pulses over a period of time. The measurements were then taken over time intervals. The power pulse is applied to the diamond resistor circuit (referred to as the circuit as described in *Section 3.5*) until steady state conditions are reached. The time and voltage across R_1 were recorded from the start of the testing and at 1 second intervals until there is no change in voltage drop across R_1 was observed. This condition indicates that the diamond resistor has reached steady state. This test was conducted on attached resistor **Att_C5**.

Figure 4.17 shows the input voltage pulse, the diamond resistor's resistance and current waveform recorded for the first pulse. The first pulse input power was ~1.03W and the dissipated power in the resistor was ~1.02W. The input and dissipated powers were calculated from Eqn. (3.6) and Eqn. (3.7) (**Chapter III**).

The above described test was performed on the attached resistor **Att_C5** with the intention to characterize the resistor under pulse heating that would reach a steady state condition (final temperature) and not suffer failure. As power pulses were applied, the diamond resistor retained heat (**Figure 4.18**) between pulses and the resistor's temperature increased. The temperature increase, due to Joule heating was presumed to reach a final temperature, which was determined by the thermal resistance associated with the resistor and its thermal environment (thermal equilibrium). It was observed that resistor **Att_C5** heated and showed minimal/no change for ~10s (from t=136s to t=147s). Then, continuing pulses resulted in further increase in the inter-pulse current as well as the intra-pulse (*within* the pulse) current as shown in **Figure 4.18**. The observed *transient* behavior indicates that resistor **Att_C5** *did not* reach steady state condition. The test was stopped when sparks were observed in the vacuum chamber after ~220s of pulsing. It appeared possible that the sudden current increase (inter-pulse; after ~150s of pulsing) might come from the development of a leakage path, e.g. through the oxide to the silicon substrate. The sparks may have then occurred due to electrical overstress (EOS) from the increased leakage current through the leakage path. EOS events typically induce failures either due to dielectric (oxide) breakdown (excessive voltage) or thermal runaway from Joule heating (excessive current). Other research indicates that field-

induced and current-induced degradation mechanisms complement one another and both are required to fully explain breakdown behavior over a wide range temperature (49), (50). According to Pantisano *et al*., the oxide breakdown that leads to a leakage current is a common failure mechanism when a thermal/electrical stress is present (51). The calculated temperature before the resistor was believed to have had leakage current was ~217℃. The temperature might not be high enough to cause damage to the oxide, but another factor known as time dependent dielectric breakdown (TDDB) could possibly contribute to oxide breakdown. It was observed that when a SiO_2 dielectric was placed under a fixed electric field, the oxide would breakdown with time (49). In this case, power pulsing for ~4 minutes could have led to the oxide breakdown. **Figure 4.19** shows the $R(t)$ corresponding to $i(t)$ of **Figure 4.18**.

In **Figure 4.20** the average current in each pulse vs. cumulative time of pulsing is plotted. The current increases not reaching a steady state even after 150s of pulsing was observed. The average temperature in each pulse over the pulsing time is shown in **Figure 4.21**.

As the temperature increases, this p-doped diamond resistor is, of course, undergoing changing (increasing) carrier (hole) concentration because more dopants are ionizing. However, in this case this effect may not be dominant as the final temperature reached before the omit of leakage current is low. This will be discussed further with the attached resistor pulsed at higher voltage.

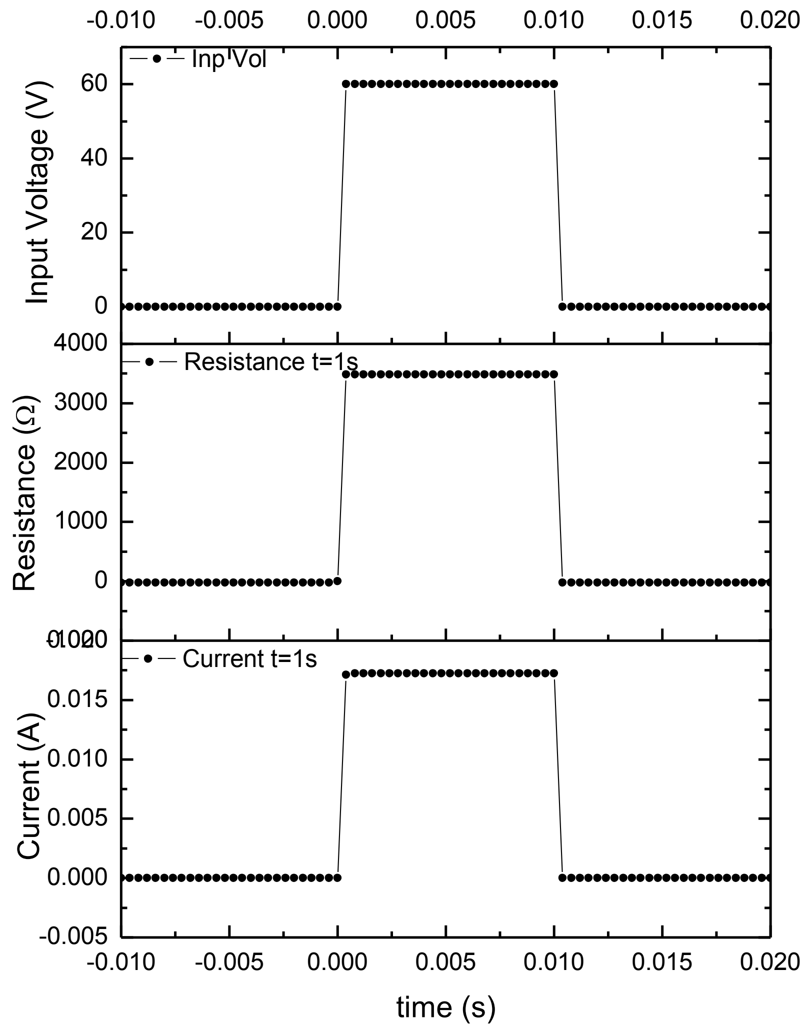

Figure 4.17: Input voltage and corresponding resistance and current waveform for resistor **Att_C5**.

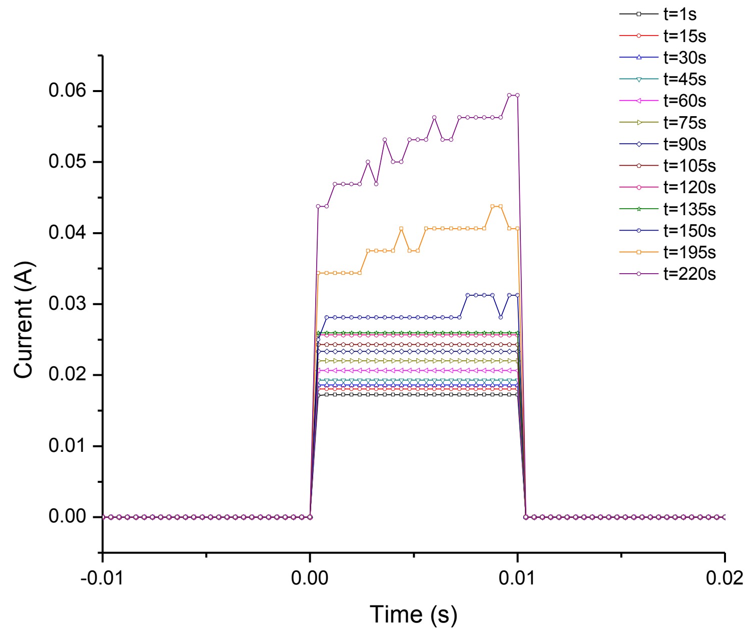

Figure 4.18: Change in the current over time (**Att_C5**).

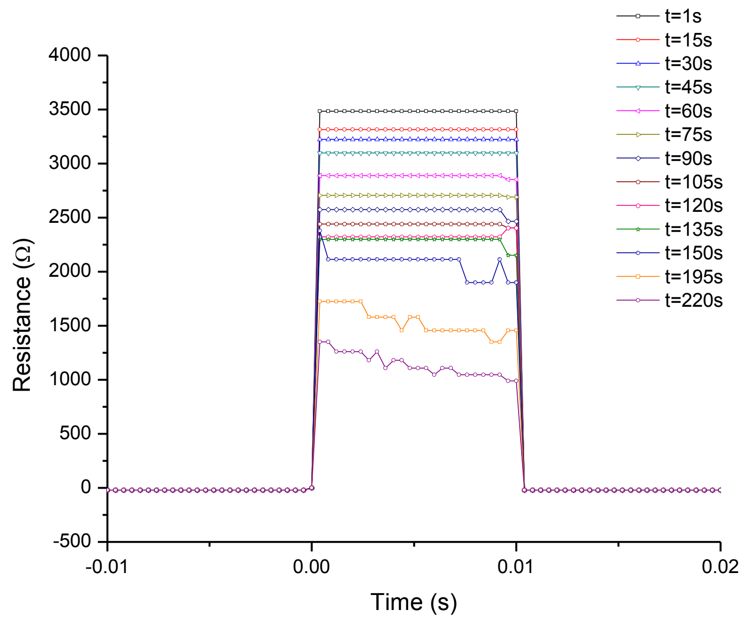

Figure 4.19: Corresponding change in resistance of $i(t)$ in Figure 4.18 over pulsing time.

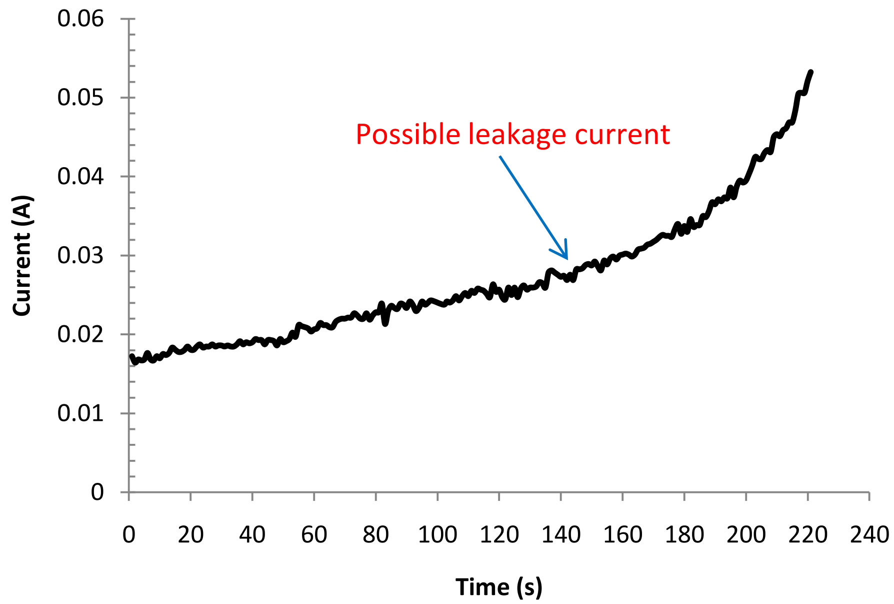

Figure 4.20: Average current per pulse over cumulative pulsing time for resistor **Att_C5**.

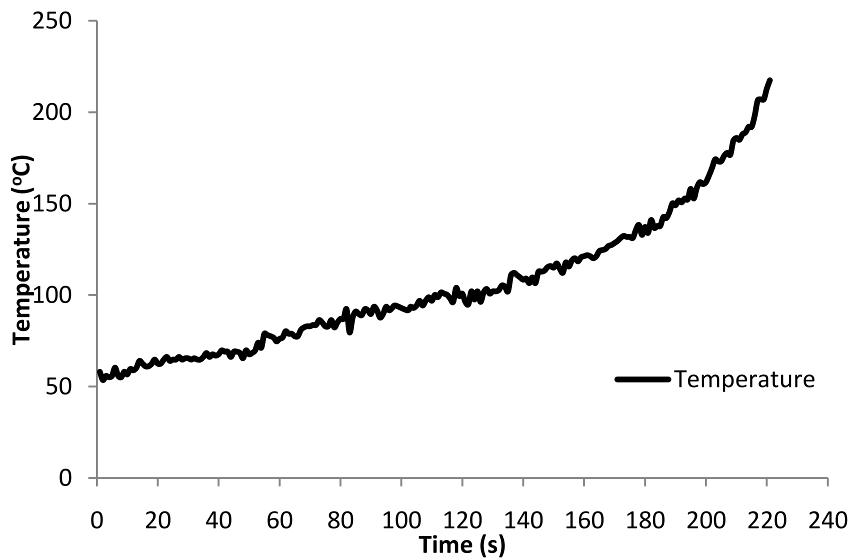

Figure 4.21: Calculated average temperature per pulse over cumulative pulsing time for resistor **Att_C5**.

4.4.2 Higher Pulse Voltage Response Characterization

We now consider the transient response of the attached diamond resistor as observed with a higher input voltage pulse. There are two resistors involved in this higher voltage pulse test; resistors **Att_C6** and **Att_C8**. The next pulsing condition was determined by further trials and a 100V pulse with a pulse frequency of 10Hz and 10% duty cycle was applied. This test was conducted on resistor **Att_C6.** Its room temperature resistance was ~5kΩ. The voltage drop across R_1 was recorded at 1 second time intervals. **Figure 4.22** shows the current over the pulsing time from t=1s to t=76s. The current was ~78mA in the first (t=1s) voltage pulse applied to the resistor. The resistance fell from its room temperature resistance to ~1.3kΩ.

The current increase in between pulses was minimal in the first 70s of the pulsing pulse and there was no visible change in the current intra-pulse profile. We then observed the current started to show transient behavior, the intra-pulse current increasing after t>72s. Apparently, the transient behavior was the onset again of the resistor developing a secondary conduction path, i.e. leakage current (**Figure 4.22**). The resistor's resistance before the leakage current occurred was ~620Ω and the estimated temperature was ~820°C. This is a temperature where it is probable that the oxide would breakdown and leakage arises. The indicated resistance then decreases during each pulse with continued pulsing as shown in **Figure 4.23**.

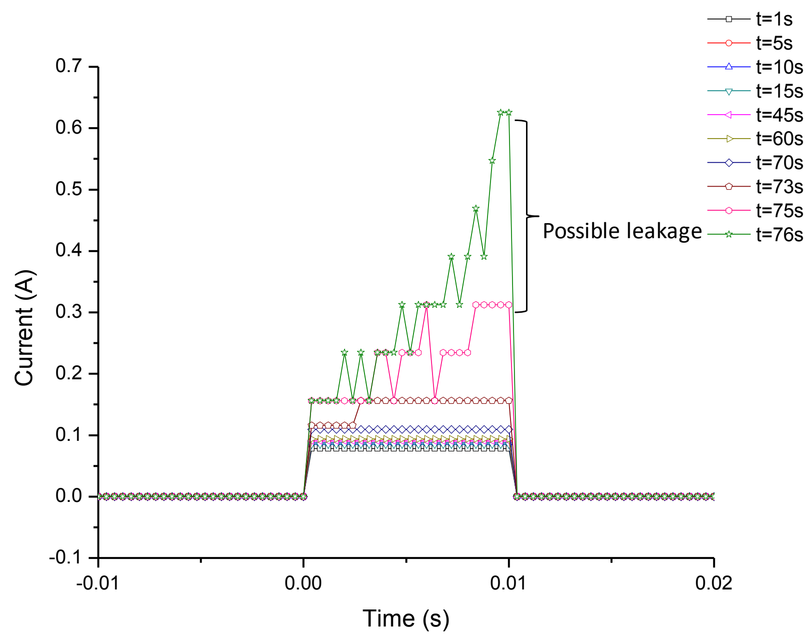

Figure 4.22: Current waveform for resistor **Att_C6** at 1s < t < 76s.The possible leakage current was observed after t > 73s.

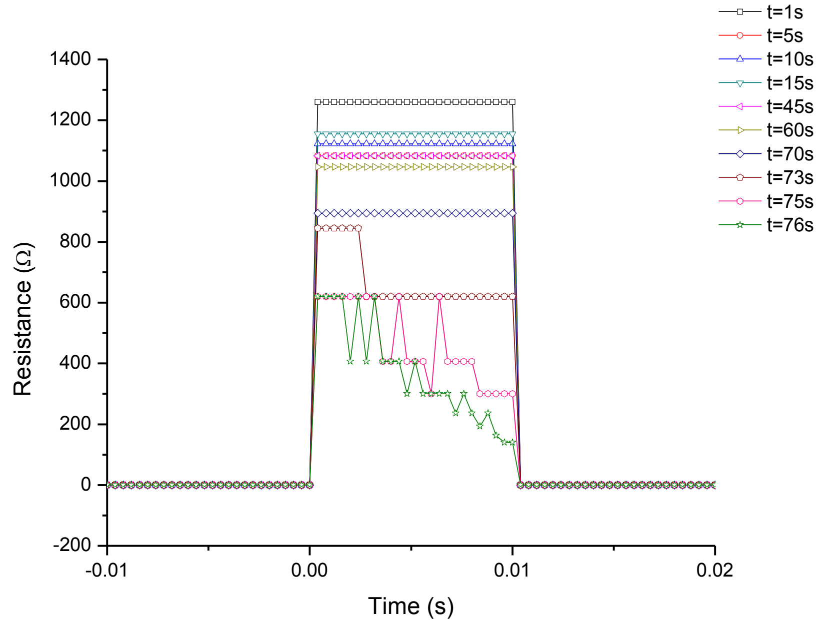

Figure 4.23: Corresponding resistance waveforms of $i(t)$ in Figure 4.22.

Figure 4.24 and **Figure 4.25** show the current and resistance respectively for t ≥76s. At this point, we note that there is a sharp current increase in the subsequent pulses indicating that the leakage current becomes more dominant. The resistance fell to a low of 10Ω at the peak of the current pulse. The test lasted for 110s of pulsing when sparks/arcing was observed in the vacuum chamber. The arcing occurred probably due to EOS of leakage current, shorting out the resistor. Thus, the 100V pulse test performed on resistor **Att_C6** lead to oxide failure and leakage to the substrate, confirming the observation with the prior resistor, **Att_C5**, that a limiting mechanism with pulsed attached diamond resistors is the oxide dielectric strength. The onset of leakage from this (100V pulse) test occurred abruptly. We wished to consider the mechanism in more

detail. With the experience from many trials and these two (60V and 100V) results, we conducted detailed pulse testing on a third resistor, **Att_C8**.

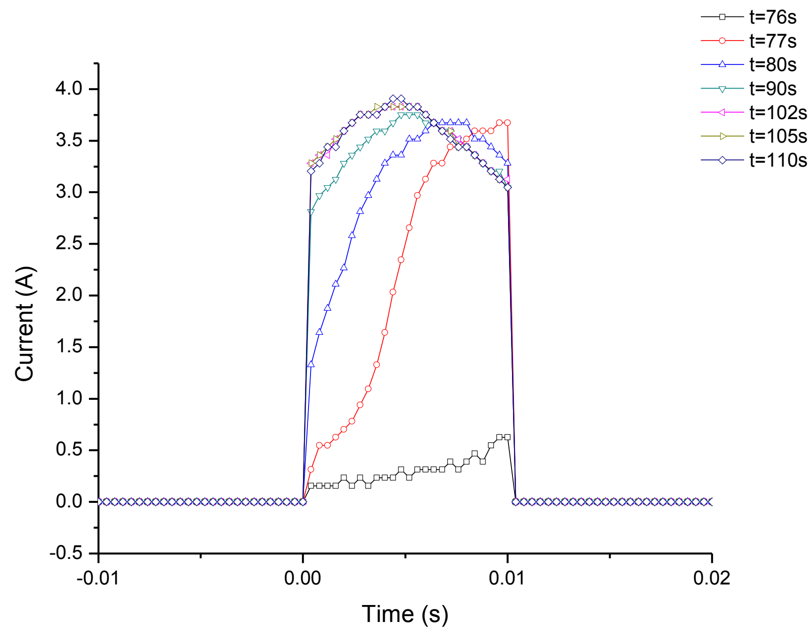

Figure 4.24: High leakage current observed in resistor **Att_C6** after $t \geq 76$s leading to electrical overstress.

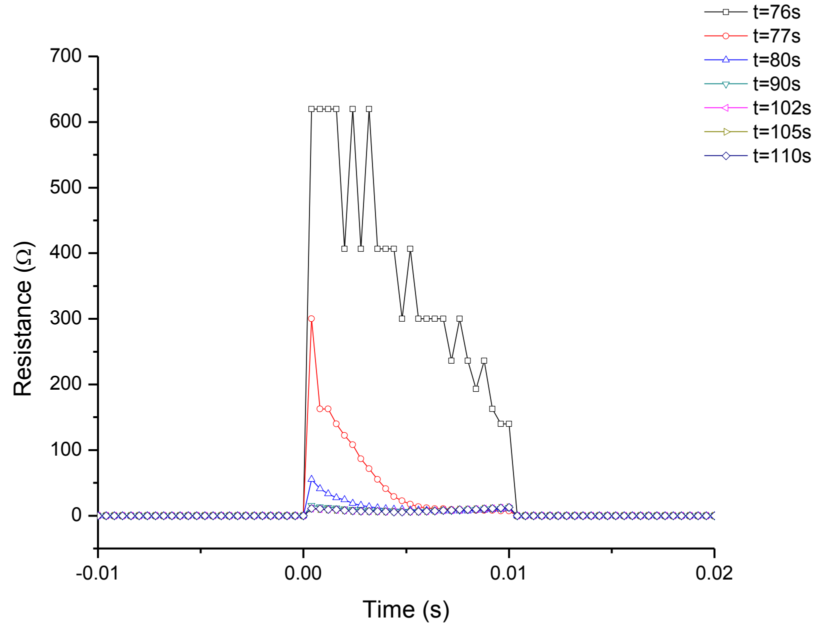

Figure 4.25: Corresponding resistance waveform of resistor **Att_C6** after t > 76s. Resistance became very low indicate it was failed to a short.

Given that the earlier test at 100V resulted in rapid resistor destruction, we reduced the voltage to examine the resistor in a more controlled manner the regime of resistor pulse response (i.e. *transient*) that would slowly lead to resistor failure. The voltage pulse was reduced to 80V and with the same pulse frequency and duty cycle (10Hz and 10% duty cycle). Although the 80V pulse is higher than the 60V pulse test, the experience gained from the prior trials and two pulse regimes allowed us to proceed with this test prepared to garner detail from high power behavior of attached diamond resistors.

The voltage drop across R_1 (equipment to the current flow though the diamond resistor, see discussion on test set up, *Section 3.3*) was recorded at 1 second time

intervals. This test was conducted on attached resistor, **Att_C8** with an initial room temperature resistance of ~5.2kΩ. (All resistors involved in this testing have the same dimensions as described in *Section 3.2*). In this test, a similar scenario as the 100V pulse test was observed, where initially minimal current increases between pulses occurred. The current was ~20mA for the first pulse and increased to ~22mA even after 115s of pulsing, when the resistance had dropped to ~4kΩ. At this point, the current pulse form in resistor **Att_C8** was similar to the previous 100V test on resistor **Att_C6**, with a longer period. **Figure 4.26** shows the typical current pulse form before 115s of pulsing. After t = 115s, a transient response was observed within a pulse. The typical transient response is shown in **Figure 4.27**, an increasing intra-pulse current. The corresponding resistance is shown in **Figure 4.28**.

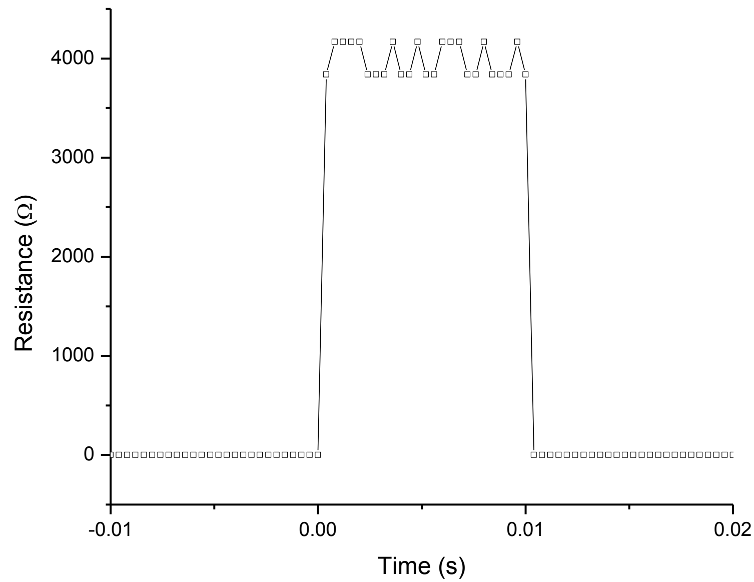

Figure 4.26: Typical resistance profile of resistor **Att_C8** shows near constant value of resistance in the pulse. In this display, the profile was at t = 70s.

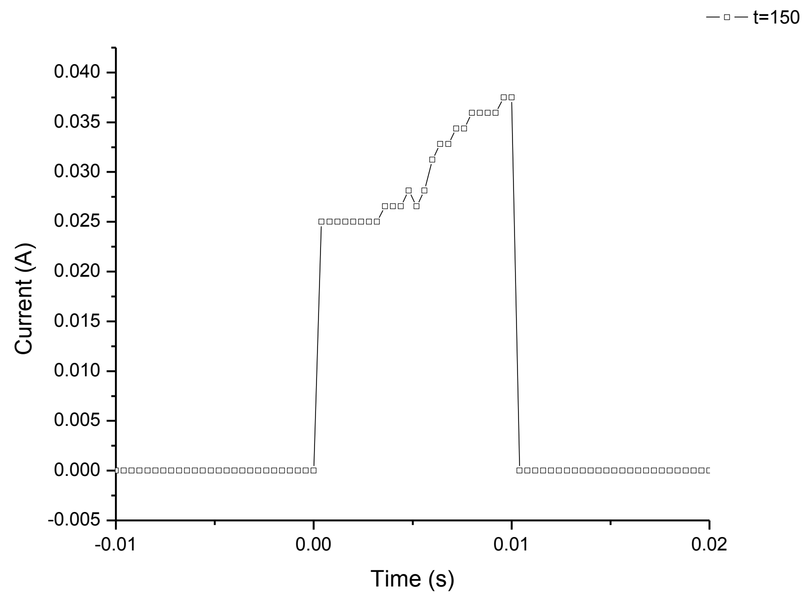

Figure 4.27: Current profile of resistor **Att_C8** at t = 150s.

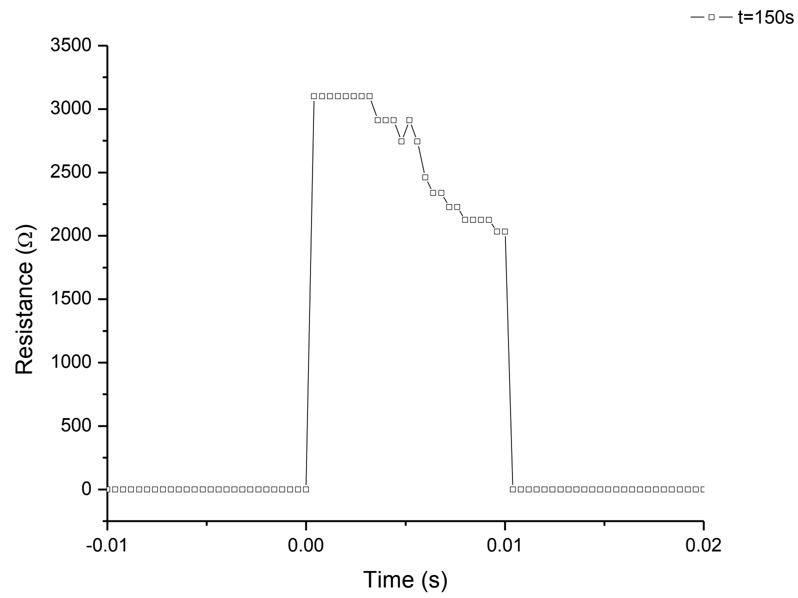

Figure 4.28: Resistance profile of resistor **Att_C8** at t = 150s shows resistance decreases across the pulse (transient).

Figure 4.29 shows the sequential current behavior of resistor **Att_C8** with successive pulses. Evidence of possible leakage current was observed when a sharp current increase was observed at pulse t = 164s. The temperature was calculated to be 553°C at t = 163s before the apparent leakage arose.

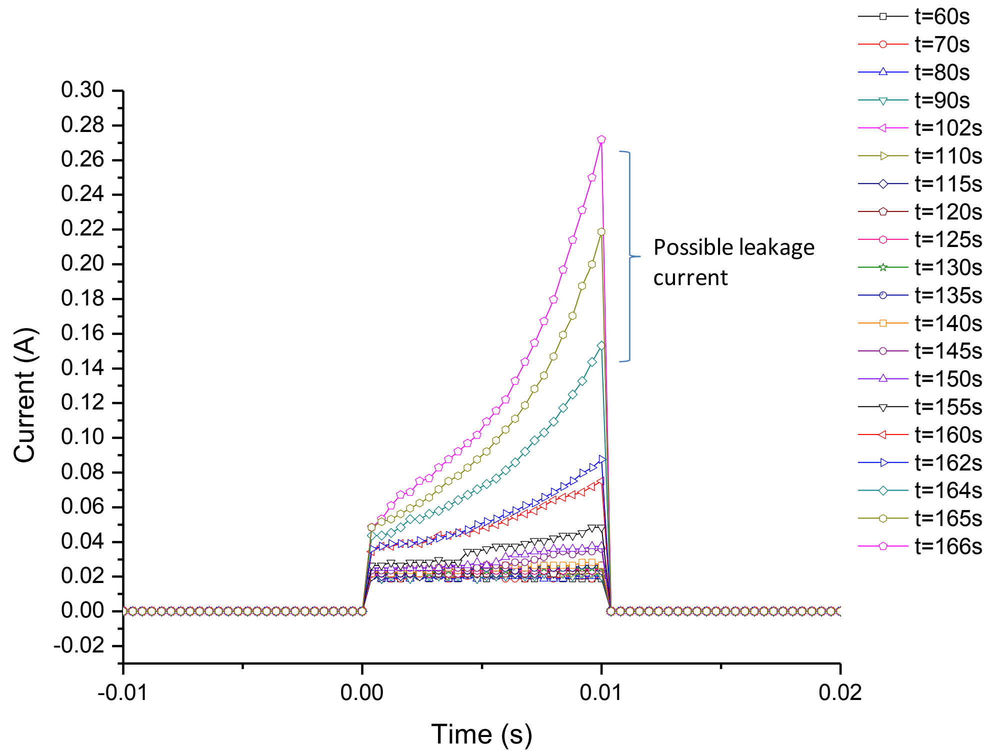

Figure 4.29: Sequential current behavior of resistor **Att_C8** with successive pulses for t > 60s. Possible leakage current was observed after 164s of pulsing.

Figure 4.30 shows $i(t)$ over the pulsing time before the observed current leakage. The effect of rising current after t > 140s and rising temperature occurring with each

pulse is apparent. The transient response in each of the later pulses is also visible. Concurrently, the average resistance in each pulse of the diamond resistor decreases as shown in **Figure 4.31** and falls off rapidly. Since the applied voltage was held constant during each pulse, higher average currents occurred with each succeeding pulse as shown in **Figure 4.32**.

We have reason to believe that before the onset of oxide breakdown and secondary leakage, we can observe the effect of carrier concentration increase from power heating and provide some quantitative interpretation of same. Consider in **Figure 4.32**, the characteristic of $i_{ave}(t)$ shows an *exponential* relationship. The exponential behavior occurs because the resistance decreases rapidly with increasing temperature. In this p-doped diamond resistor, the resistance decreases because the hole concentration, p, of thermally generated carriers is increasing, reducing the resistivity "faster" than the effect of decreasing carrier mobility that arises from increasing temperatures. The i.e., overall conductivity increases due to more holes available for conduction. This phenomenon was discussed in detail in *Boron Ionization in P-Doped Diamond, Section 2.4*.

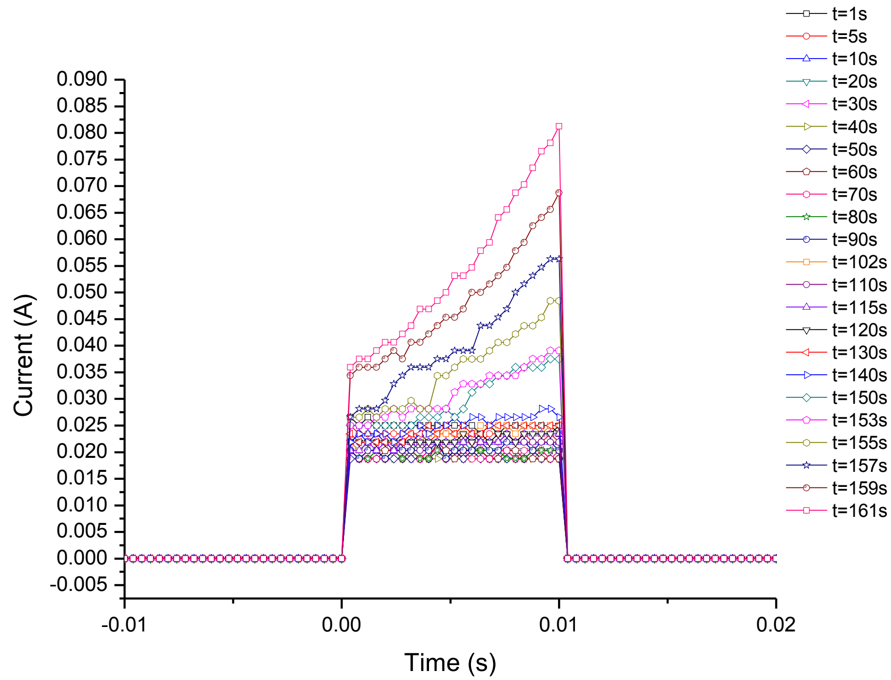

Figure 4.30: Sequential current behavior of resistor **Att_C8** with successive pulses over pulsing time before the leakage current.

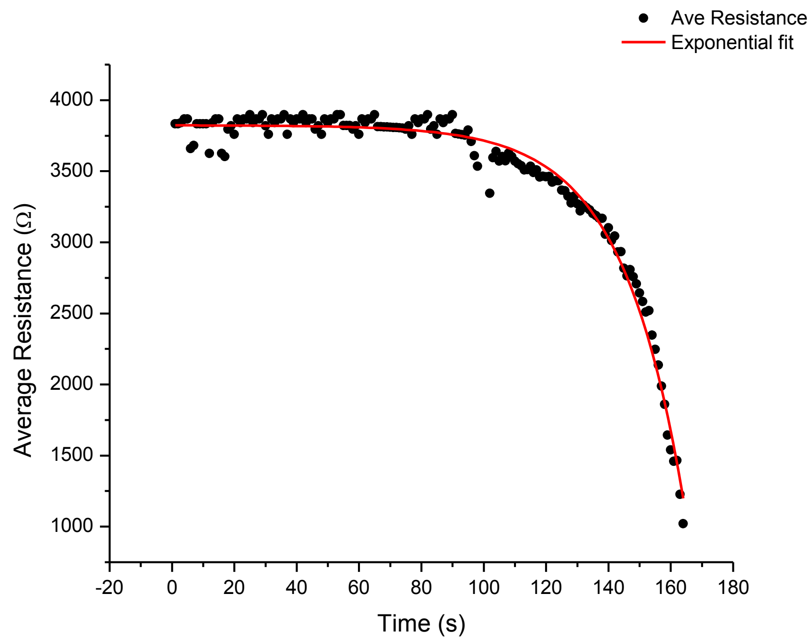

Figure 4.31: Plot of average resistance (in each pulse) over time before the leakage current.

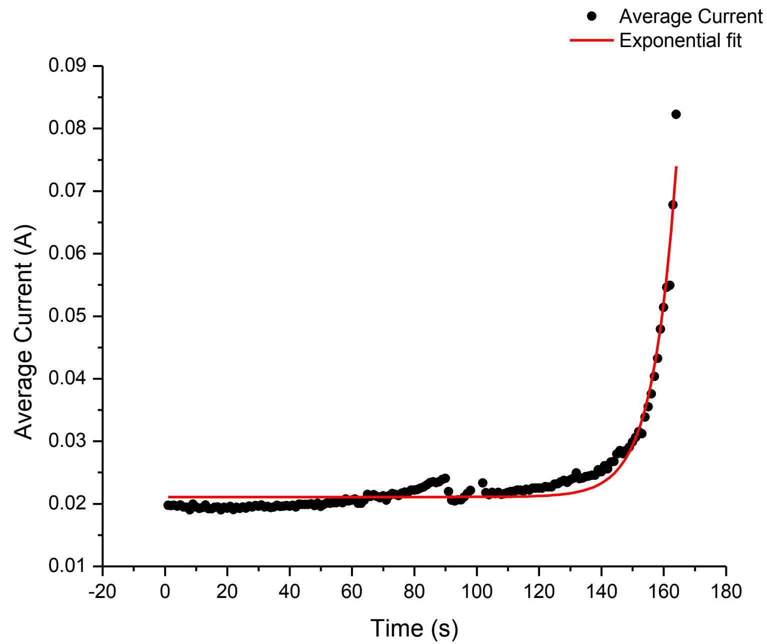

Figure 4.32: Plot of average current (in each pulse) over time.

Referring again to **Figure 4.30**, the Joule heating thus increases the resistor temperature, reduces its resistance and result in the current increase. The heat conduction to the substrate and surrounding environment contributes to the *linear* behavior observed in the current profile (intra-pulse). This is described by Fourier's Law of heat conduction, Eqn. (2.1);

$$q = -\kappa \frac{dT}{dx} \tag{4.10}$$

where q is the heat flux, or heat flow per unit area perpendicular to the flow direction (W/m^2), T is the local temperature (K or ^oC), x is the coordinate in the flow direction (m) and κ is the thermal conductivity (W/m·K) of the material. The *negative sign* indicates that heat is transferred in the direction of decreasing temperature.

The minimal increase in current, hence temperature observed at this point in this higher voltage pulse test was assumed to be due to the high thermal conductivity of diamond. The basic expression for thermal conductivity is

$$\kappa = \frac{1}{3} c_p v l \tag{4.11}$$

where c_p is the heat capacity of the thermal carriers per unit volume, v is their average group velocity in the direction of the thermal gradient, and l is their average mean free path between collisions. The factor 1/3 enters because the thermal gradient is principally only one direction in three-dimensional space, while the phonon wavevectors are distributed more or less isotropically, i.e., with the full symmetry of the crystal lattice which is cubic in the case of diamond (52).

With a band gap of 5.5eV, diamond is usually considered as an electrical insulator in which heat is carried only by phonons. For heavily doped diamond, the dopant (boron) can decrease the total thermal resistance by providing holes as heat carriers. Holes migrating through the resistor under the effect of the power pulse undergo different scattering events, namely scattering with phonons, ionized boron and vacancies as well as hole-hole scattering (53). This heat generated (Joule heating) in the resistor is due to the

flow of electricity within it and losing part of its energy to the vibration of the lattice (phonons).

The estimated temperature for each pulse is plotted in **Figure 4.33**. The temperature indicated was calculated from the temperature dependence of resistance (Arrhenius relationship, see *Section 4.2*). The calculated temperature at the pulse of t = 163s (prior to current leakage) was ~553℃.

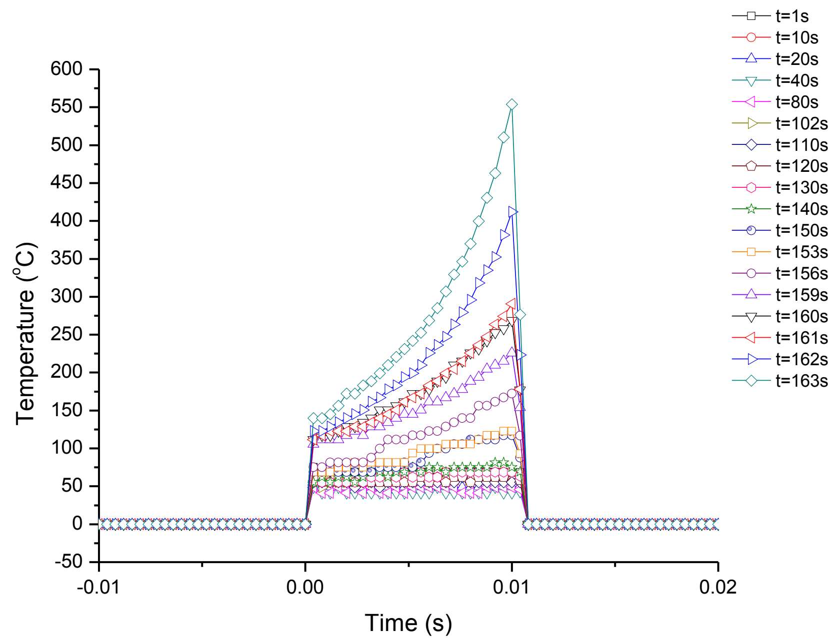

Figure 4.33: Sequential calculated temperature with successive pulses.

As the power pulses continue, the power dissipation in the resistor increases and increased Joule heating was observed. A plot of the average temperature-average power

relationship is shown in **Figure 4.34**. A straight line is observed for the average temperature range of 68°C to 276°C (341K – 549K) which suggests that the temperature increases approximately proportional to the power increase.

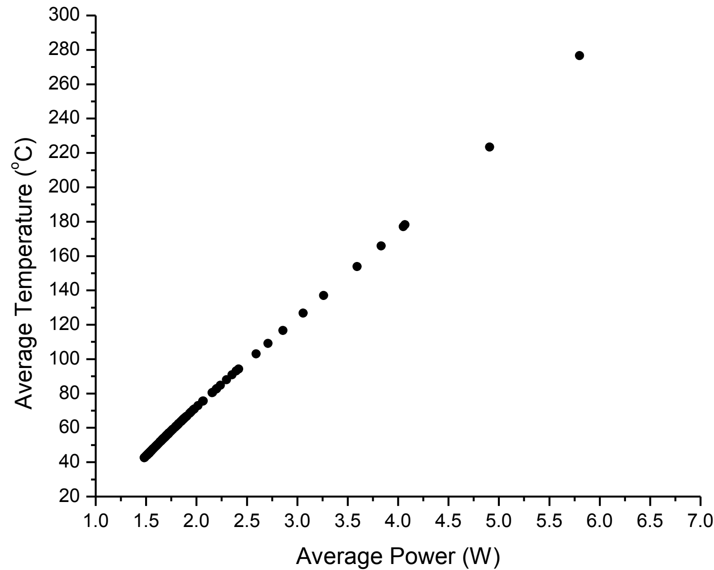

Figure 4.34: Plot of temperature vs. power shows that the temperature increases as the power increases.

The 80V pulse test on **Att_C8** was terminated due to arcing observed at the sample. The arcing occurred after the high leakage current was observed (**Figure 4.29**) in the last 5 seconds of pulsing. As was discussed earlier in *Section 4.4.1* that arcing occurred probably due to EOS from the increase of leakage current through a leakage path. EOS events typically induce failures either due to dielectric (oxide) breakdown (excessive voltage) or thermal runaway from Joule heating (excessive current). This is

known as stress induced leakage current (SILC). SILC has been shown to be one of the main problems in thin oxide MOS devices before the onset of soft or hard breakdown (54).

4.4.2.1 Discussion of the Rate of Change in Temperature over Pulsing Time

We will consider the effect of changing carrier concentration as the temperature increases over the pulsing time.

In the earlier discussion (*Section 2.3*), we stated that when power pulsing was applied to the circuit, the diamond resistor starts to warm up and when the power pulse is terminated, the resistor cools down but heat would be retained by the resistor. This phenomenon is a simple Joule heating mechanism that occurs in the diamond resistor. The power (I^2R) dissipated in the resistor causes the temperature to increase.

Concurrently, in these diamond resistors, as the temperature increases, the concentration of ionized boron dopants increases and more carriers (holes) are thermally generated. **Figure 4.35** is the plot of rate of change in temperature, dT/dt, over cumulative pulsing time for resistor **Att_C8.** The curve exhibits an *exponential* behavior.

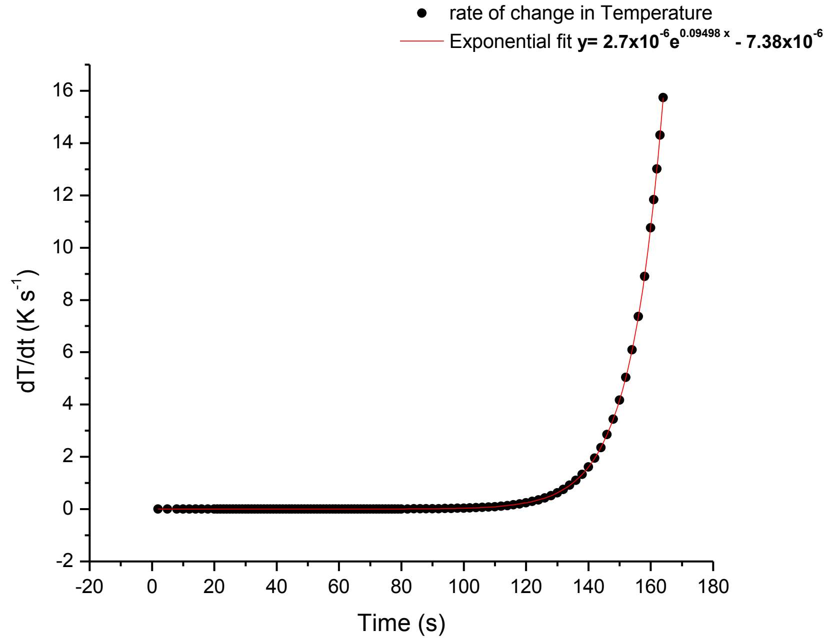

Figure 4.35: Plot of rate of change in temperature vs. cumulative pulsing time for resistor **Att_C8**.

Due to the fact that the attached resistors are sitting on a substrate (oxide layer), they can disperse heat through conduction. From the curve, at time, 1s < t < 120s there is minimal increase in the rate of change in temperature as all the heat is dispersed almost immediately. The high thermal conductivity of diamond speeds up the heat dispersion. In this case, the substrate acts as a heat sink, providing sufficient dissipation of the heat generated and keeping the power dissipated per unit volume low. This heat dissipation scenario establishes the $T(t)$ behavior in the attached resistors compared to freestanding resistors in the next section. A quasiuniform rate of change is maintained in the resistor's temperature profile. Keep in mind that in this scenario, as more holes are generated, the

system accommodates them and the resistivity decreases (conductivity increases) and the resistor doesn't warm up as quickly despite the accumulation pulses on it.

But as the power pulses continue, there comes an exponential increase in the rate of change in temperature in the last ~40s of the pulsing time before the resistor failed due to arcing. The temperature build up leads to decreasing resistance, increasing current and higher temperatures. The exponential increase in the temperature change would parallel an exponential increase in generated carrier concentration. The extra carriers that become available cause the resistor to decrease in resistance, which in turn allows more current to flow, thereby generating more resistive heating, leading to further drop in resistor resistance. This positive feedback cycle causes the temperature of the resistor to rise exponentially.

4.4.3 Examination of Power and Current at the Attached Diamond Resistor Limit

It is noteworthy to observe the maximum electrical limits for attached diamond resistors. **Table 4.2** shows the parameters upper limit for both resistors, **Att_C6** and **Att_C8**. These limits are prior to the observed leakage currents. Both resistors have the same dimension (see *Section 3.2*), however, resistor **Att_C6** was pulsed with 100V pulse and resistor **Att_C8** was pulsed with 80V. In the earlier discussion, we noted that the 100V test for **Att_C6** resulted in more rapid resistor onset of leakage and destruction. Therefore less data were taken during transient response regime. Even though resistor **Att_C6** failed sooner than **Att_C8**, both resistors have nearly the same limit in current and power density. The limits of the attached resistors are influenced by the dielectric

integrity of the thermal oxide layer as it warms up and is a subjected to a strong electric field.

Table 4.2: Parameters upper limit for attached resistors observed before leakage current.

	Resistor Att_C6	**Resistor Att_C8**
Maximum current (A)	0.16	0.15
Maximum power (W)	15.14	9.9
Maximum current density* (A/cm^2)	5.79E+04	5.67E+04
Maximum power density* (W/cm^2)	5.61E+06	3.67E+06
Maximum temperature (^oC)	820	553
Time of pulsing (s)	73	164

*****area (cm^{-2}) refers to cross section of the resistor

Though both attached resistors were tested with different power pulses, it is interesting to comprehend how the different levels of power pulse affect the resistor behavior; e.g. temperature. **Figure 4.36** shows the *average* power dissipation (for each pulse) vs. the calculated *average* temperature for both diamond resistors in one plot. The plot shows that resistor **Att_C6** which was pulsed at higher voltage dissipates more average power for the same given calculated average temperature compared to the resistor pulsed at a lower voltage (**Att_C8)**. As the power in each pulse increased, the resistor's temperature continued to rise which caused the resistance to decrease, as shown in **Figure 4.37**, due to its negative temperature coefficient. The plot is the average values of resistance plotted against the average values of current density in each pulse for both

attached resistors. The limit of the diamond resistor will be discussed in further detail with regards to the freestanding resistor in *Section 4.5.3*.

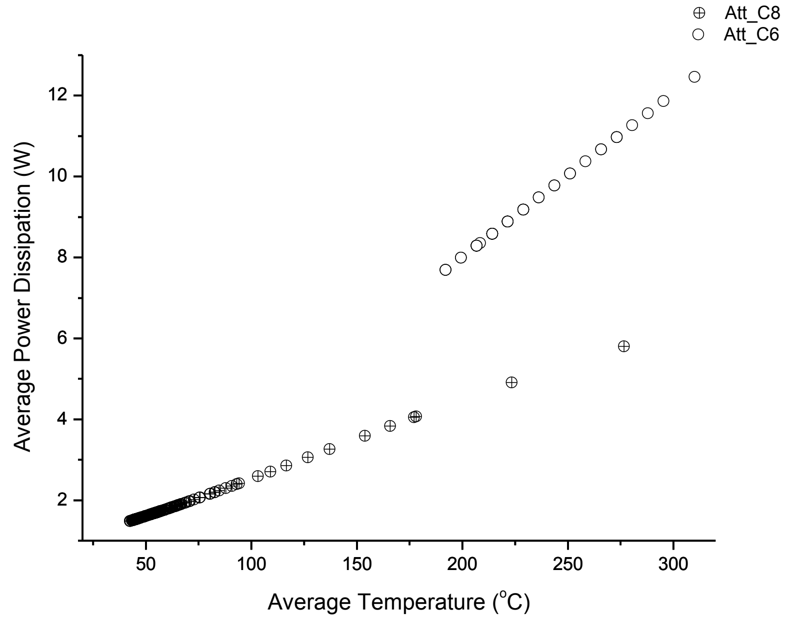

Figure 4.36: Average power dissipation vs. calculated average temperature for both resistors **Att_C8** and **Att_C6**.

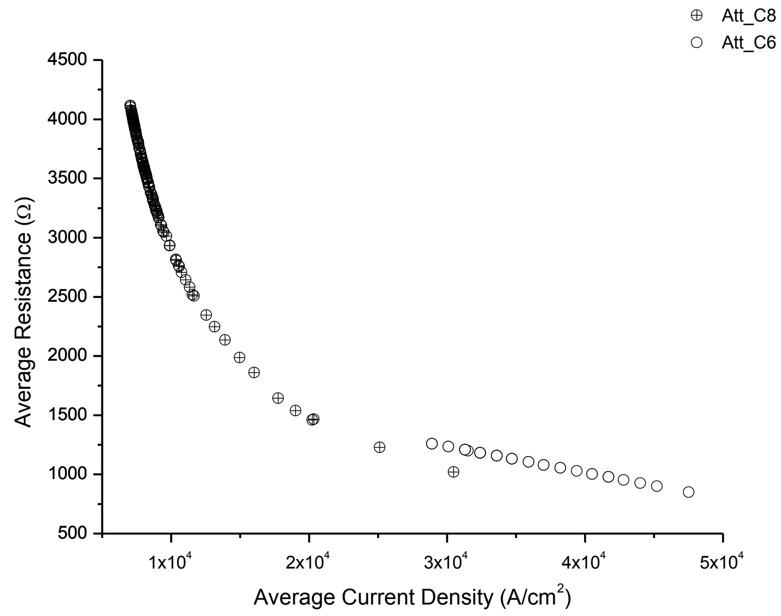

Figure 4.37: Average resistance vs. average current density over pulsing intervals for both resistors **Att_C8** and **Att_C6**.

4.5 Freestanding Diamond Resistors

We now turn our attention to the freestanding diamond resistors. In the following sections, we will discuss the thermal behavior of the freestanding diamond resistors under lower and higher voltage pulses as well as the limit of the resistors. This will allow us to view the differences between the attached and freestanding diamond resistor under similar power pulse conditions.

4.5.1 Lower Pulse Voltage Response Characterization

The freestanding diamond resistor described in *Section 3.2* and **Figure 3.10B** was examined under pulse conditions where the pulse duration and voltage were maintained low enough that the resistor would heat up to an equilibrium temperature as a result of the pulse power, but could sustain said pulsing and not fail open or suffer irreversible damage. This pulsing condition was determined by trial pulsing and found to be a 60V pulse with a pulse frequency of 10Hz and 10% duty cycle. These conditions allowed us to observe how the diamond resistor behaves as it heats up under the effect of power pulses over a period of time. The 60V is lower than the voltage levels that led to the resistors failing open. The measurements were then taken over time intervals. The power pulse is applied to the diamond resistor circuit (referred to as the circuit as described in *Section 3.3*) until steady state conditions are reached. The time and voltage across R_1 were recorded from the start of the testing and at 3 seconds intervals until no change in voltage drop across R_1 was observed. This condition indicates that the diamond resistor has reached steady state. This test was conducted on resistor **Free_A10**.

Figure 4.38 shows the input voltage pulse, the diamond resistor's resistance and current waveform recorded for the first pulse. The first pulse input power was 0.30W and the dissipated power in the resistor was 0.29W. The input power and dissipated power were calculated from Eqn. (3.6) and Eqn. (3.7) (**Chapter III**). The current fell to a constant value at an input power level of ~0.4W after approximately 180 seconds of pulsing. The temperature increases as power increases. The current remains unchanged from the magnitude of the previous pulse at steady state.

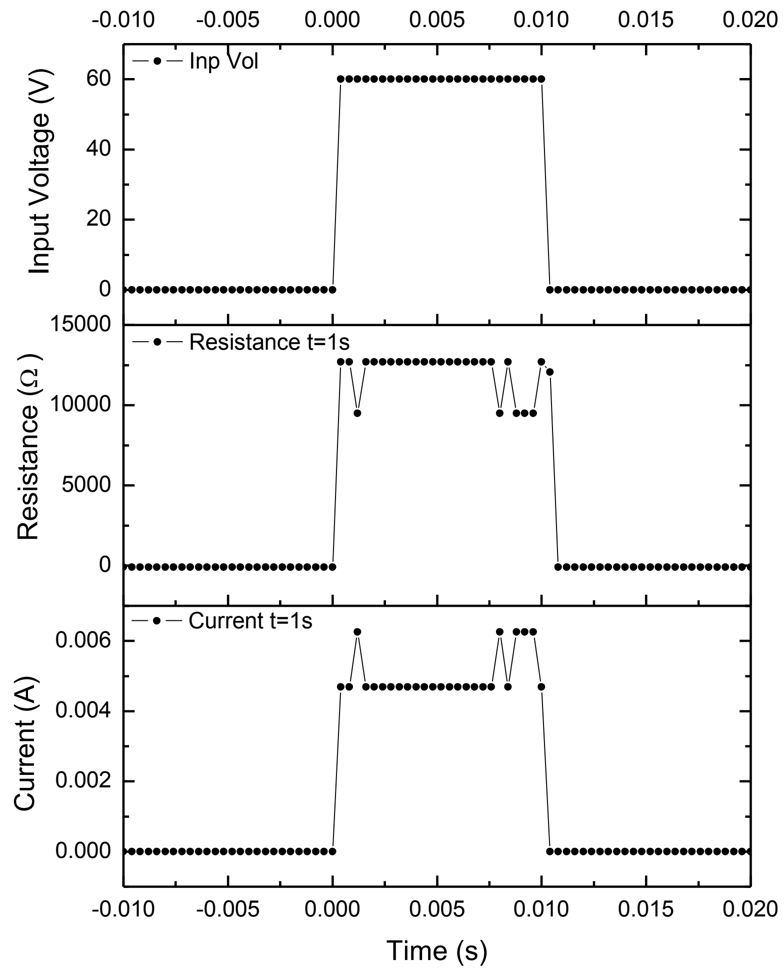

Figure 4.38: Input voltage and corresponding resistance and current waveform for resistor **Free_A10**.

As the train of power pulses was applied, the diamond resistor retained heat (**Figure 4.39**) between pulses and the resistor's temperature increased until it reached a stable condition and a final temperature, relative to the *constant* voltage of the pulses. The final temperature is determined by the thermal resistance associated with the resistor and its thermal environment i.e. attached or freestanding, in this case, the latter.

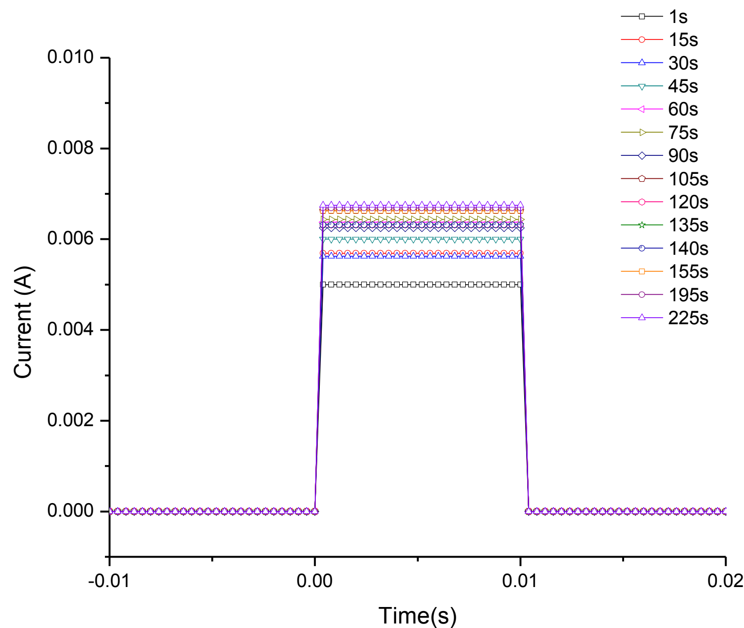

Figure 4.39: Change in the average current over time.

Similar behavior was observed pulsing the diamond resistor, **Figure 4.40,** where the average current in each pulse vs. cumulative time of pulsing is plotted. The current increases, reaching a steady state average after nominally 150s of pulsing. The resistor

could withstand this pulsing lower level of voltage indefinitely, hence it reached a stable steady state of pulse loading and an estimated temperature of 79°C (**Figure 4.41**).

The increasing temperature causes the diamond resistor to have an increasing hole concentration due to ionization. Conversely, this effect is insignificant as the final temperature reached at the steady state is low. This occurrence will be discussed in more detail under higher voltage pulsing.

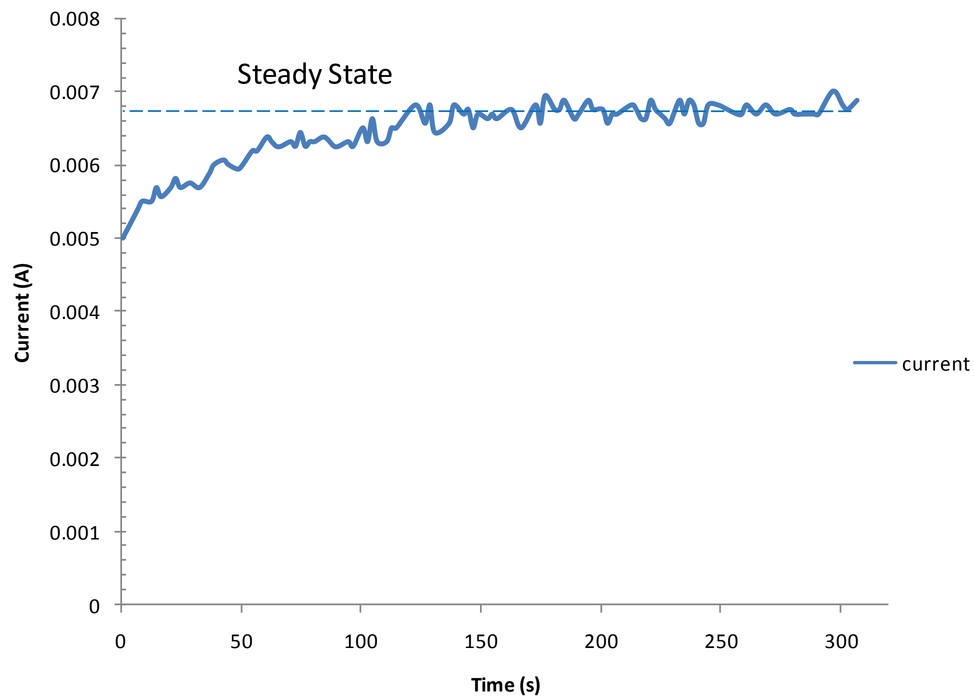

Figure 4.40: Average current per pulse over cumulative pulsing time for resistor **Free_A10**.

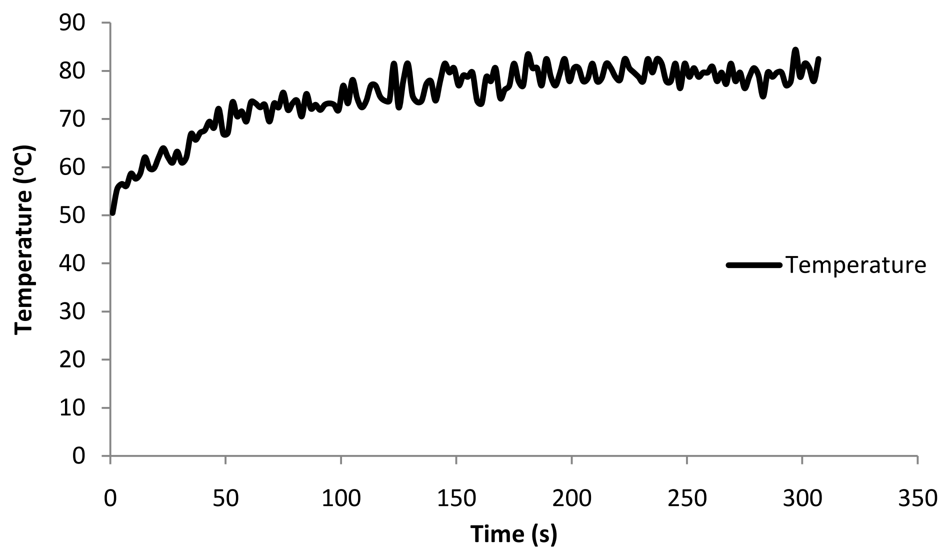

Figure 4.41: Calculated average temperature per pulse over cumulative pulsing time for resistor **Free_A10**.

The time: temperature dependence of the diamond resistor is obviously subject to the heating and cooling transiency that occurs during a pulsing event performed at higher voltages. As stated previously, when power pulsing is applied to the circuit, the diamond resistor will start to warm up (*Joule heating*) and when a power pulse terminates, the resistor will cool, but heat will be retained by the resistor (the heating and cooling principles will be identical, see **Figure 4.42**. If the pulse off-interval is short and/or the voltage (power) on-interval is high, then the resistor does not return to ambient temperature before the next pulse arrives, the resistor's resistance will be less and the temperature higher. Thus there can be a condition of pulsing where thermal stability is not reached (**Figure 4.43**). Even though the next pulse is identical in voltage (by test intent), the temperature of the resistor at the end of the pulse is greater than the previous pulse. Further pulses increase the temperature but a stable situation may be achieved relative to the level of the power pulse employed. In other words, if the pulses are sufficiently close together, the temperature decline between pulses does not decay completely before the start of the next pulse. Furthermore, the peak temperature in the resistor reached from a given train of power pulses is less than the steady-state temperature at the same power applied DC, the resulting curve has a sawtooth waveform that trends upwards (so-called *envelop*). If the pulse voltage is low enough, a quasi steady state is reached as seen in **Figure 4.40** and observed in **Figure 4.43**. The mathematical model of this phenomenon was discussed in *Section 2.6*.

However, if the voltage is higher, the resistor may not plateau in temperature, but instead continually warm up to destruction. The pulsing conditions under which one or

the other occurs are of interest. We now examine the higher voltage condition that leads to resistor failure for the freestanding resistor.

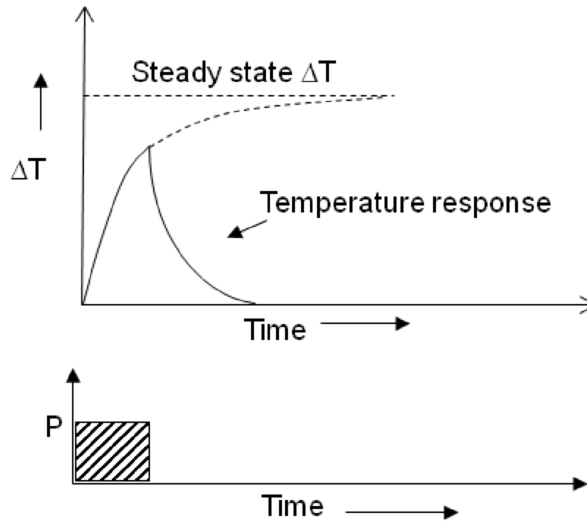

Figure 4.42: Heating and cooling follow the same principle

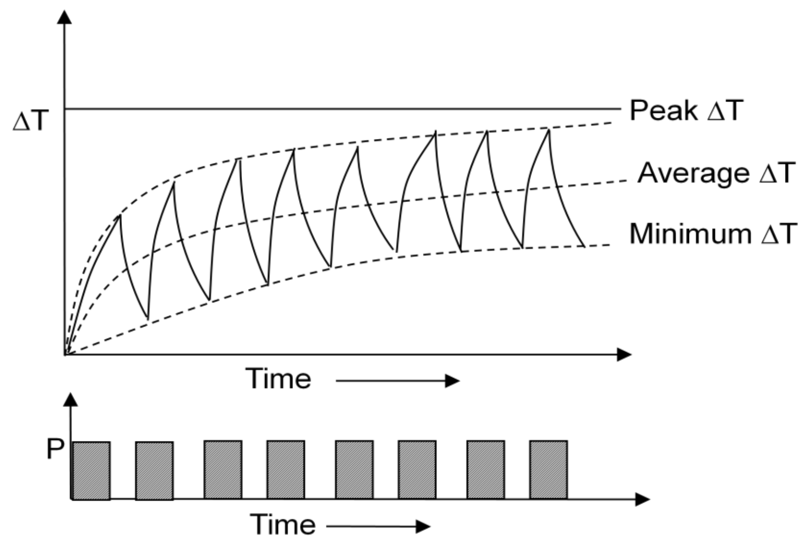

Figure 4.43: The peak temperature in the resistor reached from a given power pulse can be less than the steady-state temperature at the same power applied DC.

4.5.2 Higher Pulse Voltage Response Characterization

We now consider the transient response of the freestanding diamond resistor as observed with a higher input voltage pulse. In the earlier test on resistor **Free_A5** (*Section 4.3*), it was observed that the resistor had a dynamic intra-pulse response with a 160V voltage pulse, where the resistor heated up and failed too quickly to examine its pulse power behavior to the detail we wanted. In this pulse test, the voltage was set to 120V to examine the response. Given that the earlier test at 160V resulted in rapid resistor destruction, we reduced the voltage to hopefully examine in a more controlled manner the regime of resistor pulse response that "slowly" led to resistor failure. This test was conducted on the same resistor used in the lower pulse voltage test, resistor **Free_A10.** Other than the voltage being set at 120V, the pulse profile is per the previous experiments, namely 10Hz and 10% duty cycle. The voltage drop across R_1 was recorded at 1 second interval (please refer to the earlier discussion on the test setup). The test lasted 80s before the resistor failed open.

Through the duration of the 120V pulsing test, the overall current assumes an increasing "sawtooth" form as shown in **Figure 4.44**. Each value plotted for the $i(t)$ response of **Figure 4.44** is the minimum and maximum value of the start and end of the on state of each current pulse (**Figure 4.45)** and plotted vs. cumulative time of the test. The inset of **Figure 4.44** shows an enlarged region of the $i(t)$ curve over a larger time scale in the last 10s of the pulsing time. **Figure 4.45** will be discussed in detail in the following segment. *Note: A similar current waveform profile of **Figure 4.45**, was also observed in other freestanding resistor, **Free_B11**, see **Appendix C** for details*. Back to **Figure 4.44**, we note at $t <$ 20s the sawtooth amplitude is not as pronounced as it is at $t >$

55s. The overall character of the variation of the output quantity of the pulse system follows the *envelop* expressions (*Section 2.6*) where curves joining the maximum and minimum values of the output quantity in the transient process are imposed.

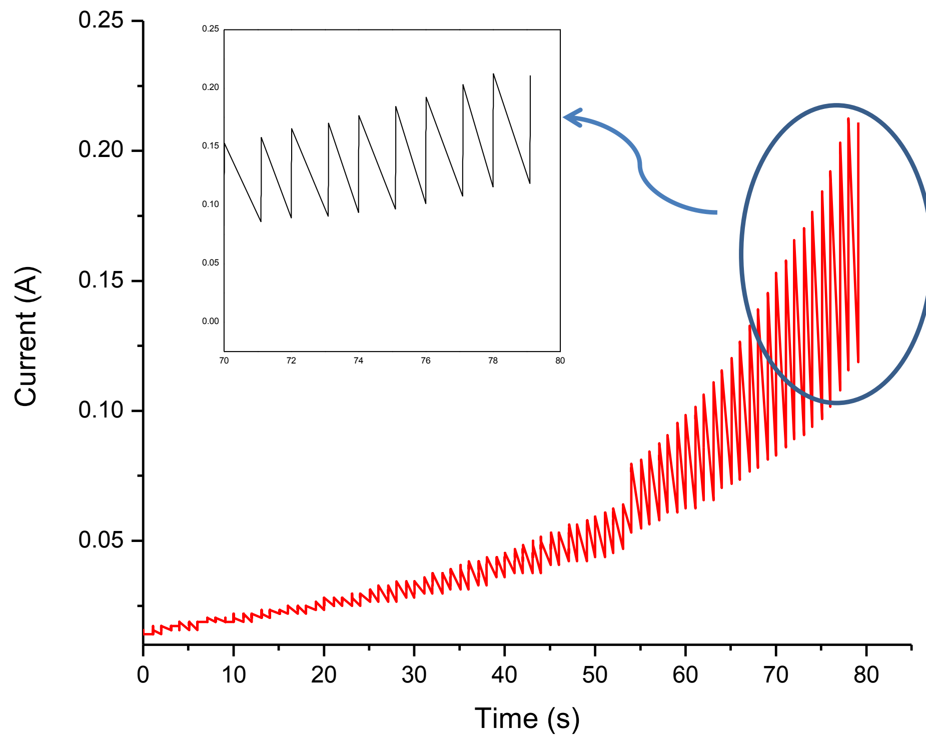

Figure 4.44: Current waveform over time shows that the sawtooth effect is less pronounced when t < 20s but is more marked when t > 55s.

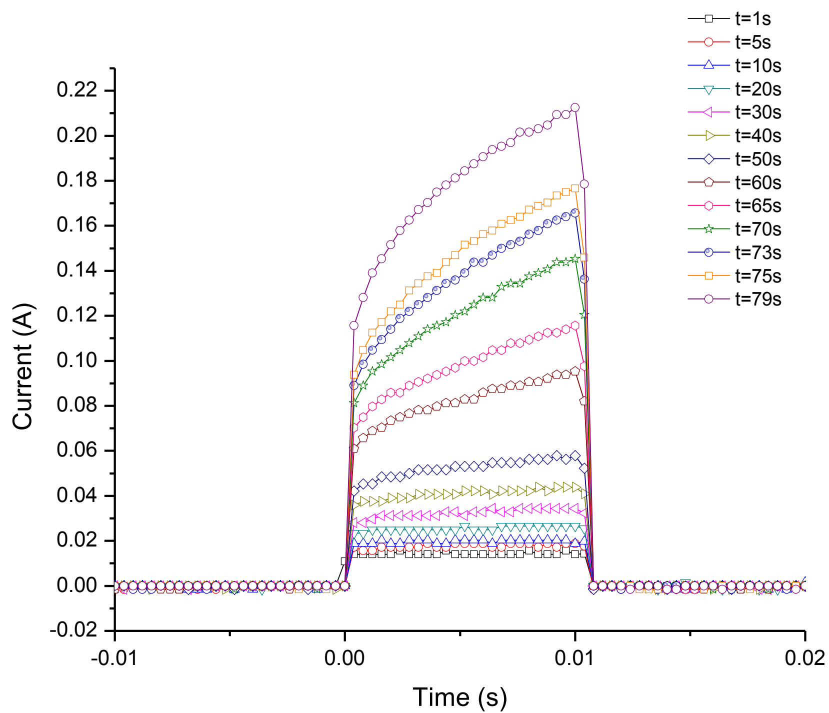

Figure 4.45: Sequential current behavior with successive pulses.

In **Figure 4.45** the effect of rising current and thus temperature occurring with each pulse is apparent. Concurrently, the resistance of the diamond resistor decreases as shown in **Figure 4.46** and since the applied voltage was held constant during each pulse, higher currents occurred in the diamond resistor with each succeeding pulse as shown in **Figure 4.45**. As previously mentioned in the attached resistor, higher voltage pulse discussion, a similar principle can be applied to the freestanding resistors. The resistance decreases because the concentration, p, of thermally generated carriers is increasing at a rate that reduces the resistivity "faster" than the thermally generated carriers exceeds the rate of decrease of carrier mobility that arises from increasing temperatures. The details on this phenomenon can be found under *Boron Ionization in P-Doped Diamond, Section 2.4*.

Figure 4.47 shows the plot of average current in each pulse over the pulsing interval. (The minor transient in the data at t~55s was a test anomaly not related to resistor behavior.)

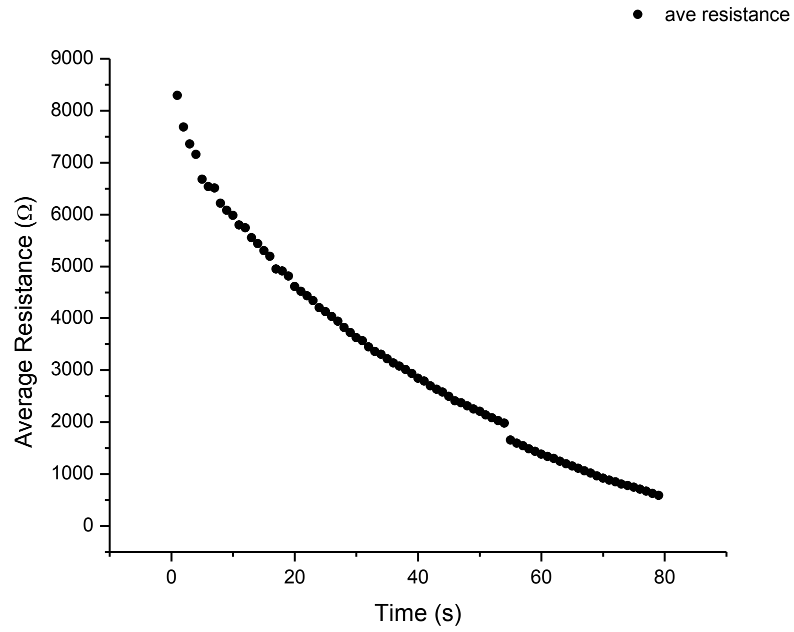

Figure 4.46: Plot of average resistance (in each pulse) over time.

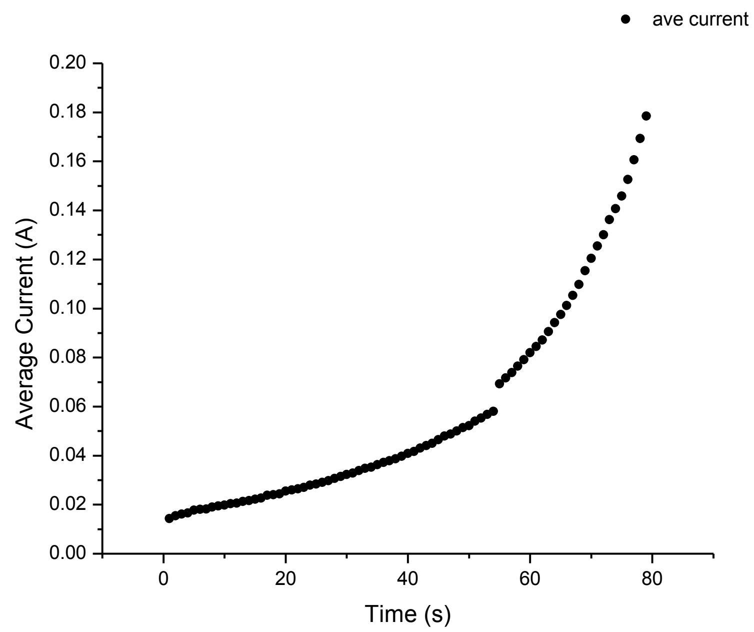

Figure 4.47: Plot of average current (in each pulse) over time.

The diamond resistor failed open circuit after 80 seconds total time elapsed or ~8000 pulses. The current increased in a power relationship (will be discussed in detail later, see **Figure 4.53**) before the resistor failure. This increase was recorded every 1s as shown in **Figure 4.45**. The resistance decreased as the resistor heated up, and because we were providing a constant voltage pulse, a corresponding increase in current occurred. The room temperature resistance of resistor **Free_A10**, prior to the testing was 16kΩ. The first pulse heated the resistor (**Free_A10**) such that its resistance fell to 8.4kΩ. The resistance continued to fall with ongoing pulsing until it reached the lowest value of 468.6Ω at the highest current. The resistor experienced enough resistive heating to cause a visual illumination in the form of a "red hot" glow, and it's temperature was definitely $>$ ~800°C. As shown in the preliminary test section, *Section 4.3*, the *radiant* phenomenon was also observed in the other freestanding resistor, **Free_A8**, see **Figure 4.14**.

The calculated temperature for each succeeding power pulse is plotted in **Figure 4.48**. The temperature shown was calculated from the temperature dependence of resistance (Arrhenius relationship). The calculated temperature at the peak of the *pulse* at t = 79s (prior to resistor failure) was ~3227°C which is improbably hot.

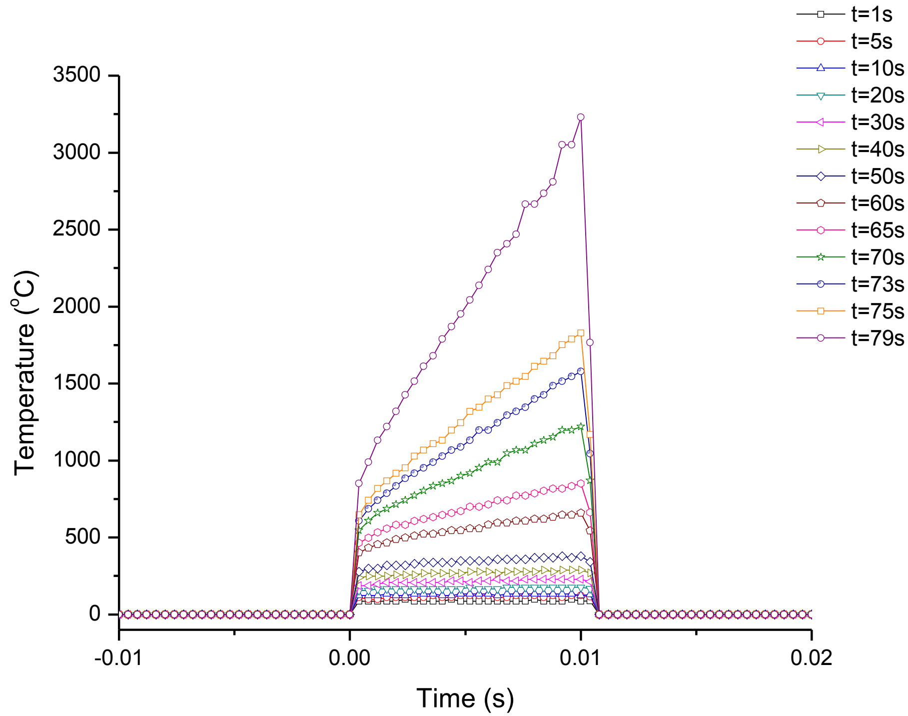

Figure 4.48: Sequential calculated temperature with successive pulses.

This anomalous high temperature from the calculation would be a predictable deviation from the Arrhenius relationship. This deviation can be explained by the findings of a study, that non-Arrhenius behavior was observed at elevated temperatures in doped semiconductors (55). The study concluded that the non-Arrhenius behavior occurred because of two scenarios. In the first scenario, the energy levels of holes on acceptor band states have a broad energy distribution, and in the second scenario, the density of states of the extended band states in the vicinity of the band edge possesses a low-energy exponential tail. Both of these scenarios lead to a nonlinear shift of the Fermi level as a function of temperature and thus results in a non-Arrhenius temperature

dependence of the resistivity (55). Therefore, the anomalous high temperatures in the high temperature regimes calculated simply from the Arrhenius relationship in **Figure 4.48** are believed to be accurately overestimated. In these high temperature regimes, the boron dopants are believed to have reached a state of full ionization and thus have a broad energy distribution in the energy levels of holes on acceptor band states. As discussed by Michel *et al*. that this scenario contributes to a non-Arrhenius relationship of temperature dependence of resistivity. This consideration is relevant at these high temperature regimes.

A plot of the average temperature-average power result is shown in **Figure 4.49**. A linear response is first observed in the temperature range (as estimated from Arrhenius behavior, *Section 4.2*) of 88°C to 870°C which suggests that the temperature increases proportional to the power (Joule heating). However, the non-linear increase in temperature at higher power suggests a different mode of heat transfer is becoming dominant.

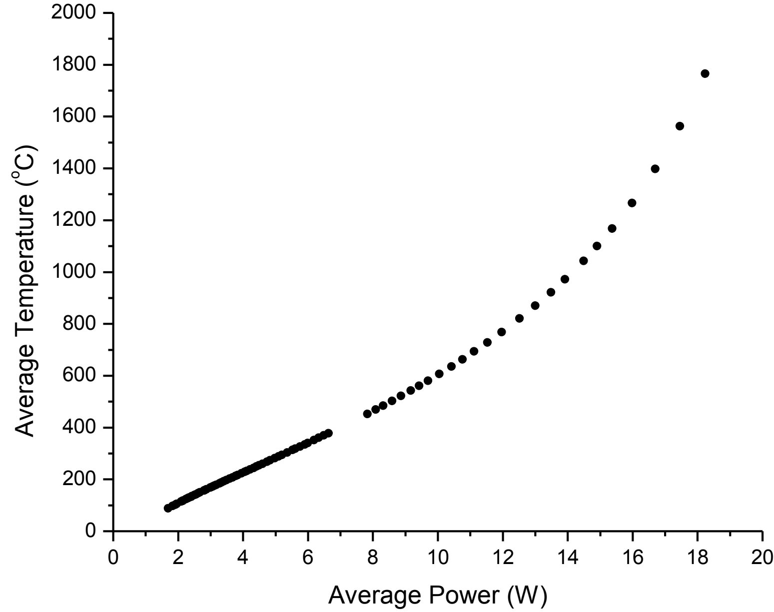

Figure 4.49: Plot of temperature vs. power shows that the temperature increases as the power increases and at high temperatures regime, the radiation mechanism is dominant and consistent with T^4.

The behavior is consistent with proportion to T^4, (*Stefan-Boltzmann law*) where radiant mechanism is dominant. That is, to indicate the relationship between temperature and thermal radiation (at the higher end of the calculated temperature range, focusing on the last 10s of the pulsing test), we can consider the Stefan-Boltzmann law which states (56) that for an object of temperature T, the radiated power P will be;

$$P_{rad} = \epsilon \sigma A_s T^4 \tag{4.12}$$

where ϵ is the emissivity of the object, A_s is the surface area, and σ is the Stefan-Boltzmann constant. The emissivity constant depends entirely on the material and is defined as 1 for an ideal blackbody. There is no definitive emissivity value reported for diamond. Indeed, the values are highly dependent on surface and growth conditions of the diamond film (57). Herchen and Cappelli reported estimated emissivity values determined from the measured diamond brightness temperature and the diamond temperature derived from the Stokes to anti-Stokes ratios (*Raman Scattering*). Their results suggest emissivities at the wavelength of 655nm close to unity in the temperature range from 1100K to 1400K.

For practical purposes, the net power being radiated is more relevant than the absolute radiated power. The net power of an object at temperature T in an environment of temperature T_0 is

$$P_{net} = P_{rad} - P_{absorb} \tag{4.13}$$

and, according to the Stefan-Boltzmann relation,

$$\begin{aligned} P_{net} &= \epsilon\sigma A_s T^4 - \epsilon\sigma A_s T_0^4 \\ &= \epsilon\sigma A_s (T^4 - T_0^4) \end{aligned} \tag{4.14}$$

where $\epsilon, \sigma \; and \; A_s$ are the aforementioned constants. In this experiment, when the temperature of the diamond resistor, T is greater than ~1500K and ambient temperature

T_0 was measured at 298K, then T^4 will be >> than T_0^4, so the environmental temperature term is negligible. This simplifies Eqn. (4.14) to

$$P_{net} = CT^4 \tag{4.15}$$

or further,

$$P_{net} \propto T^4 \tag{4.16}$$

and

$$lnP_{net} \propto 4lnT \tag{4.17}$$

Thus a plot of lnP vs. lnT of the test data will illustrate the relationship between P and T as a power law, the exponent of that power law being the slope of the curve. The experimentally determined values of lnP and calculated values of lnT are plotted in **Figure 4.50.** As noted earlier, the assumption made in the derivation of Eqn. (4.15) was that T^4 was far larger than T_0^4. Thus, Eqn. (4.15) does not hold for lower resistor temperatures, so only data points with an inferred temperature exceeding ~1500K were examined. The slope observed is ~3.2, an exact operant would be 4.0. This deviation from the expected value of 4 can occur for several possible reasons. One possibility is

that the approximation of $T^4 \approx T^4 - T_0^4$ used in Eqn. (4.15) is not valid. This seems unlikely, as the least data point is ~1586K. $(1586)^4$ is over 700x larger than $(298)^4$.

Another possible source of difference is the estimated temperature values. The temperatures were calculated from the Arrhenius relationship. Recall from *Section 4.2* that the rate constant (resistance) of the Arrhenius equation was directly determined from the temperature range of 25°C to 350°C (298K to 623K). The logarithmic rate constant is $\propto$ to $\frac{1}{T}$. Although it is possible to calculate the pre-exponential factor (constant), R_0 and activation energy, E_A (see *Section 4.2*) using one set of resistance-temperature reading, it would be more practical and reliable to use at least three sets of experimental data and determine R_0 and E_A using statistical method. Additionally, the statistical analysis of the $ln(R)$ vs. $ln\left(\frac{1}{T}\right)$ plot indicates the standard error in the slope (which determines the E_A value for the freestanding diamond resistor **Free_A**) was 56. This gives an uncertainty interval of ±123.4 or 10.52% within a 95% confidence level. This uncertainty affects the estimated temperature values at the higher end of the temperature range and can be an influential source of variation in the Stefan-Boltzmann law estimation.

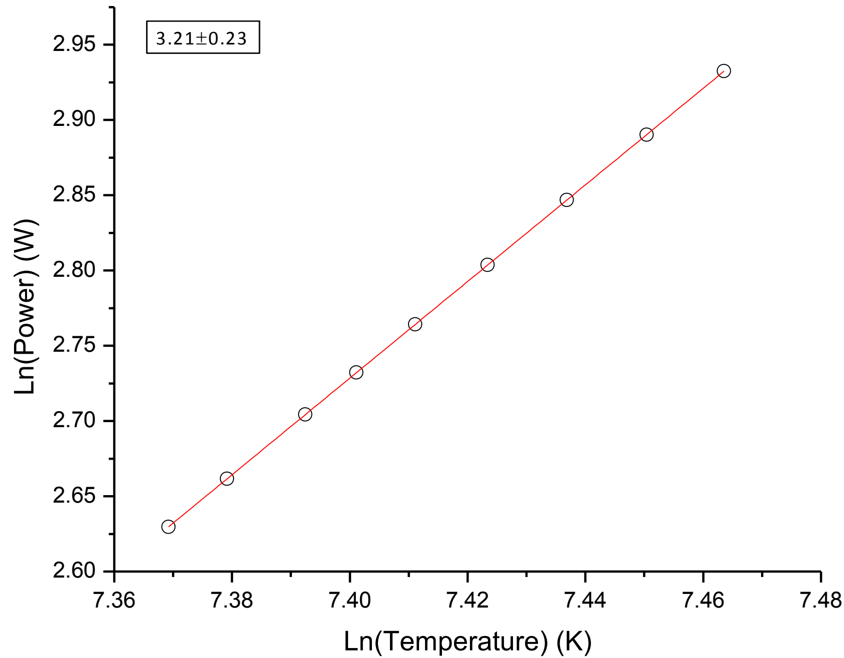

Figure 4.50: The natural log of the measured power versus the natural log of the inferred temperature. The slope of the curve fit is 3.21.

The observed slope of ~3.21 from the plot $ln(P)$ vs. $ln(T)$ resulted from the calculated temperatures from the temperature dependence of Arrhenius relationship. However, as discussed earlier, the calculated temperatures are probably inaccurate as the Arrhenius relationship has been shown to deviate at elevated temperatures (55). Assuming different temperatures, a plot to fit a T^4 dependence for the Boltzmann power law relationship was redrawn. **Figure 4.51** shows the redrawn curve of $ln(P)$ vs. $ln(T)$ with the set of predicted temperatures that ideally correlate with the Stefan-Boltzmann power relationship. When the slope had a value of ~4, the indicated temperatures used were lower than those calculated from the single Arrhenius relation. There is an average

difference of 260K lower temperatures, with the biggest difference being 287K and the smallest 236K. A tabulated table containing the considered temperatures can be found in Appendix A. This difference can be explained by the deviation from simple Arrhenius behavior at highly elevated temperatures. Based on the set of predicted temperatures that "match" the Stefan-Boltzmann T^4 dependence, for the elevated temperatures, the Arrhenius equation predicted higher temperatures than the Stefan-Boltzmann comparison. This is consistent with the observation of strong non-Arrhenius temperature dependence of resistivity (55).

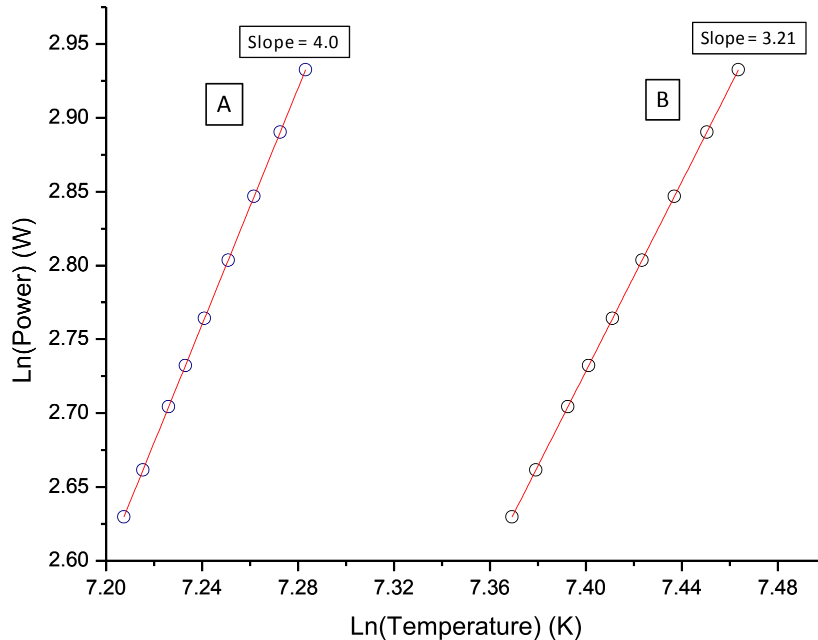

Figure 4.51: Plot of $ln(P)$ vs. $ln(T)$. A: Redrawn plot with new predicted temperatures. B: Plot with initial calculated temperatures.

We now portray the *T* vs. *P* plot (as per **Figure 4.49**), **Figure 4.51B** showing the original "Arrhenius" curve and the "matched" Stefan-Boltzmann temperature behavior. This range of temperature at the higher power should be a reasonable estimate of the actual behavior at the extremes of power density (see discussion in *Diamond Resistor Limit, Section 4.5.3*)

Referring again to the pulsing intervals in **Figure 4.45** (shown here as **Figure 4.52**), we note the rising current within each additional pulse. Power is of course dissipated as heat but as noted earlier, the body temperature of the resistor will rise above the ambient temperature of its environment if the resistor does not cool completely between pulses.

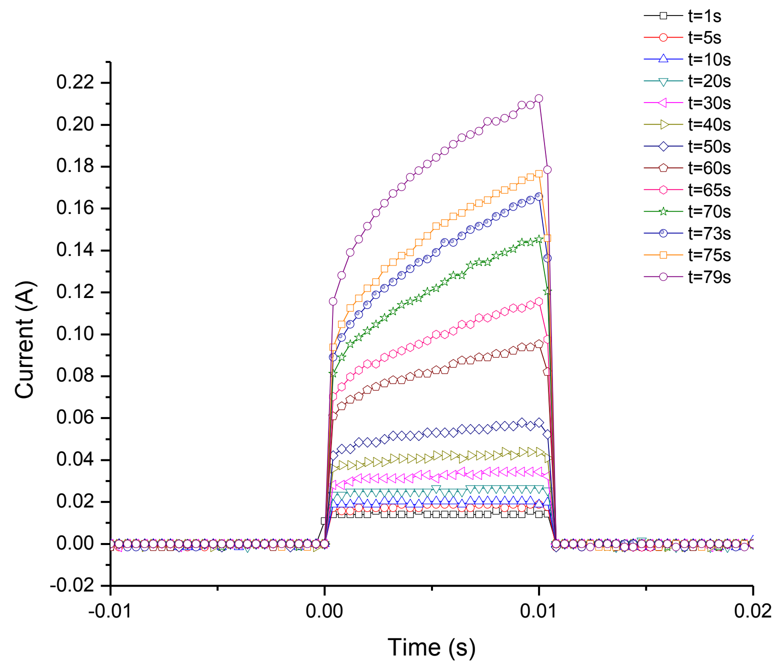

Figure 4.52: Sequential current behavior with successive pulses.

Figure 4.53 is a detailed plot of $i(t)$ for time, t at 77s, 78s and 79s which focuses on the scenario at the limit of high current and high temperature. This is the interesting testing regime just before the resistor **Free_A10** failed open. The current behavior can be described ("fit") by a *power* function consistent with a radiance governed response as the temperature increases. A similar observation was reported on thin film nichrome resistors that were characterized for infrared projector applications (58). Qualitatively, this power behavior of $i(t)$ vs. t agrees with the power relation of $ln(P)$ vs. $ln(T)$ of Stefan-Boltzmann power law estimation above. Consequently, the test data of the freestanding diamond resistor in the high temperature regime is consistent with *radiation* as the dominant mechanism of heat transfer.

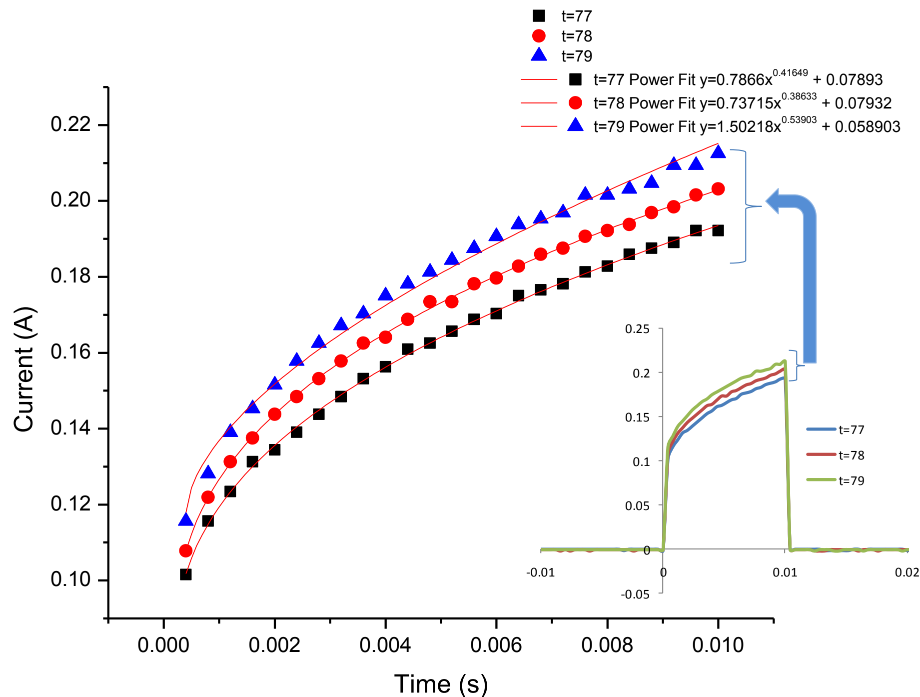

Figure 4.53: Details of the current waveforms for time, t at 77s, 78s and 79s which focuses on the scenario at high currents.

Thus, at these highest power/temperature conditions of pulsing, the levels rise at an increasing rate, consistent with a higher temperature from the preceding pulse and the T^4 dependence of radiated power. The occurrence of radiative behavior at high temperatures can be examined further based on heat transfer analysis.

As previously described in *Section 4.2.1*, the heated diamond resistor can be treated as a thermistor. A thermistor is a thermally sensitive resistor and comes from the words *thermal resistor*. Heat equation analysis has been applied to thermistors to characterize their behavior and energy transfer and can be applied to our diamond resistor configuration.

Conservation of energy dictates that the rate at which energy is supplied must equal the rate at which energy is lost plus the rate at which energy is absorbed (**Figure 4.54**):

$$\frac{dQ}{dt} = \frac{dQ_L}{dt} + \frac{dQ_A}{dt} \tag{4.18}$$

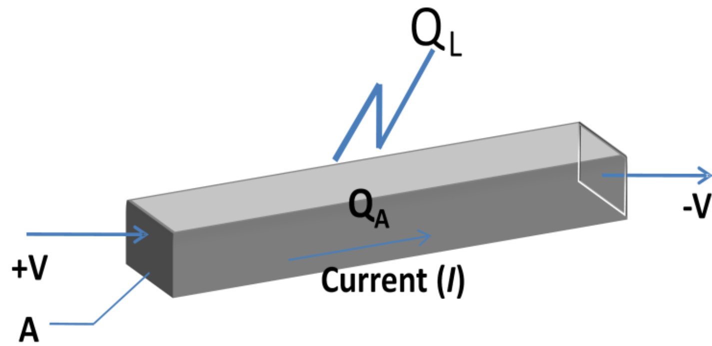

Figure 4.54: Energy balance of the resistor.

The rate at which thermal energy is *supplied* to the resistor is equal to the power dissipated in the resistor:

$$\frac{dQ}{dt} = P = I^2 R \tag{4.19}$$

The rate at which thermal energy is *lost* from the resistor to its surroundings is proportional to the temperature rise of the resistor:

$$\frac{dQ_L}{dt} = \delta \Delta T = \delta (T - T_A) \tag{4.20}$$

δ is dissipation constant which depends upon thermal conductivity (*conduction*), relative motion of the medium (*convection*) as well as heat transfer from the resistor to its surroundings (*radiation*). In the high temperatures scenarios, the radiation mechanism

will be dominant (59), (60). The rate at which thermal energy is *absorbed* by the resistor causing a specific rise in temperature can be expressed as:

$$\frac{dQ_A}{dt} = sm\frac{dT}{dt} = c_p\frac{dT}{dt} \tag{4.21}$$

where s: specific heat (kJ) , m:mass(kg) , c_p: specific heat capacity (kJ/kg·K*)*

The heat transfer equation for a thermal resistor at any instant in time after power has been applied to the circuit can be expressed as:

$$\frac{dQ}{dt} = P = I^2R = \delta(T - T_A) + c_p\frac{dT}{dt} \tag{4.22}$$

Examining the resistor thermal behavior under transient conditions, the solution for the above equation where power is constant is:

$$\Delta T = T - T_A = \frac{P}{\delta}\left[1 - exp\left(-\frac{\delta}{c_p}t\right)\right] \tag{4.23}$$

This demonstrates that when a significant amount of power is dissipated in the resistor, its body temperature will rise above the ambient temperature as a function of time. The transient conditions at “turn on”, and all applications that are based upon the *Current-Time* characteristics are governed by Eqn. (2.23).

In regards to the heat loss equation, Eqn. (4.20), in the freestanding thermal resistor, the heat loss is attributable to radiation. This assumption is based on the *freestanding* configuration of the resistor and that the experiment was performed in vacuum. At the high temperature test conditions, the heat loss due to radiation can be modeled using the Stefan-Boltzmann Law:

$$E = \varepsilon \sigma_s A T^4 \tag{4.24}$$

Substituting Eqn. (4.24) into Eqn. (4.20) yields:

$$\frac{dQ_L}{dt} = \varepsilon \sigma_s A (T_f - T_i)^4 \tag{4.25}$$

At high temperatures, small increases in the temperature lead to large changes in heat loss. The increased heat loss at higher temperatures reduces the rate of increase of the current flow through the resistor. This results in the response of the current vs. time (**Figure 4.52** and **Figure 4.53**) to roll off during the duration of the pulse in this higher temperature regime as more power in is lost through heat, i.e. the rise time is reduced, in agreement with the power law fit of the current-time plot (**Figure 4.52** and **Figure 4.53**).

4.5.2.1 Temperature Effect on Carrier Concentration

Above, we discussed this freestanding diamond resistor (**Free_A10**) having T^4 power dependence due to the radiance with respect to the temperature at high power regimes (Stefan-Boltzmann). We will now extend the discussion for the resistor when the carrier concentration increases as the temperature increases.

In the earlier discussion, we stated that when power pulsing was applied to the circuit, the diamond resistor started to warm up and when the power pulse is terminated, the resistor cooled down but sufficient heat would be retained by the resistor, that it did not return to equilibrium or ambient temperature. This phenomenon is a simple Joule heating mechanism that occurs in the diamond resistor. The power dissipated (I^2R) in the resistor causes the temperature to increase.

In diamond, boron dopants are not fully ionized at room temperature. As such, the carrier (hole) concentration is equal to the ionized dopant concentration, but not the atomic dopant concentration. As we know, the conductivity of a semiconductor is determined by two factors: the concentration of free carriers available to conduct current and their mobility (see *Section 2.4*):

$$\sigma = q[\mu_n(T)n(T) + \mu_p(T)p(T)] \quad (4.26)$$

where σ: conductivity, q: elementary charge, μ_n, μ_p: carriers mobility and n,p: carrier concentrations.

For p-type semiconductor, Eqn. (4.26) becomes

$$\sigma = q\mu_p(T)p(T) \tag{4.27}$$

Both carrier concentration and mobility are temperature dependent. When the power pulse is applied to the diamond resistor, it heats up, more boron dopants are ionized and this leads to an increase in the carrier concentration, in this case, holes. **Figure 4.55** shows a plot of the ratio of ionized boron to atomic boron concentration in the temperature range of $180 < T < 2400\ K$ $(-93 < T < 2000℃)$ calculated from Eqn. (2.32) in *Section 2.5* using the ionization energy, E_A of 0.1eV and the boron concentration of ~10^{19}/cm^3.

When the temperature rises, the ionization of boron increases and more carriers are thermally generated. Because of the increasing number of holes, the conduction in the resistor increases and hence there is a decrease in resistance as a function of time as shown in **Figure 4.46**. The conductivity also depends on the mobility of the carriers. Furthermore, the mobility of carriers in diamond is also subject to the doping concentration, e.g. at lower concentrations the mobility increases and vice versa (61). See *Section 2.4* for further discussion.

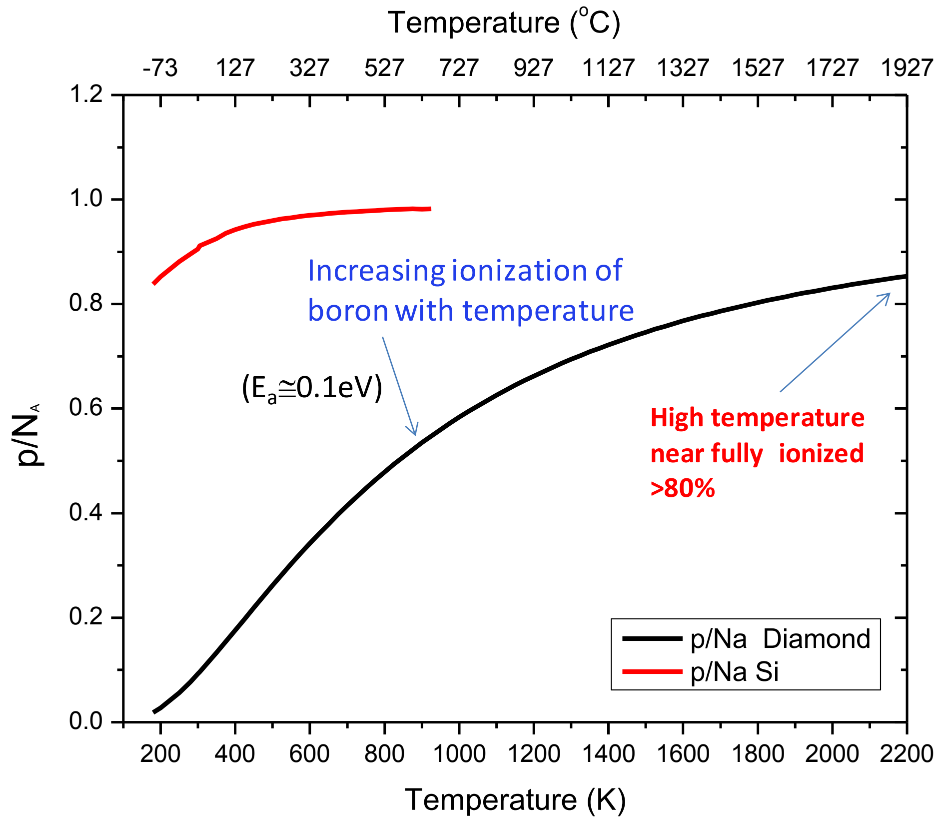

Figure 4.55: Ratio of ionized boron to boron concentration 180 K< T< 2400K (-93 < T< 2000°C).

Figure 4.56 is the plot of rate of change in temperature over cumulative pulsing time for resistor **Free_A10**. Note that, the behavior suggests two mechanisms at lower vs. higher temperature, linear and exponential.

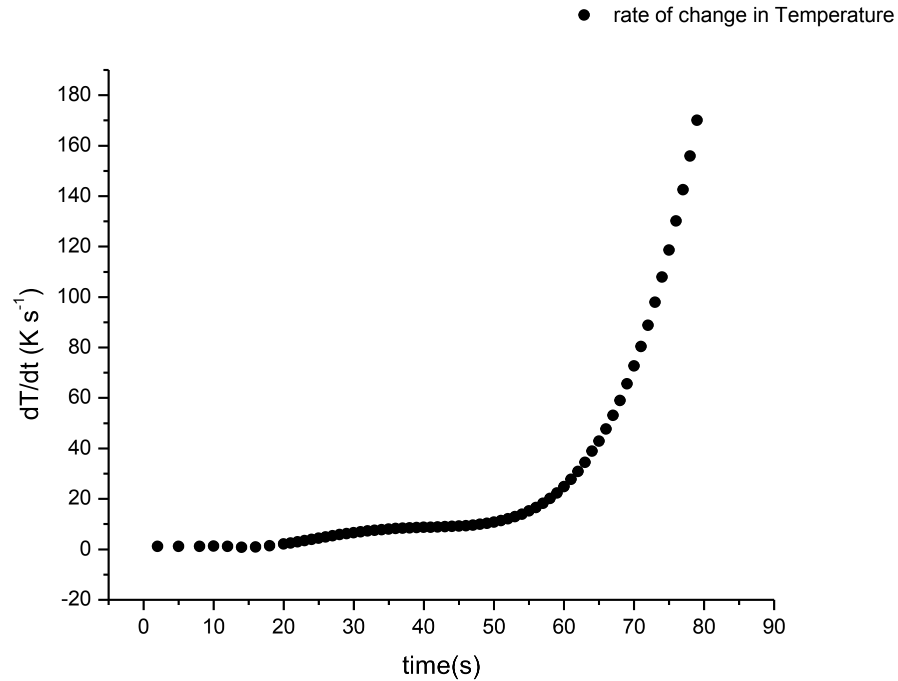

Figure 4.56: Plot of rate of change in temperature vs. cumulative pulsing time.

The low power region (early pulsing) is shown in **Figure 4.57** where we plot the rate of change in temperature vs. the first 50s of the pulsing time. The small linear increase in the rate of change in temperature in the first 50s of pulsing test suggests that the rate of Joule heating by the current equals the rate of heat transfer to the surroundings. In this scenario, more holes are generated and the system accommodates them such that the resistivity decreases and the resistor doesn't warm up quickly despite the continuous pulsing. At t = 50s it appears that this equilibrium at which power dissipation balances the heat loss to the surrounding changes.

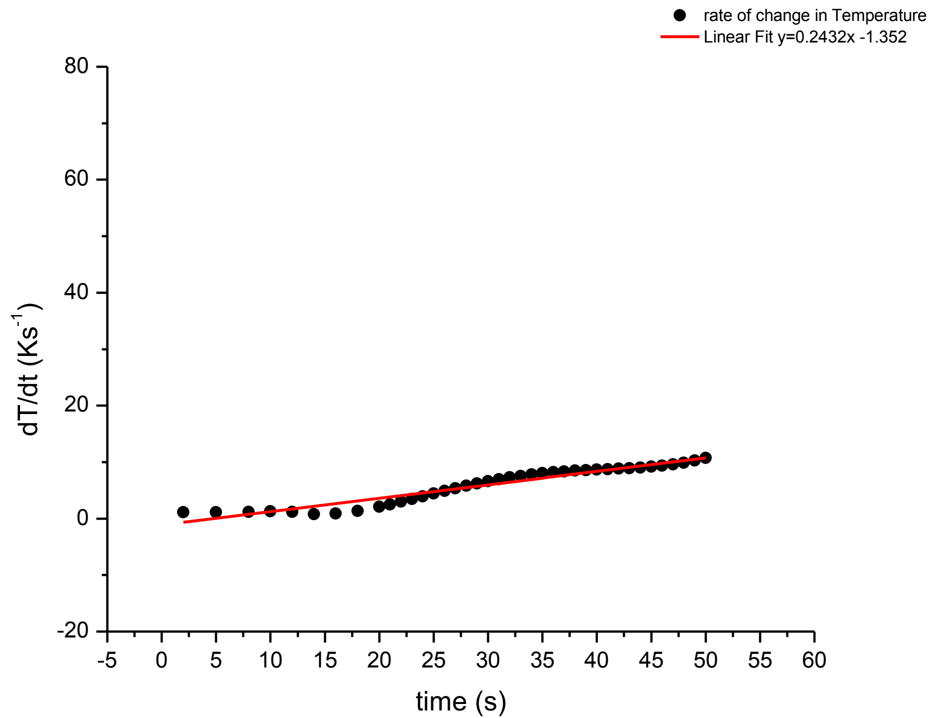

Figure 4.57: Plot of rate of change in temperature in the first 50s of pulsing time.

As the power pulses continue, the resistor is heated such that the conduction thermal mechanism becomes as discussed in previous section, principally the radiant mode. The second part of the plot in **Figure 4.56** is shown in more detail in **Figure 4.58**. There is an exponential increase in the rate of change in temperature in the last ~30s of the pulsing time before the resistor failed open. The pulsing under this particular condition is the same as earlier but the temperature build up leads to decreasing resistance, which increases the current and causes even higher temperatures. The exponential increase in the temperature change suggests that, the exponential increase in

hole concentration governs the behavior and then the resistor reaches a condition where the boron approaches full ionization, and a constant carrier concentration. At this point, the diamond resistor is believed to have semi-metallic property and act as a conventional resistor.

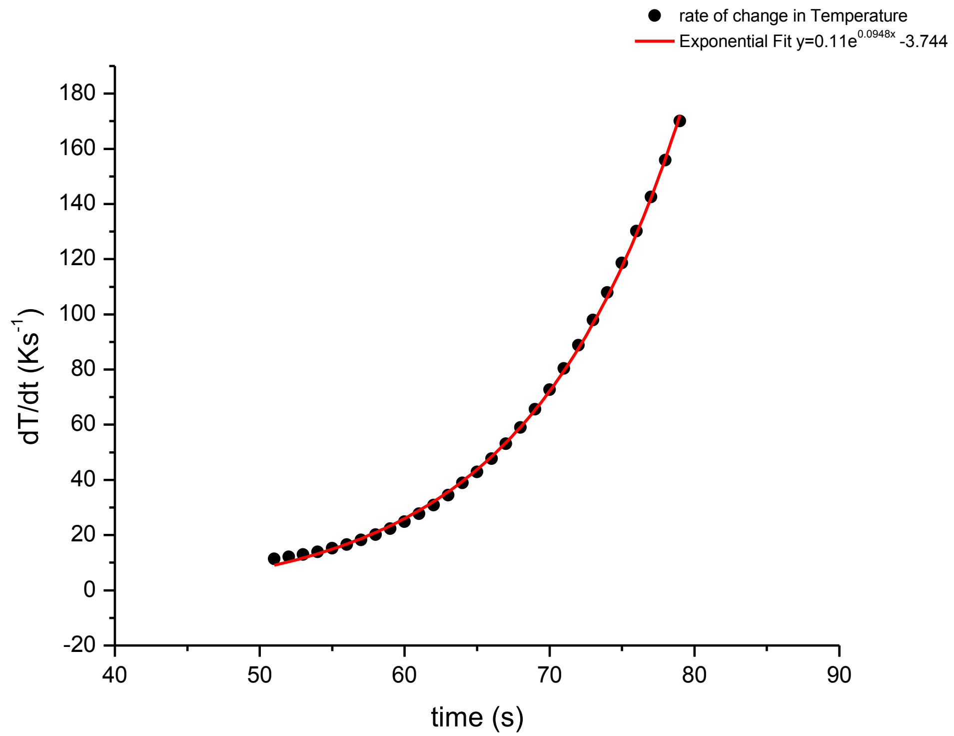

Figure 4.58: Plot of rate of change in temperature from 50s of the pulsing time until the resistor failed open.

4.5.3 Examination of Power and Current at the Freestanding Diamond Resistor Limit

It is pertinent to consider the maximum power and current density for the freestanding diamond resistor, i.e. what are the limits of the boron doped resistor body? The maximum current measured was 0.21A which for the resistor of this dimension (see *Section 4.5.2*) gives a maximum current density (cross section) of ~8.4×10^4 A/cm^2 and a maximum power density in the resistor of ~8.3×10^6 W/cm^2. The average power and current density in each pulse of resistor **Free_A10** are plotted against the cumulative pulsing time in **Figure 4.59**. **Figure 4.60** shows the average power dissipation (for each pulse) in the diamond resistor vs. the calculated temperature. As the power to the diamond resistor increases, the resistor temperature continues to rise to a maximum calculated (from Arrhenius relation, Eqn. (4.7)) *average* temperature of ~1800°C.

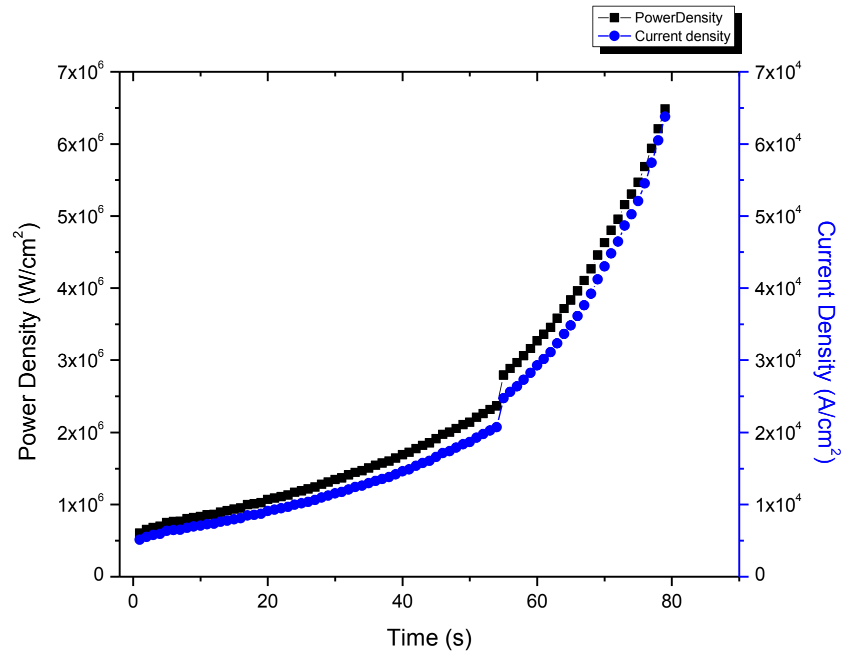

Figure 4.59: Power and current density over pulsing intervals.

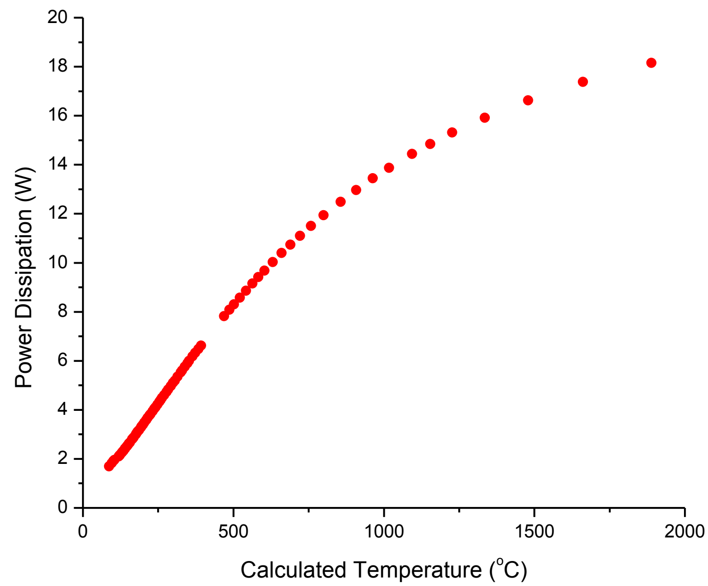

Figure 4.60: Power dissipation vs. theoretical temperature.

As the power in each pulse increased, the resistor's temperature continued to rise which caused the resistance to decrease, as shown in **Figure 4.61**, due to its negative temperature coefficient. The plot is the average values of resistance plotted against the average values of current density in each pulse.

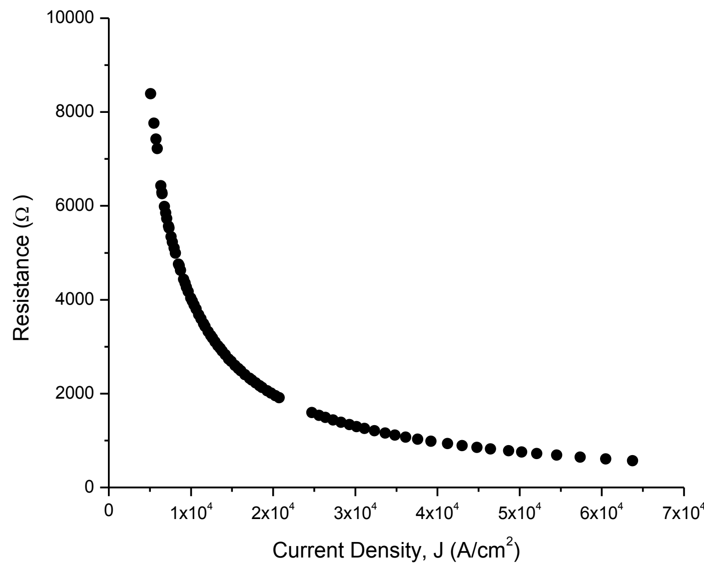

Figure 4.61: Resistance vs. current density over pulsing intervals.

Figure 4.62 shows the input voltage pulse, resistance and current combined in one plot of the last pulse recorded at 80s when the diamond resistor failed. The resistance abruptly increased and the current was measured at 0.21A before the resistor became open. This occurred before the last voltage pulse completed its cycle. **Figure 4.63** is the optical image taken before and after the experiment. The freestanding diamond resistor

body was broken and separated from the neck of the resistor. The Ti/Au contact pads were observed to be discolored and detached after the cycles of pulses, **Figure 4.64**.

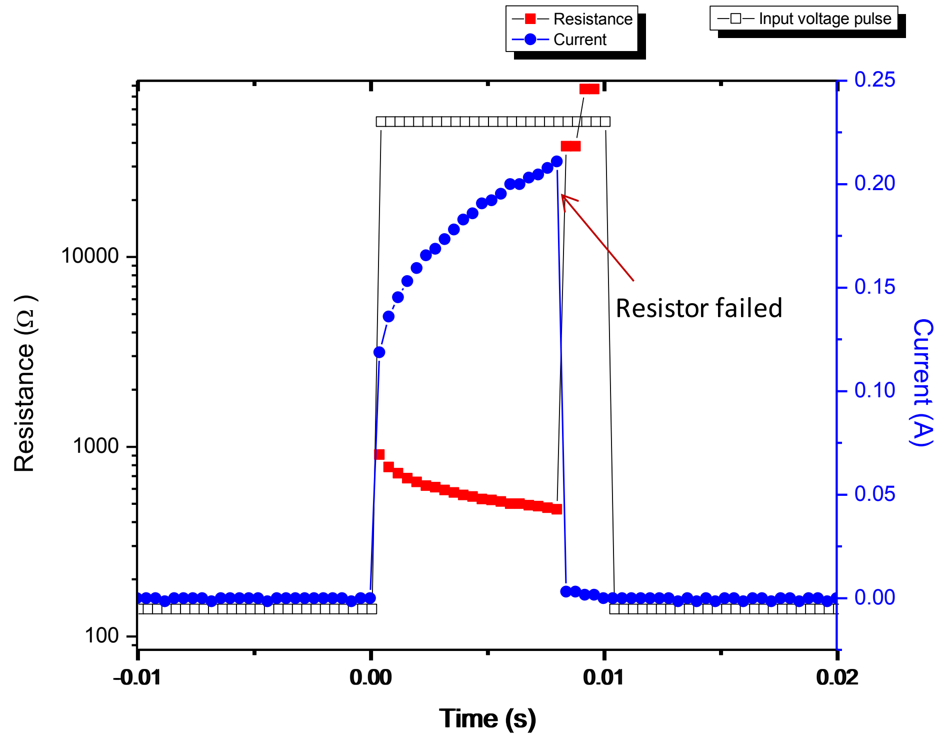

Figure 4.62: Waveforms of input voltage, resistance and current when the resistor failed.

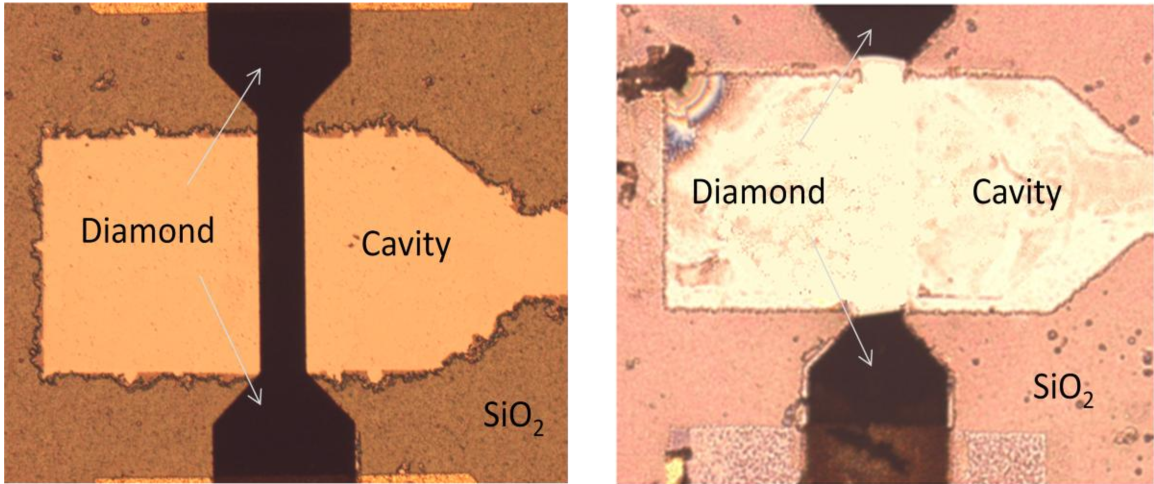

Figure 4.63: Before (left) and after (right) picture of resistor **Free_A10** at 120V power pulse.

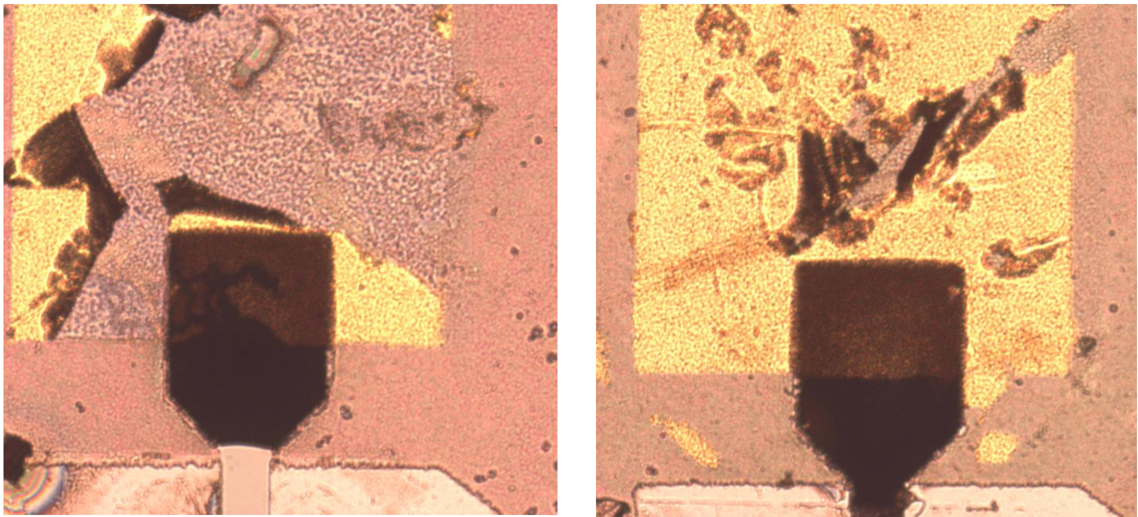

Figure 4.64: Damaged contact pads after voltage cycles.

If we consider the last current and resistance reading (~0.21A and ~468Ω) before the resistor failed, we can calculate interesting "limit" values of the diamond resistor properties.

The values of the maximum current, J_{max} and power density, P_{Dmax} (cross section) as well as the minimum resistance, R_{min} have been mentioned in the previous segment but will be cited again for comparison purposes. The J_{max} was recorded at $\sim 8.5 \times 10^4\ A/cm^2$ and the P_{Dmax} reached the value of $\sim 8.3 \times 10^6\ W/cm^2$. The R_{min} was measured at 468Ω (compared with 16kΩ of R_0, where R_0 = initial room temperature resistance. P'_{Dmax}= maximum power density per unit square = $2.1 \times 10^5\ Watts/square$ (analogous to sheet resistivity, associated with "conventional" power resistors.

It is interesting and relevant to compare P_{Dmax} with other materials used for electronic purposes. For example, the nichrome resistor is reported to have J_{max} of $4.9 \times 10^4\ A/cm^2$ (62) and P_{Dmax} of $2.63 \times 10^4\ W/cm^2$ (63). The P_{Dmax} reported for chromium silicide was only $\sim 38\ W/cm^2$ (64). Hence, we observe that diamond resistors have two orders of magnitude higher power density than that of nichrome.

As regards to the open failure of the resistor, from electrical results and test performance, it appears that the resistor's local temperature may have reached a value where it proceeded to graphitize and became physically unstable. This could happen if its local temperature became in excess of ~1800°C.

4.6 Comparing Attached and Freestanding Diamond Resistors

There are several observations to be made when comparing the pulsed behavior of the freestanding and attached resistors. Under the lower voltage conditions on freestanding resistors, current (between pulses) initially increases with time (i.e. each sequential pulse) but settles to a constant value. However, for attached resistors, the current increases steadily to a point and then rises rapidly. This increase is suspected to be the result of leakage to the substrate, i.e. through the layer of oxide on which the attached resistors sit. The leakage current was also observed in the higher voltage conditions.

Based on these observations, the current profile of the attached resistors was in contrast to the behavior of the freestanding resistor (**Free_A10**). Under higher voltage pulse conditions, the freestanding resistors show a dynamic increase in the current pulses for each successive voltage pulse. The $i(t)$ signals (**Figure 4.65**) rise in a non-linear (*power*) behavior at higher temperatures which is consistent with the effect of heat loss through radiation as described by the T^4 dependence of the Stefan-Boltzmann law. In contrast, the $i(t)$ signals of attached resistors, **Figure 4.66**, the current increase exhibits *linear* behavior in both cases, 80V and 100V voltage pulse test at higher temperatures regime. At relatively lower temperatures, the $i(t)$ signals of attached resistors follow the voltage pulse profile (square shape) and observed minimal increase in current level intra-pulse. The linear increase in the current at high temperatures is describable by the mechanism of direct conduction of heat to the substrate.

When the attached resistors failed, the failures were due to a short to the substrate and caused a spike in the current levels. The ~1 micron thick of the oxide layer

underneath the attached resistors was not sufficient to provide the dielectric insulation under thermal and voltage stressing of the pulses. That is, the continuous pulsing voltage applied to the resistors could have contributed to the thermal stress of the oxide layer. Conversely, the freestanding resistors failed open, the resistor becoming completely destroyed. Of the two physical constructions, the freestanding resistor was able to tolerate higher power density than the attached configuration.

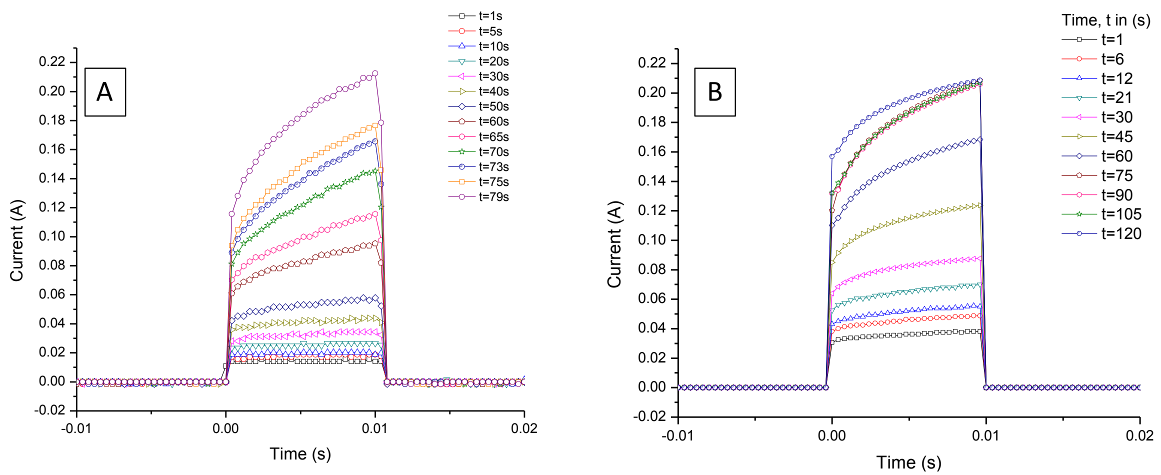

Figure 4.65: Sequential current behavior with successive pulses for freestanding resistors, (A): resistor **Free_A10** with 120V voltage pulse, (B): resistor **Free_B11** with 80V voltage pulse.

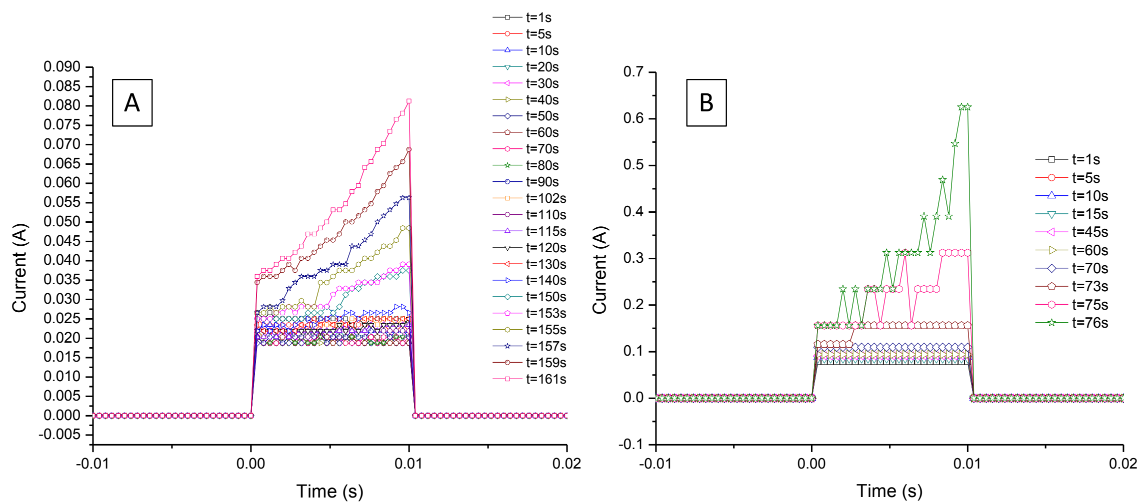

Figure 4.66: Sequential current behavior with successive pulses for attached resistors, (A): resistor **Att_C8** with 80V voltage pulse, (B): resistor **Att_C6** with 100V voltage pulse.

CHAPTER V

SUMMARY AND FUTURE WORK

Summary

Thin and thick film resistors occur regularly in electronics. In certain situations, high power into resistive elements are utilized as blackbody radiative sources. Most common is the incandescent bulb. Diamond is the hardest known material, has the lowest coefficient of thermal expansion, is chemically inert and wear-resistant, has the highest thermal conductivity and high binding energy. It is electrically insulating but can be doped to behave as a semiconductor/resistor.

These properties led to investigation of the thermal-electrical properties of diamond as fabrication and testing/characterization of diamond microelectronic resistors had not been accomplished before.

DC and temperature testing provided basic property information but given the semiconductor behavior of doped diamond, thermal runaway made behavior of diamond resistors “at the limit” difficult to ascertain. Pulsing power allowed details of the diamond resistor configuration to be examined by “stretching” out the high power behavior of attached and freestanding diamond micro resistors to learn more about the material system.

It was determined that diamond resistor could tolerate 1000x more power than conventional resistor (65) material and the freestanding configuration was potentially a better form for handling high power.

Future Work

The work done herein, can be continued in several directions. As typical with the nature of polycrystalline material, there are still many unanswered questions. For example, the influence of grain boundary in thermal transport was not discussed in this dissertation. An interesting study may involve investigating the influence of grain boundary states on the thermal behavior of the diamond resistor.

Exploring the wavelength of diamond resistor during the illumination may result in profound knowledge of temperature dependance of hole concentration at high temperatures in diamond. A simple concept may involve the deposition of a thin film on one side and the measurement of the temperature rise on the other side by means of an infrared imager.

Another area of study, which would yield valuable results, is the study of the temperature dependent thermal conductivity in diamond resistor, as a function of thickness and film morphology. It would be interesting to measure the local thermal conductivity of diamond films, on roughly the scale of a grain, using specialized microscale techniques (e.g. Scanning Thermal Microscopy).

APPENDIX A

RESISTANCE AND CONDUCTANCE

Electrical resistance and its reciprocal, electrical conductance are the basic concepts that govern the travel of electricity through a conducting medium. Resistance is a ratio of the degree to which a material opposes an electrical current, whereas conductance is a measurement of the ease with which electricity can travel through the material. The units used in resistance and conductivity are ohms (Ω) and Siemens (S) respectively. Resistance can be expressed as:

$$R = \frac{\rho L}{A} \tag{A-1}$$

Where L is the length, A is the cross sectional area and ρ is the specific electrical resistance of the material. Also known as resistivity, specific electrical resistance is the value that denotes how strongly a material opposes the flow of an electrical current.

The base equations that express the relationships held between resistance with voltage, current and electrical power are rearrangements of Ohm's law with additions of Joule's laws, and are as follows:

$$R = \frac{V}{I} \tag{A-2}$$

$$R = \frac{V^2}{P} \tag{A-3}$$

$$R = VI \tag{A-4}$$

$$R = \frac{P}{I^2} \tag{A-5}$$

Where R is resistance, V is voltage in volts (V), I is current in Amperes (A) and P is power in watts (W). The equations above show that when the voltage across a resistor is kept constant, the power dissipated in the resistor will increase as current increases. The dissipated power is lost in the form of thermal energy which increases the temperature of the resistor. For semiconductors such as the diamond resistor, a higher temperature leads to reduced resistance. This in turn increases the current flowing through it and causes even greater power losses. This is a phenomenon known as Ohmic heating, joule heating, or electrical resistance heating (ERH). The theory behind ERH has been extensively studied, and is very well understood.

APPENDIX B

P-SPICE SIMULATION

Following are P-Spice circuit simulation to illustrate the circuit simulation for diamond resistor measurement.

```
**** 06/13/09 16:51:51 ********* PSpice 9.1 (Mar 1999) ******** ID# 0 ********
 Circuit simulation for resistor measurement
 ****     CIRCUIT DESCRIPTION****************************************************
VS  1 0 DC 60V
RA 1 2 100k
RB 2 0 1k
Rd 1 3 5k
R1 3 0 100
.DC Vs 60 60 1
.PRINT DC V(1) V(2) V(3)
.PRINT DC V(2,0)
.PRINT DC V(1,3)
.PRINT DC V(3,0)
.PRINT DC I(RA)
.PRINT DC I(RB)
.PRINT DC I(R1)
```

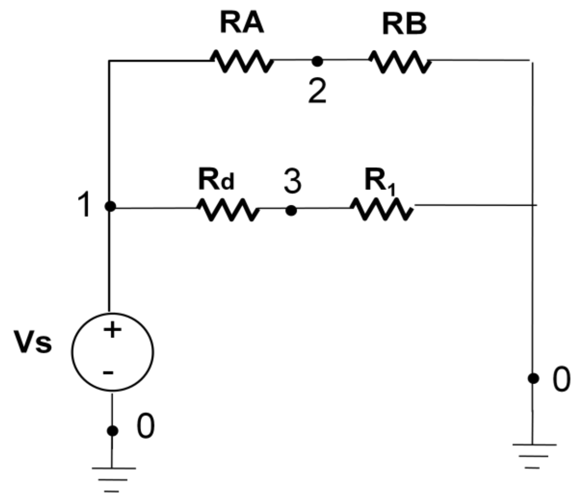

```
.PRINT DC I(Rd)

.END




**** 06/13/09 16:51:51 ********* PSpice 9.1 (Mar 1999) ******** ID# 0 ********

 Circuit simulation for resistor measurement

 ****     DC TRANSFER CURVES              TEMPERATURE =   27.000 DEG C

******************************************************************************

      VS              V(1)           V(2)            V(3)

   6.000E+01   6.000E+01   5.941E-01   1.176E+00


**** 06/13/09 16:51:51 ********* PSpice 9.1 (Mar 1999) ******** ID# 0 ********

 Circuit simulation for resistor measurement

 ****     DC TRANSFER CURVES              TEMPERATURE =   27.000 DEG C

******************************************************************************

        VS          V(2,0)

   6.000E+01   5.941E-01
```

```
**** 06/13/09 16:51:51 ********* PSpice 9.1 (Mar 1999) ******** ID# 0 ********

 Circuit simulation for resistor measurement

 ****     DC TRANSFER CURVES              TEMPERATURE =   27.000 DEG C

******************************************************************************

        VS          V(1,3)

  6.000E+01   5.882E+01


**** 06/13/09 16:51:51 ********* PSpice 9.1 (Mar 1999) ******** ID# 0 ********

 Circuit simulation for resistor measurement

 ****     DC TRANSFER CURVES              TEMPERATURE =   27.000 DEG C

******************************************************************************

        VS          V(3,0)

  6.000E+01   1.176E+00


**** 06/13/09 16:51:51 ********* PSpice 9.1 (Mar 1999) ******** ID# 0 ********

 Circuit simulation for resistor measurement

 ****     DC TRANSFER CURVES              TEMPERATURE =   27.000 DEG C

******************************************************************************

        VS          I(RA)

  6.000E+01   5.941E-04


**** 06/13/09 16:51:51 ********* PSpice 9.1 (Mar 1999) ******** ID# 0 ********

 Circuit simulation for resistor measurement

 ****     DC TRANSFER CURVES              TEMPERATURE =   27.000 DEG C

******************************************************************************

        VS          I(RB)

  6.000E+01   5.941E-04
```

**** 06/13/09 16:51:51 ********* PSpice 9.1 (Mar 1999) ******** ID# 0 ********

Circuit simulation for resistor measurement

****   DC TRANSFER CURVES   TEMPERATURE =   27.000 DEG C

****

```
        VS          I(R1)

  6.000E+01   1.176E-02
```

**** 06/13/09 16:51:51 ********* PSpice 9.1 (Mar 1999) ******** ID# 0 ********

Circuit simulation for resistor measurement

****   DC TRANSFER CURVES   TEMPERATURE =   27.000 DEG C

* **

```
        VS          I(Rd)

  6.000E+01   1.176E-02

        JOB CONCLUDED

        TOTAL JOB TIME            .03
```

**** 06/13/09 16:51:51 ********* PSpice 9.1 (Mar 1999) ******** ID# 0 ********

************ ***CIRCUIT DESCRIPTION********************************

APPENDIX C

PRELIMINARY TEST

Resistor Free_B11

As mentioned previously, the transient response characteristics of the diamond resistor can be readily observed at a higher input voltage pulse. The transient response was observed with the 80V voltage pulse. The test was conducted on resistor **Free_B11**. The pulse frequency was set at 10Hz with 10% duty cycle. The voltage drop across R_1 was recorded at 3s interval (see earlier discussion on the experimentation setup for details). The test lasted for 4mins and 9s before the resistor failed open. **Figure C.1** shows the instantaneous current waveforms over the pulsing intervals of resistor **Free_B11**. It is noted that Joule heating becomes appreciable as the power pulse continues. The resistance of the diamond resistor decreases while the applied voltage was constant during the pulse leading to higher currents in the diamond resistor. The corresponding resistance waveforms are depicted in **Figure C.2**. **Figure C.3** shows SEM image of the resistor's failure after the power pulse.

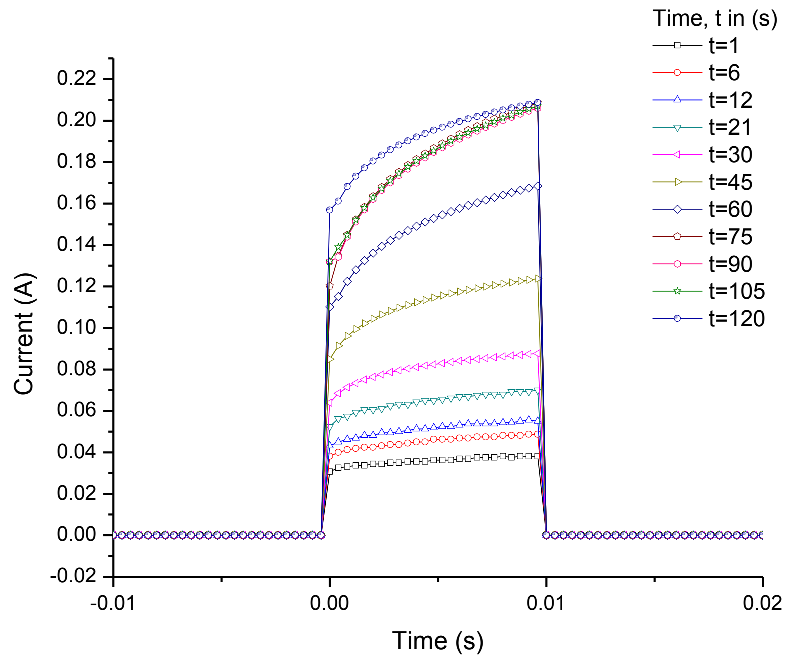

Figure C.1: Current waveforms over pulsing intervals.

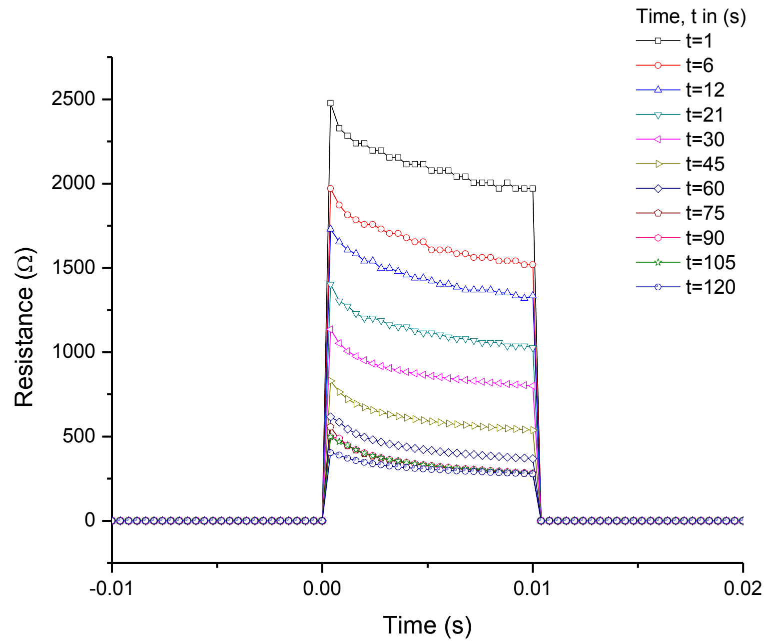

Figure C.2: Resistance waveforms over pulsing intervals.

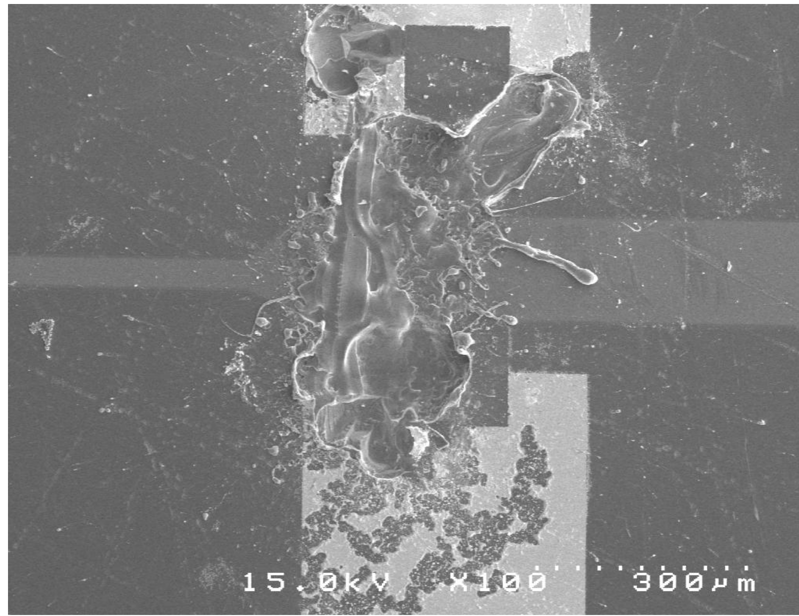

Figure C.3: SEM image of resistor **Free_B11** failed during pulse test.

APPENDIX D

TEMPERATURE TABLE

Table D.1: Tabulated table of calculated temperatures from Arrhenius relationship and predicted temperatures that correlate to ideal Stefan-Boltzmann relationship.

Initial calculated average temperature* , T (K)	**Predicted average temperature, T_{new} (K)**	**Power (W)**	**Ln(Power)**	**Ln(T)**	**Ln(T_{new})**
1586.393	1349.410	13.869	2.630	7.369	7.207
1602.234	1360.212	14.319	2.662	7.379	7.215
1623.711	1374.825	14.944	2.704	7.392	7.226
1637.852	1384.425	15.366	2.732	7.401	7.233
1654.252	1395.539	15.865	2.764	7.411	7.241
1674.717	1409.377	16.504	2.804	7.423	7.251
1697.382	1424.663	17.232	2.847	7.437	7.262
1720.534	1440.237	17.998	2.890	7.450	7.273
1783.326	1455.528	18.774	2.932	7.464	7.283

* Calculated from Arrhenius relationship

REFERENCES

1. *Diamond Field Emission Devices.* **Davidson, J.L., Kang, W.P., Wisitsora-At,A.** 3-7, 2003, Diamond Related Materials, Vol. 12, pp. 429-433.

2. **Kittel, C.** *Introduction to Solid State Physics.* New York : Wiley-Interscience, 1986, pp. 19-20.

3. **Davidson, J.L.** [book auth.] K.E. and Dismukes,J.P. Spear. *Synthethis Diamond: Emerging CVD Science and Technology.* New York : Wiley-Interscience, 1994, p. 356.

4. **Van Enckevort, W.J.P.** [book auth.] K.E., Dismukes, J.P. Spear. *Synthetic Diamond: Emerging CVD Science and Technology.* New York : Wiley-Interscience, 1994, pp. 322-332.

5. **Pankove, J.I., Qiu, C.H.** [book auth.] K.E., Dismukes, J.P. Spear. *Synthetic Diamond: Emerging CVD Science and Technology.* New York : Wiley-Interscience, 1994, pp. 403-407.

6. *Optical Absorption and Luminescence in Diamond.* **Walker, J.** 10, 1979, Reports on Progress in Physics, Vol. 42, p. 1605.

7. **Zaitsev, A.M.** *Optical Properties of Diamond: a Data Handbook,.* Berlin : Springer-Verlag, 2001. pp. 389-393.

8. *Photothermal Ionization and Photon-Induced Tunneling in the Acceptor Photoconductivity Spectrum of Semiconducting Diamond.* **Collins, A.T. and Lightowlers, E.C.** 3, 1968, Physical Review, Vol. 171, pp. 843-855.

9. *CVD Diamond - A New Technology For The Future?* **May, P. W.** 3, 1995, EndeavourMagazine, Vol. 19, pp. 101-106.

10. *Optical Properties of GaAs.* **Memon, A. and Fakhro, S.Q.** 11, 2008, International Journal of Infrared and Millimeter Waves, Vol. 8, pp. 1391-1397.

11. *Surface Micromachining for Microelectromachanical Systems.* **Bustillo,J., Howe, R.T., and Muller, R.S.** 8, August 1998, Proceedings of the IEEE, Vol. 86, pp. 1552-1574.

12. *Nucleation of Diamond Powder Particles in an RF Methane Plasma.* **Mitura, S.** 2, February 1987, Journal of Crystal Growth, Vol. 80, pp. 417-424.

13. *Generation of Diamond Nuclei by Electric Field in Plasma Chemical Vapor Deposition.* **Yugo, S., Kanai,T., Kimura, T. and Muto, T.** 10, 1991, Applied Physics Letters, Vol. 58, p. 1036.

14. *Characterization of Bias-Enhanced Nucleation of Diamond on Silicon by Invacuo Surface Analysis and Transmission Electron Microscopy.* **Stoner,B.R., Ma, G.-H.M., Wolter, D.S. and Glass, J.T.** 19, 1992, Physical Review B, Vol. 45, p. 11067.

15. *Electrical Conduction In Homoepitaxial, Boron-Doped Diamond Films.* **Visser, E.P., Bauhuis, G.J., Janssen, G., Vollenberg, W., Enckevort, W.J.P. and Giling, L.J.**, 1992, Journal of Physical Condensed Matter, Vol. 4, pp. 7365-7376.

16. **Incropera,F.P. and DeWitt,D.P.** *Fundamentals of Heat and Mass Transfer* . 2nd. New York : John Wiley & Sons Inc., 1990.

17. **Lienhard IV, J.H.** *A Heat Transfer Textbook.* 3rd Ed. Cambridge : Phlogiston Press, 2003.

18. **Kohn, E., Ebert, W. and Wild,C.** Electronic devices on CVD diamond. [book auth.] C. Wild Ed. B. Dischler. *Low Pressure Diamond -. Manufacturing and Applications.* s.l. : Springer, 1998, pp. 331-359.

19. **Beardsmore,G.R. and Cull,J.P.** *Crustal Heat Flow- A Guide to Measurement and Modelling.* Cambridge : Cambridge University Press, 2001.

20. *Simulation of the Thermal Behavior of Thermal Flow Sensor by Equivalent Electrical Circuits.* **Auerbach, F.J., Meiendras,G., Muller,R. and Scheller,G.J. E.** 1994, Sensors and Actuators A, Vols. 41-42, pp. 275-278.

21. *The Design and Electro-thermal Modeling of Micro Devices in CMOS Compatible MEMS Technology.* **Wojciak,W., Orlikowski,M., Zubert,M. and Napieralski, A.** Cannes-France : s.n., September 1997, Proc. of 3rd Int. Workshop on Thermal Investigations of ICs and Microstructures, pp. 159-161.

22. **Meijer, G.C. M. and Herwaarden, A.W.** *Thermal Sensors.* Bristol and Philedelphia : Institute of PhysicsPublishing, 1994.

23. Wikipedia. *The Free Encyclopedia. http://en.wikipedia.org/wiki/Joule_heating.* [Online]

24. *The Dopant Density and Temperature Dependence of Hole Mobility and Resistivity in Boron Doped Silicon.* **Li, S.S.** 9, 1978, Solid-State Electron, Vol. 21, pp. 1109-1117.

25. *The Dopant Density and Temperature Dependence of Electron Mobility and Resistivity in N-type Silicon.* **Li, S.S. and Thurber, W.R.** 7, 1977, Solid-State Electron, Vol. 20, p. 609.

26. *Electrical Properties of Pure Silicon and Silicon Alloys Containing Boron and Phosphorus.* **Pearson, G.L. and Bardeen, J.** 5, 1949, Physics Review, Vol. 75, pp. 865-883.

27. *Resistivity of Chemical Vapor Deposited Diamond Films.* **Landstrass, M.I. and Ravi, K.V.** 10, 1989, Applied Physics Letters, Vol. 55, pp. 975-977.

28. *Electrical Properties of Boron-Doped Diamond Films Prepared by Microwave Plasma Chemical Vapor Deposition.* **Deguchi,M., Kitabatake,M. and Hirao, T.** 1-2, 1996, Thin Solid Films, Vols. 281-282, pp. 267-270.

29. *Electrical properties of B-doped homoepitaxial diamond (001) film.* **H. Kiyota, E. Matsushima, K. Sato, H. Okushi, T. Ando, J. Tanaka, Mutsukazu, and Y. Sato.** 1997, Diamond and Related Material, Vol. 6, pp. 1753-1758.

30. *Temperature Dependent Mobility in Single Crystal Vapor-Deposited Diamond.* **Pan,L.S., Kania, D.R., Pianetta,P., Ager.,J.W., Landstrass,M. I. and Han, S.** 6, 1993, Journal of Applied Physics, Vol. 73, pp. 2888-2894.

31. *Hopping Conduction in Semiconducting Diamond.* **Massarani, B., Bourgoin, J.C. and Chrenko, R.M.** 4, 1978, Physical Review B, Vol. 17, pp. 1758-1769.

32. **Mihir, S.** *Principles of Thermal Control.* Department of Aerospace and Mechanical Engineering, University of Notre Dame. Notre Dame, IN 46556, U.S.A. : Mihir, S., 2004.

33. *Temperature Measurement Using Thermistor with Pulsed Operation of Circuit Containing Thermistor and Linear Resistor.* **Minkin, S.B., Shashkov, A.G. and Ulashchik, V.E.** 6, June 1976, Journal of Engineering Physics and Thermophysics, Vol. 30, pp. 710-716.

34. **Mahan, J.R.** *Radiation Heat Transfer: A Statistical Approach.* New York : John Wiley & Johnson, 2002.

35. **Hudson, R.D.** *Infrared System Engineering.* New York/London/Sydney/Toronto : John Wiley & Sons, 1969.

36. **Mooney, W.J.** *Optoelectronic Devices and Principles.* New Jersey : Prentice Hall, 1991.

37. **Nave, C.R.** Hyper Physics Department of Physics and Astronomy. *Radiation Blackbody.* [Online] Georgia State University, 2001. http://hyperphysics.phy-astr.gsu.edu/HBASE/bbrc.html.

38.**Pattison,G.** http://www.egglescliffe.org.uk/physics/astronomy/blackbody/bbody.html. *Blackbody Radiation.* [Online] 2000/2001.

39. **Hamari, Puteri S. M.** *Thermal Behavior of Powered Miniature Diamond Resistors.* Vanderbilt Univeristy. Nashville : Master's Thesis, 2004.

40. *Microstructure, Electrical Properties, and Thermal Stability of Ti-Based Ohmic Contacts to N-GaN.* **Smith,L.L., Davis,R.F., Liu,R-J., Kim,M.J. and Carpenter,R.W.** 2, 1999, Material Research Society, Vol. 14, pp. 1032-1038.

41. *Piezoresistive Microsensors using P-type CVD Diamond Films.* **Taher,I., Aslam, M., Tamor, M.A., Potter,T. J. and Elder, R.C.** 1, 1994, Sensors and Actuators A, Vol. 45, pp. 35-43.

42. *Growth and Characterization of Diamond Films on SiO2/Si Substrates.* **Jiang, N., Noguchi, S., Nishimura,K., Inaoka,T., Shintani,Y. and Hiraki, A.** Part 1, 11A, November 2002, The Japan Society of Applied Physics, Vol. 41, pp. 6493–6497.

43. *Multiwavelength Reflectometric Technique for Normal Spectral Emissivity Measurements by a Pulse-Heating Method.* **Yi,F., Sun Xiaogang,S. and Righini,F.** 3, May 2003, International Journal of Thermophysics, Vol. 24, pp. 849-857.

44. *Pulse Testing a Model Heat Exchange Process.* **Sidney, L.** 6, 1956, Industrial and Engineering Chemistry, Vol. 48, pp. 1064–1068.

45. *Joule Heating and Determination of Temperature in Capillary Electrophoresis and Capillary Electrochromatography Columns.* **Rathore, A.S.** 1-2, 2004, Journal of Chromatography A, Vol. 1037, pp. 431–443.

46. *Thermistor Made of P-Type Synthetic Diamond.* **Vereshchagin,L.F., Demidov, K.K., Revin,O.G. and Slesarev, V.N.** 1975, Soviet Physics Semiconductors, Vol. 8, pp. 1581-1582.

47. *Thermister Made of Diamond Thin Film.* **Nakahata,H., Imai,T., Shiomi,H., Nishibayashi,Y. and Fujimori, N.** 1990, Science and technology of New Diamond, pp. 285-289.

48. *Short-Time Failure of Metal Interconnect Caused by Current Pulses.* **Murguia,J. and Bernstein,J.** 10, October 1993, IEEE Electron Device Letters, Vol. 14, pp. 481-483.

49. *Complementary Model for Intrinsic Time-Dependent Dielectric Breakdown in SiO2 Dielectrics.* **McPherson,J.W., Khamankar,R.B. and Shanware, A.** 9, 2000, Journal Of Applied Physics, Vol. 88, pp. 5351–5359.

50. *A Unified Gate Oxide Reliability Model.* **Hu,C. and Lu,Q.** Piscataway, NJ : s.n., 1999, International Reliability Phyics Proceedings IEEE, pp. 47–51.

51. *Stress-Induced Leakage Current (SILC) and Oxide Breakdown: Are They From the Same Oxide Traps?* **Pantisano,L. and Cheung,K.** 2, June 2001, IEEE Transactions On Device and Materials Reliability, Vol. 1, pp. 109-112.

52. **Carslaw,H.S. and Jaeger,J.C.** *Conduction of Heat in Solids.* s.l. : Oxford University Press, USA; 2 edition (April 10, 1986), 1986.

53. *Joule Heating in Single-Walled Carbon Nanotubes.* **Ragab,T and Basaran,C.** 6, 2009, Journal of Applied Physics, Vol. 106, p. 63705.

54. *Stress Induced Leakage Current Under Pulsed Voltage Stress.* **Cester,A., Paccagnella,A. and Ghidini,G.** 3, 2002, Solid-State Electronics, Vol. 46, pp. 399-405.

55. *Strong Non-Arrhenius Temperature Dependence of the Resistivity in the Regime of Traditional Band Transport.* **Michel,C., Baranovskii,S.D., Klar,P.J., Thomas,P. and Goldlücke,B.** 2006, Applied Physics Letters, Vol. 89, pp. 112-116.

56. **Kittel,C. and H. Kroemer,H.** *Thermal Physics.* s.l. : W. H. Freeman and Co, 1980.

57. *High-Temperature Raman Scattering Behavior in Diamond.* **Herchen,H. and Cappelli,M.A.** 1991, Proceedings SPIE, Vol. 1534, p. 1047.

58. *Performance Characteristics of Thin Film Resistor Arrays for Infrared Projector Applications.* **Williams, O.M.** 1992, Proceedings SPIE, Vol. 1687, pp. 71-81.

59. *Transient Energy Transfer By Radiation and Conduction.* **Lick, W.** s.l. : Pergamon Press, 1965, Int.. J. Heat Mass Transfer, Vol. 8, pp. 119-127.

60. *Simultaneous Conduction and Radiation in Porous and Composite Materials: Effective Thermal Conductivity.* **Chlew,Y.C. and Glandt, E.D.** 3, 1983, Industrial Engineering Chemistry Fundamentals, Vol. 22, pp. 276-282.

61. *Heat Generation in Semiconductor Devices.* **Lindefelt, U.** 2, January 15, 1994, J. Appl. Phys, Vol. 75, pp. 942-957.

62. **Lane, C. H.** *Nichrome Resistor Properties and Reliability.* s.l. : National Technical infermation Service, 1973.

63. *Pulse De-rating and End of Life (EOL) for High Reliability Resistors.* **Cozzolino, M.J.** Jacksonville FL. : Electronic Components Associations, 2009. CARTS USA.

64. *Influence of IR-laser irradiation on -SiC–chromium silicides ceramics.* **Vlasova,M., Marquez Aguilar, P.A., Resendiz-Gonzalez,M.C., Kakazey,M., Bykovb,A., Gonzalez Morales,I. .** 2005, Materials Science and Engineering A, Vol. 404, pp. 64–70.

65. *Properties of High-Resistivity Cr-Si-O Thin-Film Resistor.* **Narizuka,Y., Kawahito,T., Kamei,T. and Kobayashi,S.** 4, December 1988, IEEE Transactions On Components, Hybrids And Manufacturing Technology, Vol. 11, pp. 433-438.